Photosynthesis-inspired device architectures for organic photovoltaics

by

Timothy David Heidel

S.B., Massachusetts Institute of Technology (2005)
M.Eng., Massachusetts Institute of Technology (2006)
S.M., Massachusetts Institute of Technology (2009)

Submitted to the Department of Electrical Engineering and Computer Science
in partial fulfillment of the requirements for the degree of

Doctor of Philosophy

at the

MASSACHUSETTS INSTITUTE OF TECHNOLOGY

February 2010

Author .....
Department of Electrical Engineering and Computer Science
January 29, 2010

Certified by .....
Marc A. Baldo
Associate Professor
Thesis Supervisor

Accepted by .....
Professor Terry P. Orlando
Chair, Department Committee on Graduate Students

Photosynthesis-inspired device architectures for organic photovoltaics

by

Timothy David Heidel

Submitted to the Department of Electrical Engineering and Computer Science
on January 29, 2010, in partial fulfillment of the
requirements for the degree of
Doctor of Philosophy

Abstract

Organic semiconductor photovoltaics offer a promising route to low-cost, scalable, emissions-free electricity generation. However, achieving higher power conversion efficiencies is critical before these devices can play a larger role in our future energy generation landscape. Organic photovoltaic devices are currently limited by two primary challenges: (1) a trade-off between light absorption and exciton diffusion and (2) low open-circuit voltage due to charge recombination at the donor-acceptor interface. In this work, we demonstrate two new device architectures inspired by photosynthesis that aim to overcome these two challenges.

First, we overcome the trade-off between light absorption and exciton diffusion by introducing an external light absorbing antenna layer. We model energy transfer from the antenna to the charge generating layers via surface plasmon polariton modes in the interfacial thin silver contact and via radiation into waveguide modes. We experimentally demonstrate devices with both single layer antennas and strongly absorbing resonant cavity antennas. We measure energy transfer efficiency from the antenna layer to the PV active layers as high as $51\pm10\%$. We discuss structural design criteria and describe ideal antenna material characteristics.

Second, we reduce charge transfer state recombination in organic photovoltaics by inserting a thin interfacial layer at the donor-acceptor interface. The thin interfacial layer creates a cascade energy structure that destabilizes the Coulombically bound charge transfer state formed immediately following exciton dissociation. We find the optimal interfacial layer thickness to be approximately 1.5 nm. In CuPc/C_{60} devices, under simulated solar illumination the short-circuit current increased 34%, the open-circuit voltage increased 33%, and the power conversion efficiency increased 49%. Thin interfacial layers can also be used to study the physics of exciton separation.

Thesis Supervisor: Marc A. Baldo
Title: Associate Professor

Acknowledgments

First and foremost, I thank my research supervisor, Professor Marc Baldo, for his unceasing guidance and support of both this research and my development as a researcher. Marc was always available to discuss new ideas or to tackle difficult research questions. I also thank him for his enthusiastic support of all of my activities beyond the laboratory at MIT including my work in the Technology and Policy Program and my leadership of the MIT Energy Club.

I would also like to thank all of the other members of the Soft Semiconductor Group who I have had the privilege to work alongside including Matthias Bahlke, Dr. Mihai Bora, Kemal Celebi, Mike Currie, Dr. Shalom Goffri, Daniel Hochbaum, Priya Jadhav, Jiye Lee, Dr. Benjie Limketkai, Dr. Jonathan Mapel, Dr. Kaveh Milaninia, Carlijn Mulder, Phil Reusswig, Dr. Carmel Rotschild, Dr. Michael Segal, Dr. Madhusudan Singh, and Dr. Luke Theogarajan.

This work would not have been possible without the generous financial support of organizations willing to dream big and take risks on new technologies. The Air Force Office of Scientific Research, the Defense Advanced Research Projects Agency, the Martin Family Society for Sustainability, the National Science Foundation, and the Department of Energy have all contributed to the work described in this thesis.

I thoroughly enjoyed interacting with brilliant and passionate individuals throughout the MIT campus over the past several years. The Executive Committee (past and present) and other members of the MIT Energy Club have contributed a great deal to my growth. I also owe thanks to all of my friends without whom I would have never finished this thesis including Abe, Chris, Jesse, Joseph, Junjay, Kyle, Zoe, and many more.

Finally, I would like to thank my parents and my girlfriend Nicole. Their neverending support and love has played a large part in my successful pursuit of this milestone. I would also like to thank Nicole for contributing countless hours helping to edit drafts of this thesis.

Contents

List of Figures

Chapter 1

Introduction and Motivation

1.1 The energy challenge

The capture, conversion, and consumption of energy is a multi-trillion dollar industry that impacts the lives of every human being at every level of society in every country on Earth every day. Global energy use has grown dramatically since the start of the industrial revolution, rising from approximately 27.4 exajoules (EJ) in 1850 [1] to 474 EJ in 2008 [2], a twenty-seven-fold increase. During this time the global population grew from approximately 1.25 billion to just over 6 billion [3]. By the middle of the twenty-first century the global population is projected to grow to over 9 billion and global energy demand is projected to double again [4]. Energy is a basic need underlying all aspects of the global economy.

Unfortunately, all energy sources currently in widespread use are derived from finite, exhaustible resources that are distributed disproportionately throughout the world. As the global population continues to grow and the economies of developing countries continue to grow rapidly, energy resources will become increasingly constrained. Furthermore, our understanding of the potential risks associated with anthropogenic climate change, primarily driven by human energy consumption, con-

tinues to grow. Procuring adequate, environmentally-benign energy supplies is poised to become a defining technological, economic, and political challenge of the coming century.

The resurgence of interest in alternative sources of energy is due to three primary drivers: (1) economic opportunity, (2) national security, and (3) climate change and environmental risk.

Increasingly, the pursuit of new energy technologies is being viewed as an important economic opportunity. Energy is one of the largest industries on Earth. Countries with technical leadership in new energy technologies in the next century could lead the global economy. In recent years price volatility for oil has become an increasing concern. For example, over the past decade the spot price for oil has ranged between $17 per barrel in January 1999 to more than $140 per barrel in July 2008 [5]. As the demand for oil and other energy resources continues to rise, price volatility is likely to continue to be a major concern. High energy costs could threaten the competitiveness of nations.

Security concerns are also driving the pursuit of alternative energy sources. A large portion of the world's petroleum is found in regions of the world characterized by political instability. For example, the United States currently imports over 30% of its primary energy, including significant volumes of petroleum from potentially unstable countries such as Iraq and Venezuela. Today, energy security concerns are also driven by international threats of terrorism, nationalist backlash in exporting countries, fears of a scramble for limited international energy supplies, and geopolitical rivalries [6]. Further, security concerns are not limited to oil supplies. Electric power blackouts, such as the August 2003 blackout in North America, cause enormous economic losses and present serious national security concerns. Indeed, recent evidence has indicated that the security of the US centralized electric power grid is at risk of foreign intrusion [7]. Natural gas supplies are also becoming increasingly linked throughout the world.

Disputes over European imports of natural gas from Russia and the Ukraine have been a political challenge in Europe in recent years. As the demand for energy supplies continues to grow, energy security concerns are likely to become even more prominent.

Finally, anthropogenic climate change is motivating the pursuit of new energy sources. Fossil fuel based energy sources including petroleum and coal emit large amounts of CO_2 and other greenhouse gases into the atmosphere. The average atmospheric CO_2 concentration has increased from approximately 280 ppm by volume at the start of the industrial revolution in the mid-nineteenth century to approximately 387 ppm by volume today [8]. The specific risks associated with higher atmospheric greenhouse gas concentrations are subject to significant uncertainty [9]. However, these risks could include increased mean global temperatures leading to dramatic local climate shifts, increased occurrences of droughts, fires and floods, higher ocean water levels, and increased intensity or volatility of storm systems like hurricanes. In turn, these natural changes could put enormous pressures on global food production [10] and change the dynamics of the transmission of diseases throughout the world [11]. The majority of climate scientists now believe climate change imposes significant risk and that efforts should be undertaken to reduce future greenhouse gas emissions [8]. Decarbonizing global energy supplies is one of the most direct ways to stabilize atmospheric greenhouse gas concentrations [12]. The development of technologies to economically exploit renewable, carbon-free energy resources is critical to minimize the potential risks of climate change.

Combined, these three constraints are driving the pursuit of new sources of energy. A dramatic shift to renewable sources of energy would not be the first dramatic change in energy production the US has experienced. The United States primary energy mix has evolved continuously since the start of the industrial revolution. In the United States, primary energy use grew from approximately 0.5 EJ in 1800 to over 105 EJ in 2008. As illustrated in Figure 1-1, during this time the country's primary source of

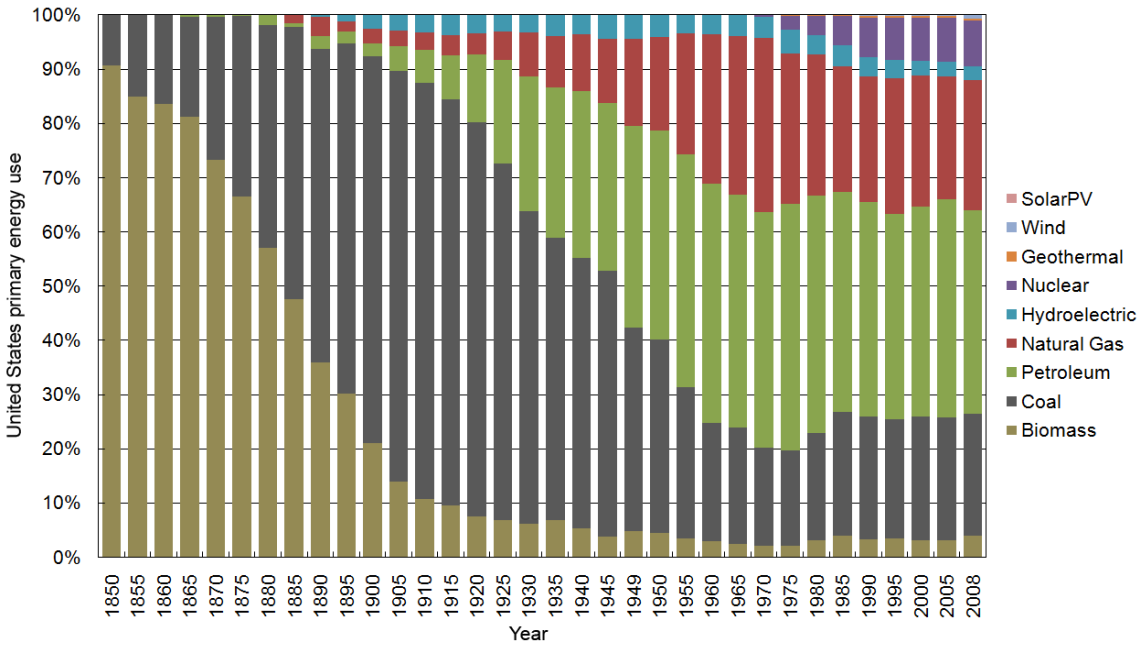

Figure 1-1: Primary energy sources in the United States since 1850. The primary sources of energy used in the United States have evolved since the start of the industrial revolution. Biomass (primarily wood) was the dominant fuel initially. However, by the early 1900s, coal became the most widely used fuel. Petroleum and natural gas use grew significantly by the middle of the last century. Renewable sources of energy currently account for a relatively small proportion of the nation's total energy use. Data from [4].

energy shifted from over 90% biomass (mostly wood) to a diversified mix dominated by coal, natural gas, and petroleum. Historically, non-renewable sources of energy have fueled most of the United State's total primary energy use. Carbon-neutral sources of energy play a small role in the United States energy consumption today.

Significant research effrots are underway to develop renewable sources of power including harnessing energy from wind, geothermal resources, waves, tides, and the sun. Expanding the civilian use of nuclear power is also an area of active research and development. Ultimately, all of these energy sources are likely to play a role in our future energy consumption. This thesis is focused on organic solar cells, a technology with promise to inexpensively harvest energy from the sun over large areas.

1.2 Solar power

The sun is an inexhaustible, carbon-neutral source of energy that has the potential to supply all of mankind's energy needs. Every hour the sun delivers over 4.3 x 10^{20} J of energy to the Earth, more than humans currently consume in an entire year [13]. The sun is a particularly attractive alternative source of energy as it is available in large supply throughout the world and, therefore, could reduce countries' energy interdependence, easing energy-related economic and national security fears. Finally, the carbon-neutral nature of the energy in sunlight means that it could be utilized at large scale with no widespread environmental harm.

The United States has an abundant solar resource potential. As illustrated in Figure 1-2, some regions of the United States have the potential to capture over 6 kWh/m^2 of solar energy on average each day. Furthermore, it has been estimated that a square land area approximately 161 km on a side or approximately 1.6% of the total US land area, could generate all of the US energy needs with 10% efficient solar cells [14]. Due to the intermittent, variable nature of the solar resource, it will likely never be feasible to source all of our energy from the sun. However, this calculation gives a sense for just how large the resource truly is.

The solar resource can be utilized in several different ways. First, solar radiation can be used directly for heating buildings. Many efforts have focused on integrating passive solar energy capture into the architectural design of buildings. The energy in solar radiation can also be used to heat water for domestic use. Roof-mounted solar water heaters have been adopted widely in some regions of the world. For example, over 85% of households in Israel currently utilize solar water heaters [16]. Finally, solar radiation can also be used to generate electricity.

Electricity generation with solar radiation can be accomplished using two primary methods. First, solar radiation can be used to heat water or other liquids that

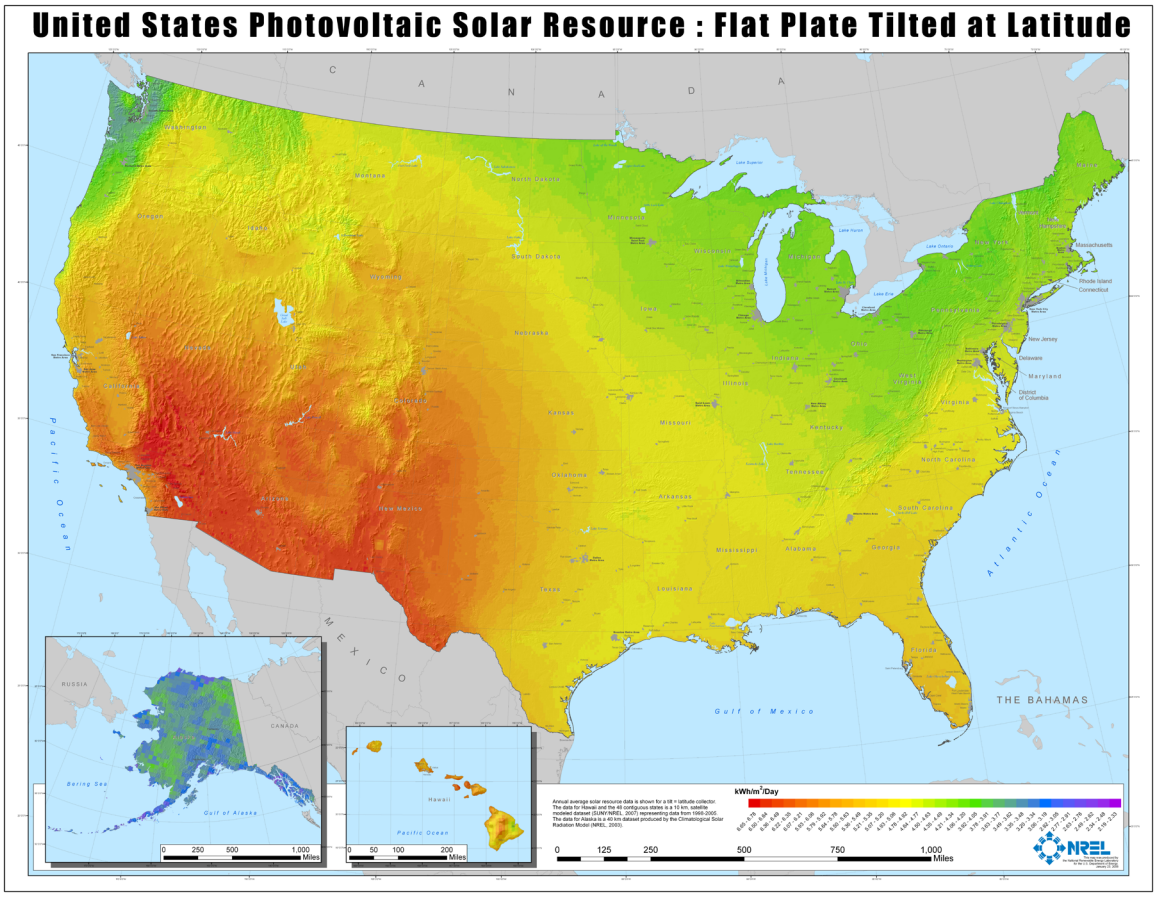

Figure 1-2: Solar resource potential in the United States. The southwestern region of the United States receives the most solar radiation on average. Some areas average over 6.5 kWh/m^2 per day of solar radiation. While the total magnitude of solar energy reaching the United States each day is far more than the country currently uses, the low-density nature of the resource complicates efforts to economically capture it at large scale. From [15].

are subsequently used to fuel steam turbines in what is known as "solar thermal" generation [17]. Solar thermal power generation facilities have demonstrated great promise to provide large amounts of baseload power generation at competitive prices [18]. Second, the energy in solar radiation can be directly converted to electricity using the photovoltaic effect. The photovoltaic effect was first discovered in 1839 by Edmund Becquerel who observed a photo induced current in a device consisting of two electrodes, one composed of silver chloride, immersed in an electrolyte solution [19]. While the photovoltaic effect was studied throughout the subsequent century, the first modern solar cell consisting of a *pn*-junction in silicon was demonstrated by Chapin *et al.* at Bell Labs in 1954 [20].

In the past half century, significant progress has been made towards achieving high power conversion efficiency in photovoltaic devices, as illustrated in Figure 1-3. Inorganic, crystalline semiconductor photovoltaics have successfully borrowed expertise and fabrication techniques from the rapidly advancing microelectronics industry. Power conversion efficiencies as high as 25.0±0.5% for crystalline silicon cells, 26.1±0.8% for III-V (GaAs) semiconductor cells, and 9.5±0.3% for amorphous silicon devices have been reported and verified by independent test centers [21]. The maximum achieveable efficiency for single *pn*-junction solar cells is limited by the Shockley-Queisser limit to approximately 31% [22].

However, despite advances in power conversion efficiency, photovoltaics remain prohibitively expensive relative to other sources of electricity and have not achieved widespread success as an alternative means of producing electricity [23]. For much of the past half century, the use of solar cells was limited to specialized niche markets such as for satellites [24] or for rural electrification [25]. In these applications, generating electricity via conventional methods such as using gas or coal burning power plants would have been too expensive or simply impractical. In addition to high cost, the intermittent and variable nature of solar radiation complicates efforts to integrate

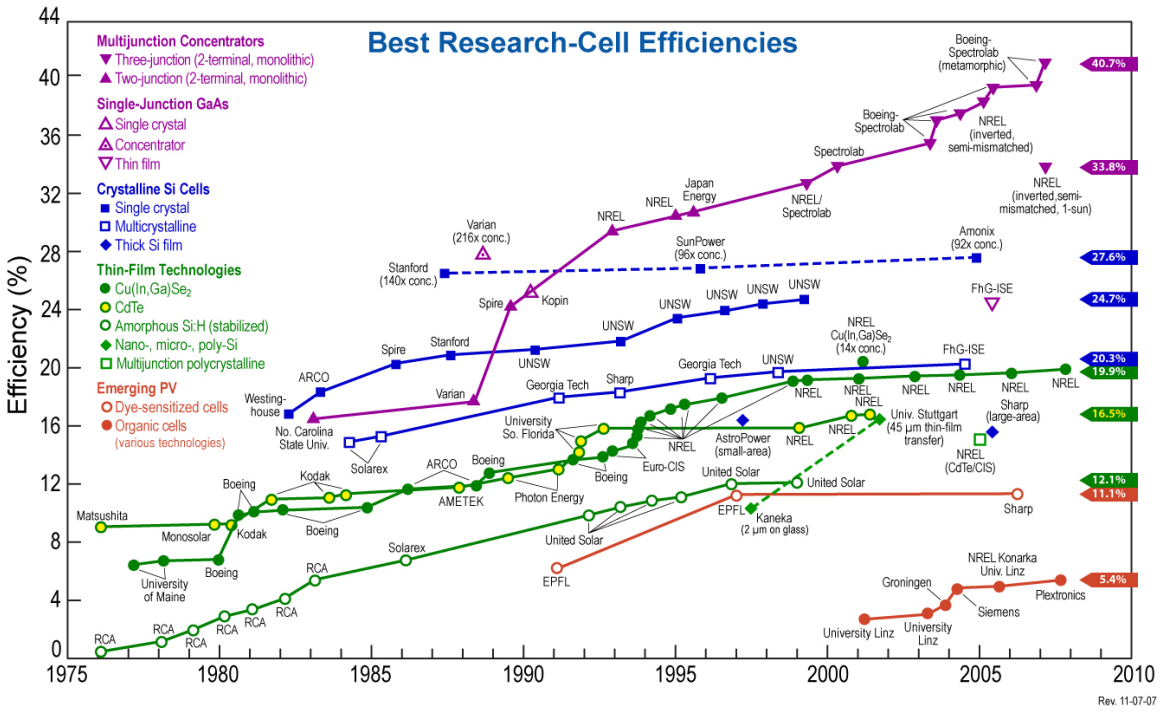

Figure 1-3: Record research solar cell efficiencies. The history of progress in power conversion efficiency is indicated for a range of photovoltaic technologies. Record cell efficiencies have increased from approximately 9% in 1975 to over 40% in 2008. The use of multiple junctions in photovoltaics have allowed efficiencies to increase beyond the single junction limit. However, higher efficiency devices are typically prohibitively expensive for most applications. Many of the technologies illustrated have yet to achieve commercial viability. Organic solar cell progress is displayed in the lower right corner of this plot.

large amounts of solar electricity generation into the bulk power system.

Photovoltaics remain too expensive for widespread terrestrial use [26]. In 2008, solar electricity generation accounted for less than 0.03% of total US electricity generation [4]. However, advances in power conversion efficiency, reductions in manufacturing costs, and aggressive policy mechanisms including feed-in-tariffs, investment tax credits, and renewable portfolio standards have resulted in rapid growth in the deployment of photovoltaics over the past decade. Over the past 20 years, PV manufacturing output has grown by a factor of 200, reaching over 5,950 MW in 2008 [27]. The total accumulated installed capacity surpassed 15 GW in 2008 [28]. While this is less than 0.4% of the world's total installed electricity generation capacity of 4000

GW, many industry leaders expect rapid industry growth to continue throughout at least the next decade [29].

Despite recent growth, photovoltaics remain more expensive than alternative generation sources. The high fabrication costs associated with crystalline semiconductors has limited conventional, inorganic solar cells from achieving truly large scale. The average price for a solar module at the end of 2009 was approximately $4.31 per peak Watt. Furthermore, installation and balance of system components including inverters, charge controllers, circuit breakers, wiring, and mounting frames continue to add significant additional cost. The average system cost for photovoltaics was estimated to be approximately $7.50 per peak Watt in 2007. Estimates of the levelized cost of electricity (LCOE) with photovoltaics vary widely from as low as approximately $0.15/kWh to over $0.40/kWh [30, 27]. Calculations of LCOE depend not only on the cost of solar modules but also on geographic location and financing terms. While estimates vary, most remain well above the average cost of retail electricity in the United States, $0.093/kWh in 2007. While incremental improvements in efficiency and reductions in balance of systems costs are likely to sustain growth in the short term, new device materials and/or architectures may be needed before photovoltaics can achieve truly large scale and make a significant contribution to total energy use.

Figure 1-4 illustrates a roadmap for solar cell development originally developed by Professor Martin Green at the University of New South Wales, Sydney, Australia. The roadmap suggests that photovoltaics can be classified into three broad technology generations. The first generation, including the vast majority of current commercial photovoltaics, are characterized by efficiencies below the single junction limit [22] at relatively high costs. Figure 1-4 includes dotted lines indicating module costs. Current solar modules cost between approximately $1/W and $3.50/W to manufacture. Second generation photovoltaics are predicted to exhibit slightly lower efficiencies but significantly lower costs. Thin-film inorganic solar cells, discussed in more detail

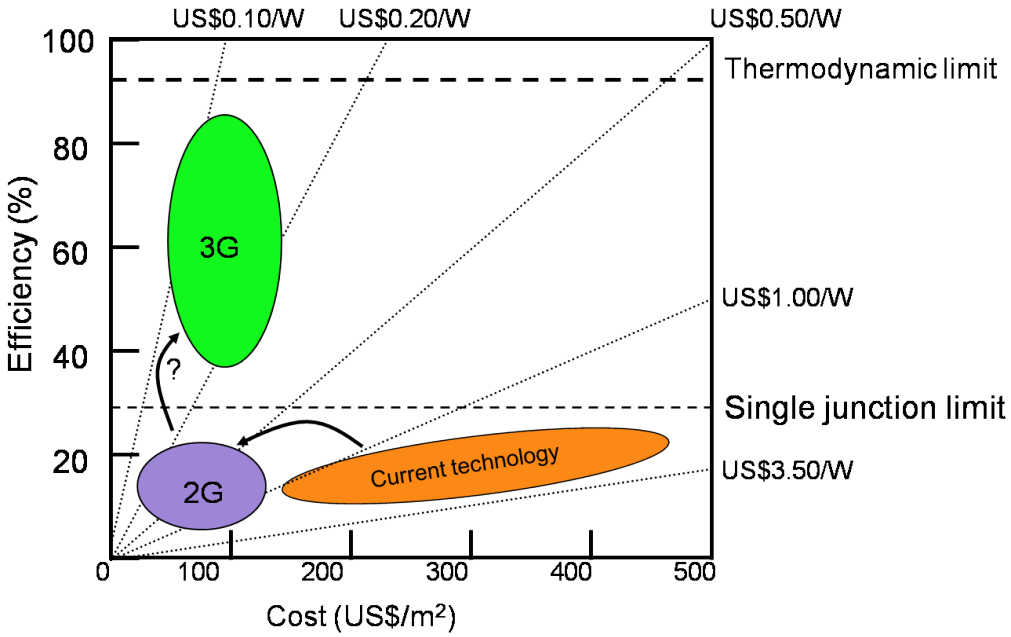

Figure 1-4: Roadmap to higher efficiency photovoltaics. Photovoltaics are expected to mature via three broad generations of technology. Current generation technology including single crystal silicon solar cells achieve relatively high efficiencies, but still below the single junction limit, at relatively high cost. Second generation devices are predicted to achieve slightly lower efficiencies at significantly lower costs. Thin film solar cells are an example of second generation devices. Finally, third generation devices are expected to use new physical concepts or architectures that overcome the single junction limit at low cost. Organic solar cells are also second generation solar cells. After Martin Green [31].

below, are considered second generation devices. Organic solar cells are typically also considered second generation solar cells. Finally, third generation photovoltaic devices are predicted to utilize new physical phenomenon that will allow efficiencies to increase beyond the single junction limit and approach the thermodynamic limit [31]. These cells could employ physical phenomenon such as hot carrier conduction, multiple carrier photon emission, or multiple band gap structures.

Recently, thin film solar cells have attracted significant interest. Thin film inorganic semiconductor photovoltaics utilize far less expensive semiconductor material compared to conventional crystalline devices and can be manufactured at large scale

using less expensive manufacturing processes such as chemical vapor deposition or printing. The thin semiconductor layers, on the order of microns, allow large areas to be coated with very little material. Thus far, thin film devices based on amorphous silicon (α-Si), cadmium telluride (CdTe), and cadmium indium gallium selenide (CIGS) have attracted the most attention [32]. While thin film devices exhibit lower efficiencies relative to crystalline silicon devices, typically in the range of 9-13%, the significant cost advantages achieved result in lower overall costs on a dollars per Watt basis. For example, First Solar, a thin film solar cell leader, recently announced that it had achieved a solar module production cost of \$0.98/W [33]. The market share for thin film solar cells, primarily CdTe devices, has expanded rapidly in recent years. Thin film devices captured approximately 13% of global PV production in 2008 [27]. Furthermore, many analysts have predicted that the market share for thin film photovoltaics will continue to expand throughout the next decade. While recent advances have yielded significant growth in thin film inorganic solar cells, it is not yet known whether these devices will be able to achieve costs low enough to compete broadly with alternative electricity generation sources.

Organic semiconductor solar cells, the focus of this thesis, are another type of second generation thin film solar cell. These devices are introduced in the next section and discussed in detail in Chapter 2.

1.3 Organic semiconductor photovoltaics

Research into organic semiconductor based PVs, using small molecule pigments or polymers, has gained significant momentum in recent years as efficiencies have continued to rise steadily. The latest organic semiconductor based solar cells have exhibited power conversion efficiencies over 6% [34]. Organic semiconductor based devices have the potential for very low-cost production using techniques common in other indus-

tries such as roll-to-roll and web-based processing [35]. Many of these techniques are also well suited for making very large area devices. Finally, the variety of organic materials available and the ability of chemists to continually synthesize new molecules for specialized applications may also allow organic solar cells to be designed for innovative form factors and applications.

However, for any of these potential benefits to be realized the efficiency of organic PVs must be increased. Current bi-layer heterojunction organic PVs are limited by two primary challenges. First, the devices are limited by the amount of light they can absorb. Photogenerated excitons must reach the interface between the donor and acceptor semiconductor layers in order to be dissociated. Excitons that do not reach the interface cannot contribute to power generation. Unfortunately, the exciton diffusion length in organic molecules is typically significantly shorter than the absorption length [36]. Therefore, the absorption efficiency and exciton diffusion efficiency in conventional organic solar cells are coupled, opposing quantities; increasing absorption by increasing the device thickness leads to a decrease in exciton diffusion efficiency and vice versa.

Second, recombination of charges immediately following exciton dissociation is a major loss mechanism in current bi-layer heterojunction organic photovoltaics. Excitons dissociate via electron transfer forming a charge transfer (CT) state at the donor-acceptor interface. In the charge transfer state, the electron is localized on an acceptor molecule and the hole is localized on a donor molecule at the interface. Unfortunately, the two charges are Coulombically bound in the CT state and eventually recombine. The mechanism that allows some carriers to escape the charge transfer state is an area of debate [37, 38, 39, 40, 41]. Reducing charge transfer state recombination is an area of growing focus in the organic solar cell literature [42, 43, 44, 45]. Charge transfer state recombination is discussed in more detail in Chapter 4.

These two challenges will likely have to be overcome before organic photovoltaics

can achieve the power conversion efficiencies required to compete with alternative generation technologies. Device structure modifications represent one of the most promising routes to overcoming these challenges and achieving higher efficiency.

1.4 New device architectures for organic solar cells

In this thesis, we demonstrate two novel device structures that yield increased organic photovoltaic device performance. First, we demonstrate devices with external light-absorbing antennas. These devices aim to overcome the trade-off between light absorption and charge separation by decoupling these two processes. Second, we demonstrate devices with a thin interfacial layer located at the exciton dissociation interface. The interfacial layer creates a graded exciton dissociation interface that serves to reduce recombination of separated charges. These device architectures are illustrated in Figure 1-5. This thesis will describe the theoretical basis underlying these device structures and will discuss the results of experimentally fabricating and characterizing the devices.

The motivations for both of the device structures explored in this thesis come from photosynthesis. Therefore, prior to introducing the two new solar cell device architectures, we first briefly review the mechanism for energy transduction in photosynthesis.

1.4.1 Energy transduction in photosynthesis

Photosynthesis is the dominant energy conversion process on Earth. The vast majority of life depends on photosynthesis as a source of energy and the process helps maintain the Earth's atmosphere. The amount of energy trapped by photosynthesis has been estimated to be approximately 100 terawatts [46], nearly six times larger than the current power consumption of humans [4]. The process has evolved over

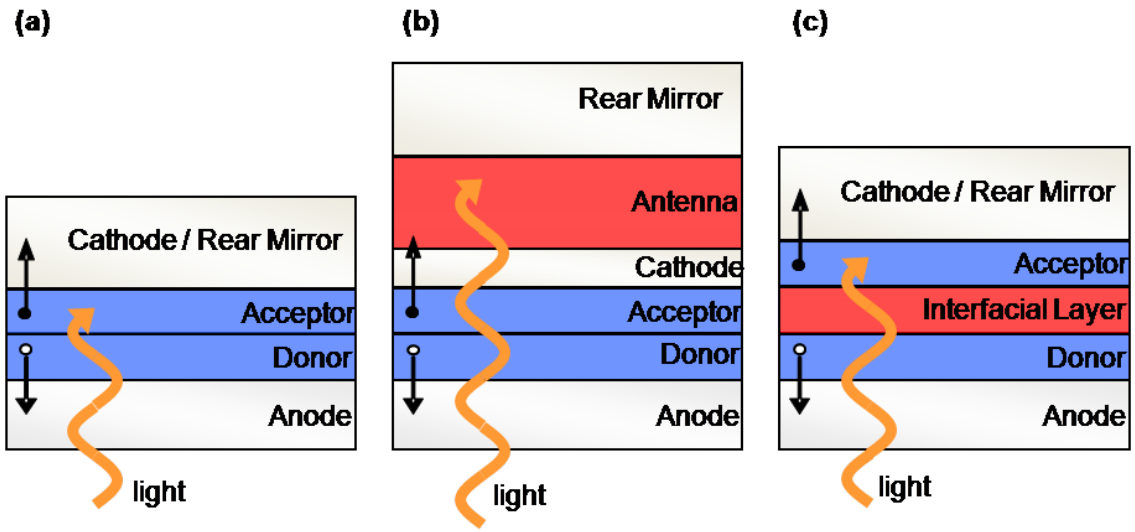

Figure 1-5: The device architectures studied in this work. (a) Conventional organic heterojunction PV cells are comprised of two organic semiconductor layers sandwiched between a transparent conducting anode and a reflecting cathode. The devices are designed such that the energy level offset at the interface between the two semiconductor layers makes it energetically favorable for excitons to split at the interface. (b) An external antenna layer can be used to overcome the tradeoff between light absorption and exciton diffusion in organic solar cells. (c) An interfacial layer creates a cascade energy structure at the interface that reduces recombination and, therefore, increases the efficiency of charge collection.

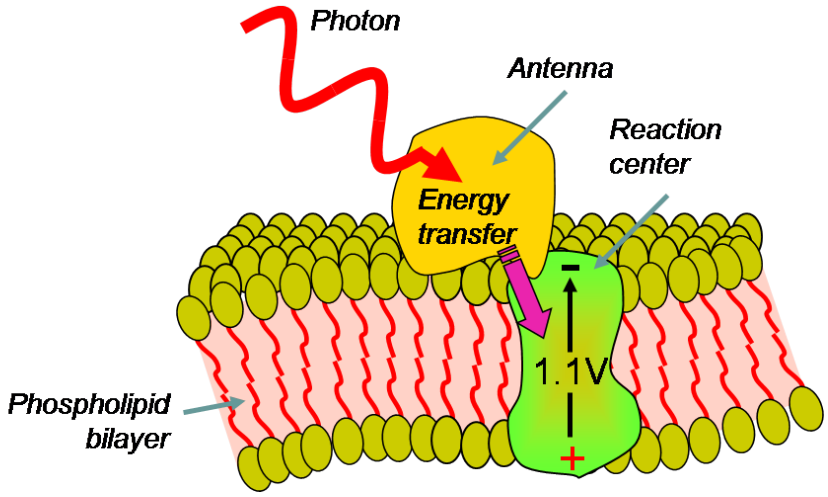

Figure 1-6: Structures involved in photosynthesis. The light harvesting antenna and reaction center serve as the sites of photon absorption and exciton dissociation respectively. A wide range of light harvesting antenna structures have been observed in nature. However, reaction centers are similar across all photosynthetic organisms. After Purves *et al.* [47].

several billion years and is the source of all the biomass and fossil fuels that we use today as energy sources.

Photosynthesis is the process that plants, algae, and many species of bacteria use to convert carbon dioxide into organic compounds using energy from sunlight. The diversity of species that perform photosynthesis requires that the process occur differently in different species. However, some features of the process are always the same. The process starts with the conversion of solar energy into electrical energy. The electrical energy is then used to drive a series of chemical reactions. Architecturally, photosynthesis can be divided into three distinct energy transduction phases, as illustrated in Figure 1-6.

First, light is typically absorbed in a protein structure known as a light harvesting antenna complex. Antenna structures vary widely throughout nature [48]. Antennas are primarily comprised of strongly absorbing chlorophyll pigment molecules [49]. However, antennas also typically employ additional pigments such as carotenoids and

phycobilins to ensure sufficient absorption throughout the visible spectrum. Pigment molecules in photosynthetic antennas capture photons and generate bound excitations known as excitons. Excitons consist of a bound electron-hole pair localized on a single molecule. After exciton generation, the antenna structures energetically funnel the excitons to charge generation complexes, known as reaction centers via resonant energy transfer [50]. Antenna structures in many biological systems have evolved a specific molecular orientation that promotes efficient funneling of excitons to the reaction centers.

Next, the photogenerated excitons are split into separated charges in the reaction center protein structures. Reaction centers consist of van der Waals bonded chlorophyll derivatives and other electron transfer cofactors that are carefully arranged to enhance electron transfer and charge separation [51]. While a wide variety of antenna complexes have been observed in nature, reaction centers are strikingly similar across most photosynthetic organisms [52]. In particular, reaction centers contain one particular chlorophyll dimer known as the special pair. The special pair is the lowest energy site for excitons in the system. Excitons generated in antenna systems are guided to the special pair before splitting [53]. Once an exciton arrives at the special pair, the exciton is split via a series of redox reactions known as an electron transfer cascade that rapidly carries the electron away from the special pair where the hole remains. The electron transfer cascade quickly separates the charges to $\sim$3 nm, suppressing back transfer of the electron. The multi-step electron transfer cascade employed in the reaction center yields highly efficient exciton dissociation [49]. A typical photosynthetic electron transfer cascade is illustrated in Figure 1-7. The potential formed by the separated charges varies from approximately 0.5 V in purple bacteria to approximately 1.1 V in more advanced systems [54].

Finally, the oxidized and reduced species are stabilized by secondary reactions, yielding a chemical potential across the photosynthetic membrane. The energy har-

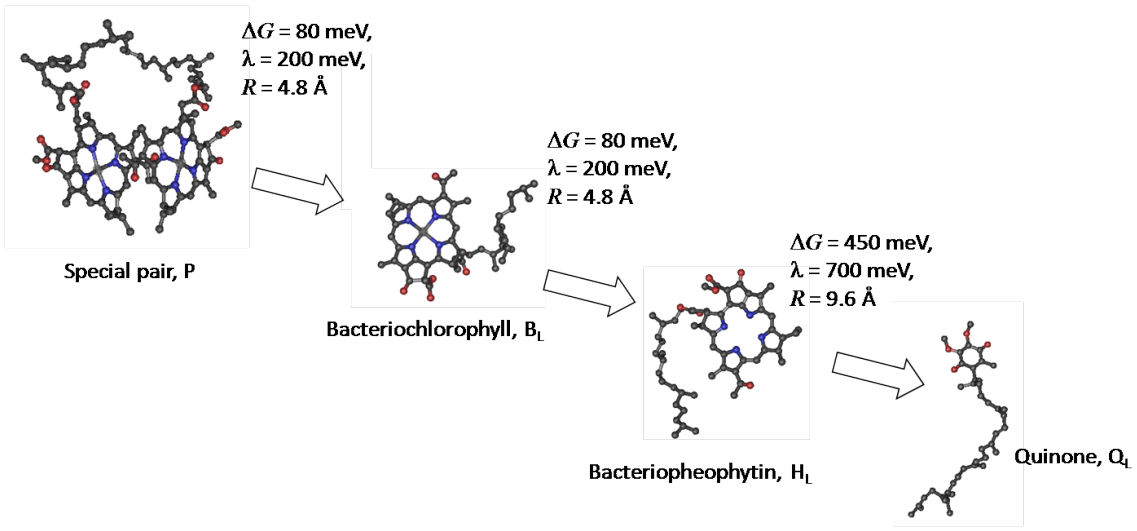

Figure 1-7: Electron transfer cascade in photosynthetic reaction centers. The special pair and electron transfer co-factors in the reaction center complex of *Rhodobacter spaeroides*. ΔG, λ, and R correspond to the Gibbs free energy change, the reorganization energy, and the spatial separation, respectively, for each step in the electron transfer cascade. Electron transfer reactions are discussed in detail in Chapter 4. Figure produced from the Protein Data Bank file 1AIJ using Visual Molecular Dynamics [55].

vested via the light reaction is stored by forming the chemical adenosine triphosphate (ATP). This chemical is made of the nucleotide adenine bonded to a ribose sugar bonded to three phosphate groups. The details of the chemical reactions in photosynthesis that occur after the initial exciton separation have been described elsewhere and are beyond the scope of this thesis.

Photovoltaics are essentially an artificial form of photosynthesis. However, the energy transduction process in photovoltaics stops prior to the chemical stabilization of the oxidized and reduced species. Instead of completing the conversion of sunlight into organic compounds, photovoltaics produce the intermediate product of separated charges which are then collected to generate electrical power. However, in contrast to the spatially separated components utilized in photosynthesis, conventional photovoltaic devices use the same material and structure to perform both of the first two phases of energy transduction. The semiconductor material absorbs the light, serving

the function of the photosynthetic antenna and the *pn*-junction, formed by doping the semiconductor, serves to separate the charges.

The spatial separation between the light absorbing antenna and the reaction center in photosynthesis and the use of a multiple step electron transfer cascade for charge separation motivate the new device architectures demonstrated in this thesis.

1.5 Organic solar cells with external antennas

The first new device structure described in this thesis is that of organic solar cells with an external light absorbing "antenna" layer. In this architecture, illustrated in Figure 1-5b, light is absorbed by the external antenna and subsequently transferred into the organic photovoltaic cell. By decoupling the optical and electrical functions of the cell, this new architecture has the potential to circumvent the tradeoff between light absorption and charge separation efficiency.

To study this architecture, we first model energy transfer mediated via surface plasmon polariton modes in the interfacial thin silver contact and via radiation into waveguide modes. We calculate the expected optical absorption in each layer of the device and then model energy transfer from the antenna layer into the active semiconducting layers. The model allows the study of the wavevector dependence of energy transfer from the antenna to the PV and the dipole coupling efficiency to each layer in the PV stack. The model is also used to optimize the thickness of layers throughout the device and predict the energy transfer efficiency.

Next, we experimentally demonstrate devices with external antennas. First, we demonstrate devices with single layer antennas with high photoluminescence efficiency achieving high energy transfer efficiencies. Next, we experimentally measure the energy transfer efficiency from an antenna layer to the PV active layers utilizing a strongly absorbing material that absorbs significant light near the device cathode. We

compare this measurement to the model described above. Finally, we demonstrate devices with strongly absorbing resonant cavity antennas resulting in increased device performance over specific regions of the solar spectrum. These results yield structural design criteria for this device architecture and allow us to describe ideal antenna material characteristics.

We also demonstrate the use of external antennas applied to conventional inorganic solar cells in luminescent solar concentrators (LSCs) in Appendix A [56, 57]. LSCs are planar waveguides with a thin-film organic coating on the face and inorganic solar cells attached to the edges. As in the organic PV devices discussed above, light is absorbed by the coating and re-emitted into waveguide modes for collection by the solar cells. We demonstrate optimized single-waveguide and tandem-waveguide luminescent solar concentrators with increased quantum efficiencies. We exploit near-field energy transfer, solid-state solvation, and phosphorescence to achieve increased concentration without the need for solar tracking.

1.6 Organic solar cells with interfacial layers

Second, we introduce a device architecture for organic solar cells that includes a thin interfacial layer between the donor and acceptor materials, illustrated in Figure 1-5c. The thin interfacial layer in this architecture creates a cascade energy structure at the exciton dissociation interface reducing recombination of separated charges. As introduced above, recombination of separated charges at the exciton dissociation interface in organic PVs represents a major loss mechanism. Devices with interfacial layers exhibit greater open-circuit voltages (V_{OC}) and short-circuit currents (J_{SC}) leading to higher power conversion efficiencies [58]. We describe an experimental study of charge collection efficiency in organic PVs using thin interfacial layers.

To study this architecture, we first fabricate devices exhibiting increased charge

separation efficiency due to the addition of an interfacial layer. Previous efforts to add an interfacial layer in organic PVs have suffered due to poor materials selection. We study how the energy level alignment of the interfacial layer impacts recombination and we develop criteria for optimal interface material design and selection.

Finally, we quantify the optimal thickness of the added interfacial layer by fabricating devices with a range of different interfacial layer thicknesses. Devices with too thin an interfacial layer demonstrate limited improvements in charge collection due to partial layer coverage. Devices with interfacial layers that are too thick suffer from carrier transport problems in the interfacial layers. Determining the optimal interfacial layer thickness gives greater insight into the physical mechanism of charge carrier recombination at the exciton dissociation interface in organic PVs.

1.7 Thesis roadmap

This chapter has given a brief background and context for the work described in this thesis. The energy industry is likely to face many new opportunities in the years ahead. The motivation for photovoltaic devices and recent progress towards their widespread adoption have been discussed. Finally, this chapter gave an introduction to organic photovoltaics and briefly introduced the two new device architectures that are the focus of this thesis.

Chapter 2 gives a brief overview of organic photovoltaics and details the mechanism of power generation in these devices. The two primary challenges limiting devices from achieving higher efficiencies: (1) the tradeoff between light absorption and exciton diffusion and (2) low open-circuit voltage due to charge transfer state recombination at the donor-acceptor interface are discussed. The chapter concludes with a description of previous efforts to overcome these challenges.

Chapter 3 discusses organic PVs with external light absorbing antennas. The

chapter first details the physics of surface plasmon polariton mediated energy transfer across a thin metal film. Devices with external light absorbing antennas are modeled to optimize energy transfer efficiency. The results of fabricating devices with single layer light absorbing antennas and resonant cavity antennas are discussed. Finally, the outlook for devices with external antennas is discussed.

Chapter 4 discusses organic PVs with a thin interfacial layer added between the donor and acceptor semiconductor layers. The physics of exciton dissociation and charge transfer state recombination are discussed. The chapter then describes the results of fabricating devices with interfacial layers. While interfacial layers are found to increase the efficiency of charge separation in some devices, the efficiency is unchanged in other devices. Several possible explanations are given for these results and the outlook for devices with interfacial layers is discussed.

Finally, Chapter 5 concludes and suggests future work.

Chapter 2

Organic Solar Cells

Organic semiconductor photovoltaics (PV) are a promising route to low-cost, scalable, emissions-free electricity generation [59]. Organic solar cells can theoretically achieve similar efficiencies to conventional inorganic photovoltaics [60]. Their compatibility with inexpensive manufacturing techniques makes organic semiconductor technology particularly attractive as a route to ubiquitous solar energy generation. However, achieving higher power conversion efficiencies is critical before organic photovoltaics can play a larger role in our future energy generation landscape.

Early organic photovoltaic cells were composed of a single organic semiconductor sandwiched between two metal electrodes with different work functions [61]. The rectification seen in these devices was due to the formation of a Schottky barrier between the organic layer and the metal contact with the lower work function [62]. However, these devices exhibited extremely poor power conversion efficiencies.

The introduction of the bi-layer heterojunction device architecture first demonstrated by Tang in 1986 was a major step forward [63]. Organic heterojunction devices are constructed from two distinct semiconducting layers placed between metal electrodes. The device structure is similar to inorganic semiconductor *pn*-junction solar cells. However, in inorganic devices the p and n layers are created by oppositely

doping two adjacent volumes of the same semiconductor. Organic heterojunction solar cells employ a different semiconducting material for each layer, one having good transport properties for holes (also known as a donor layer) and the other favoring the transport of electrons (also known as an acceptor layer).

Power conversion efficiencies of organic photovoltaic devices have been increasing steadily in recent years. A small-molecule organic solar cell was reported with an efficiency of 5.7% under 1 sun AM1.5G simulated solar radiation [64, 65]. Devices utilizing polymer materials have been demonstrated with power conversion efficiencies over 6% [34, 66]. It has been suggested that power conversion efficiencies could be achieved as high as 20% if the quantum efficiency of devices was improved across the visible spectrum [60]. Increasing the sensitivity of organic photovoltaics in the near-infrared could lead to even higher efficiencies.

In inorganic cells the electric field generated by the *pn*-junction acts to separate excited charge pairs [67]. In contrast, in organic photovoltaics the energy-level offset between the two different semiconductor materials is needed to dissociate excitons. This means that the power generation mechanism for organic cells is fundamentally different than those found in conventional inorganic devices.

The next section discusses the primary power conversion processes found in organic photovoltaics. Then, the primary barriers to higher efficiency are discussed. Finally, a brief overview is given of the methods that have previously been employed to overcome these challenges.

2.1 Mechanism of power conversion

The conversion of light into electrical power in organic photovoltaics occurs in four distinct steps as illustrated in Figure 2-1. The absorption of light in one of the semiconducting layers initiates the process. Optical absorption generates tightly bound,

charge-neutral hole and electron pairs referred to as excitons [68]. The weak intermolecular interactions and lack of long range order found in organic semiconductors gives rise to highly localized excitons [69]. In order to extract power from the device, the excitons must be separated into their constituent charges. The excitons diffuse throughout the layer where they originate via Förster energy transfer between molecules. If the excitons reach the interface between the donor and acceptor layers before they recombine they can dissociate into separate charges. The distance excitons travel before recombination is a material dependent parameter, quantified as the exciton diffusion length, L_D [36]. L_D is typically on the order of $10-50$ nm. Organic heterojunction PVs are designed such that the energy level offsets at the interface between the two semiconductors makes it energetically favorable for the charges to separate. Charge separation results in electrons being found in the lowest unoccupied molecular orbital (LUMO) of the electron transport layer and holes in the highest occupied molecular orbital (HOMO) of the hole transport layer. Finally, the separated charges diffuse toward the contacts to generate power [70]. The efficiency of each of these steps is discussed below.

2.2 Quantifying the performance of organic photovoltaics

The performance of organic solar cells is typically quantified in two ways. First, current density-voltage characteristics (J-V) are measured in the dark and under simulated solar illumination. Second, the external quantum efficiency (EQE) of devices, defined as the number of electrons flowing in the external circuit per photon incident on the PV cell, is measured under monochromatic illumination.

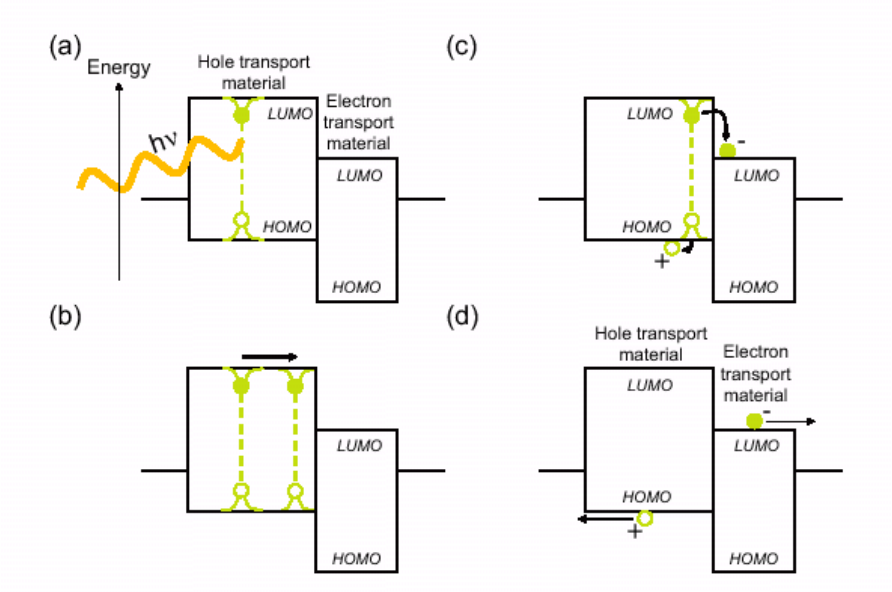

Figure 2-1: Summary of power conversion processes in organic photovoltaics. (a) Optical absorption in the semiconductor layers creates locally bound electron-hole pairs or excitons. (b) Excitons diffuse in the semiconducting layer. (c) Excitons reaching the interface between the acceptor and donor semiconductor layers before recombination are dissociated. (d) Separated electrons and holes diffuse to opposite electrodes. After Peumans *et al.* [70].

2.2.1 Current-voltage characteristics

Current density-voltage (J-V) characteristics reveal how solar cells would operate under actual solar illumination. The spectrum of the sun's radiation is close to that of a black body with a temperature of 5,800 K. While the intensity of actual solar radiation varies throughout the day, standard test conditions have been established to allow for consistent comparison of different solar cell devices. Standard test conditions correspond to a radiant intensity of 1000 W/m^2 with a spectral distribution defined as "AM1.5G" and a cell temperature of 25 °C.

As illustrated schematically in Figure 2-2, under illumination, the J-V curve for solar cells shifts into the fourth quadrant where power is generated (the product of current and voltage in this quadrant is negative). Solar cell J-V curves are typically parameterized using three values: the short-circuit current density (J_{SC}), the open-circuit voltage (V_{OC}), and the fill factor (FF). The FF corresponds to the ratio of the product of the current and voltage at the maximum power point to the product of J_{SC} and V_{OC}.

In organic solar cells, the three parameters described above are dependent on material selection and device architecture and vary widely. short-circuit current densities under 1 sun illumination vary widely based on materials selection and are typically directly proportional to the light intensity. Open-circuit voltages in organic solar cells range from approximately 0.3 V to over 1 V. Finally, a wide range of fill factors have been reported. However, state-of-the-art devices exhibit fill factors of approximately 0.6. As discussed below, the origin of the open-circuit voltage in organic solar cells is not well understood.

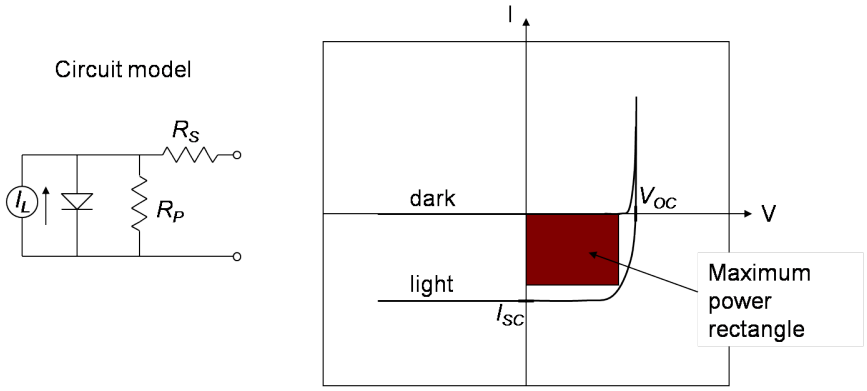

Figure 2-2: Solar cell equivalent circuit model and J-V curve schematic. (a) The equivalent circuit model for a solar cell consists of a parallel combination of a current source, a diode, and a parallel resistance in series with a series resistance. (b) The current density-voltage (J-V) curve of a solar cell. Solar cell performance is often parameterized using the short-circuit current density (J_{SC}), the open-circuit voltage (V_{OC}), and the fill factor. The shaded box corresponds to the power at the solar cell operating point. The fill factor corresponds to the ratio of the shaded area to the larger rectangle formed by the origin, the short-circuit current density, and the open-circuit voltage.

2.2.2 External quantum efficiency

The performance of organic solar cells is also quantified by the external quantum efficiency (EQE) of the cells. The EQE is defined as the number of electrons flowing in the external circuit per photon incident on the PV cell. The EQE is a function of the efficiency of each of the power generation steps described above:

$$\eta_{EQE} = \eta_{abs}\eta_{diff}\eta_{diss}\eta_{cc} \tag{2.1}$$

where η_{abs} is the efficiency of photon absorption leading to creation of an exciton, η_{diff} is the efficiency of exciton diffusion to the donor-acceptor interface, η_{diss} is the efficiency of the dissociation of excitons that reach the interface, and η_{cc} is the efficiency with which separated charges are collected at the electrodes.

The efficiency of each of the individual processes listed above is dependent on device structure and material selection. For example, η_{abs} depends on the absorption

coefficient of the semiconductor materials and the thickness of the layers. Thicker device layers typically lead to higher absorption efficiency. However, η_{diff} is also dependent on layer thickness and decreases as the thickness of the semiconductor layers is increased. The trade-off between η_{abs} and η_{diff} is discussed in more detail below. As will be discussed in detail in Chapter 4, the specific mechanism of exciton dissociation is currently subject to debate. However, the device architecture demonstrated in Chapter 4 illustrates that η_{diss} can be enhanced via device structure modifications. Finally, the efficiency of charge collection, η_{cc}, is believed to be near 100% in most practical devices.

2.3 Primary challenges limiting device efficiency

Organic photovoltaics are currently limited by two primary challenges: (1) a trade-off between light absorption and exciton diffusion and (2) low open-circuit voltage due to charge recombination at the donor-acceptor interface.

First, electronic localization in organic semiconductors yields structured optical absorption spectra with pronounced regions of weak absorption; η_{abs} is not uniform across the solar spectrum. Increasing the thickness of the active semiconducting layers improves absorption in these weakly absorbing regions of the solar spectrum. However, as layer thicknesses are increased, photogenerated excitons must travel farther to the charge separation interface. Exciton diffusion lengths, L_D, for organic materials are typically on the order of 10-50 nm. This is much shorter than typical optical absorption lengths ($(1/\alpha) \approx$ 50-100 nm). Thus, despite being composed of highly absorptive organic materials with absorption coefficients exceeding 10^{-5} cm^{-1}, organic PV cells are limited by the amount of light they can absorb. Only the light absorbed near the interface between the active layers contributes to generated power. The absorption efficiency and exciton diffusion efficiency in conventional organic solar

cells are coupled, opposing quantities; increasing absorption by increasing the device thickness leads to a decrease in exciton diffusion efficiency and vice versa.

Second, organic semiconductor solar cells exhibit low V_{OC}. The V_{OC} observed in organic photovoltaic devices is significantly less than the lowest energy absorbed photon (the optical gap of the materials) divided by the elementary charge q. The low V_{OC} represents a major efficiency loss in these devices. While there is some debate about the origin of V_{OC}, it is becoming increasingly clear that recombination of separated charges at the exciton dissociation interface reduces the open-circuit voltage and represents a major loss mechanism [42]. Immediately following exciton dissociation at the donor-acceptor interface a charge transfer (CT) state is formed that consists of the electron on an acceptor molecule and the hole on a donor molecule. Unfortunately, these two carriers are still partially bound in the CT state. Efficient separation of the charge transfer state is required for higher open-circuit voltage and efficient power generation.

2.4 Overcoming the light absorption and exciton diffusion trade-off

The trade-off between exciton diffusion efficiency and optical absorption drives a great deal of the current research in organic photovoltaics. Previous efforts to overcome this trade-off have primarily employed one of two main strategies. First, new device architectures have been demonstrated that employ increased surface areas for exciton dissociation. Second, an array of strategies have been demonstrated to trap light in organic PV devices more effectively. Some of the most relevant results are briefly described in the next sections.

2.4.1 Increasing the surface area for exciton dissociation

Several classes of organic solar cells have emerged to address the trade-off between light absorption and exciton diffusion including bulk heterojunction cells and multiple junction tandem photovoltaics. These architectures increase the surface area of the exciton dissociation interface, thereby decreasing the distance between exciton generation and dissociation and enabling the use of thicker, more absorptive organic films.

Bulk heterojunction solar cells. Bulk heterojunction organic photovoltaic cells were first demonstrated using blends of donor and acceptor semiconducting polymers [71]. Upon deposition (usually via spin coating) and subsequent solvent evaporation, the polymers have been shown to partially phase separate forming an interpenetrating network [72]. This vastly increases the interfacial surface area between the materials, decreasing the average distance between exciton generation and dissociation.

Bulk heterojunctions are limited by the necessity for continuous pathways within the two phases for charge collection at each electrode. Disorder in the exciton dissociation region can hinder charge collection and limit performance. Reduced charge carrier mobilities due to intermixing on the molecular level can lead to recombination of separated charges. Nonetheless, this technique has led to significant improvements in the efficiency of polymer devices with internal quantum efficiencies demonstrated as high as 100% at some wavelengths and power conversion efficiences as high as 6.1% under 1 sun, AM1.5 solar illumination [66]. Efforts at improving polymer bulk heterojunction cells have included optimizing the relative concentrations of each polymer in solution as well as the exploration of postproduction treatments such as annealing.

The bulk heterojunction concept has also been demonstrated in cells utilizing co-evaporated small molecule organic materials [73]. However, simply co-depositing the two materials leads to devices with very poor charge collection as the materials do not

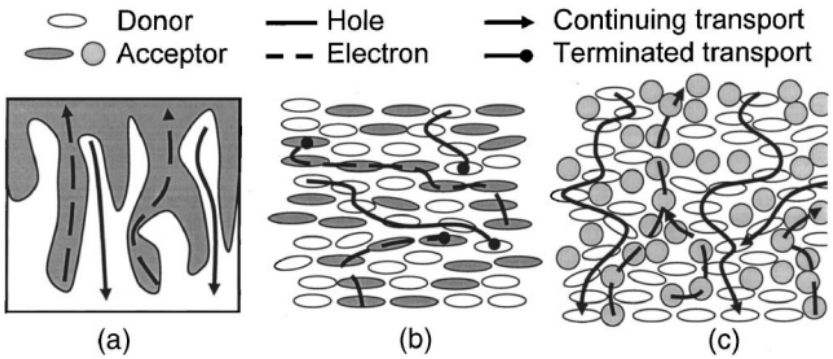

Figure 2-3: Conduction in bulk heterojunction devices. (a) Idealized interdigitated structure of donor and acceptor layers with lateral feature sizes no larger than the exciton diffusion lengths in both materials. (b) Poorly structured mixing of donor and acceptor molecules with few continuous pathways for hole and electron conduction. Devices with this structure would suffer from trapping and recombination. (c) Improved mixing conditions with continuous pathways for hole and electron conduction after exciton dissociation. After Xue *et al.* [65].

readily phase separate, as illustrated in Fig 2-3. Increasing the substrate temperature during growth leads to phase separation and crystalline domains. However, increasing the substrate temperature also yields rougher films that suffer from pinholes, resulting in lower device yields.

An extension of the bulk heterojunction cell architecture for co-evaporated small molecules have been referred to as hybrid planar-mixed heterojunctions (PM-HJ) and organic *p-i-n* solar cells [74, 65, 75]. In these devices, co-deposited mixed layers of organic semiconducting materials are sandwiched between films of hole and electron transport materials. The mixed layer increases the surface area of the interface allowing more light to be absorbed while the sandwich films assist in charge collection.

Multiple junction (tandem) devices. Devices with multiple, stacked heterojunctions have also been demonstrated [76]. In these devices, thin semi-transparent heterojunctions were constructed in layers separated by extremely thin, discontinuous layers of silver clusters. The Ag clusters serve as charge recombination sites for un-

paired charges generated in the interior of the device. In the design of these so-called "tandem cells," the optical absorption of each individual heterojunction must be balanced so that the photocurrent from each heterojunction is approximately equal. In principle, each heterojunction can be designed to absorb a separate part of the solar spectrum. This is especially attractive as most materials only absorb strongly over a narrow range of wavelengths. In addition, stacking the cells has the effect of significantly increasing the open-circuit voltage for the devices. The total open-circuit voltage is the sum of the built-in voltages of each individual cell.

Initial demonstrations of tandem cells resulted in power conversion efficiencies nearly double those using single heterojunctions with the same materials [76]. Subsequent efforts stacking hybrid planar-mixed heterojunctions have resulted in the demonstration of cells with power conversion efficiencies as high as 5.7% [64, 65]. The fabrication of polymer-based tandem cells is complicated by the need to spin coat multiple layers; the lower layers in the cells can be destroyed by the solvent used in subsequent layer depositions. Nonetheless, working polymer stacked structure devices have recently been demonstrated with power conversion efficiencies over 6% [34].

2.4.2 Enhanced light trapping strategies

Another strategy to overcome the trade-off between light absorption and exciton diffusion is to employ strategies to trap light in PV devices more effectively. This has been accomplished by modeling optical field intensities within devices [77, 78], by using diffraction gratings [79, 80, 81], and by utilizing the field enhancing properties of metal nanoclusters [82, 83].

Optical modeling. Modeling the optical interference in devices has been used to increase the light absorbed in organic PV structures while making only minor changes

to layer thicknesses [77]. The generation of excitons at a given position in a device is dependent on the optical electric field intensity at that position. Reflections at each interface in the device modify the electric field distribution. The reflection and transmission coefficients at each layer can be determined numerically, using matrix methods and the optical constants of each material. These values can then be used to determine the location of optical electric field intensity maxima. To maximize device efficiency, the maxima in the field intensities should be centered on the charge separation interface.

Figure 2-4, from Pettersson *et al.* [84], illustrates this method of optimizing layer thicknesses. The PV devices illustrated are composed of the same materials but in the top structure the electric field intensity is at a maximum at the charge separation interface between PEOPT and C_{60} whereas in the bottom structure there is minimal field intensity and, therefore, minimal absorption in the vicinity of the interface.

Furthermore, optical interference modeling has been used to predict the wavelength resolved photocurrent or action spectra of devices [78]. Comparisons of the predicted and experimental photocurrents have been used to estimate the diffusion coefficients of various materials [84].

Diffraction Gratings and Buried Nanoelectrodes. The use of diffractive optical structures built into devices has also been explored as a means of increasing light absorption. Several different implementations have been demonstrated. In one, a soft embossed grating was built into an active layer polymer [79]. The structure was designed to diffract incident light into guided modes in the thin polymer film. In other attempts, a comb-like array of electrodes embedded in a polymer were used. As shown in Figure 2-5 the structure of the electrodes was designed to diffract the incoming light, producing an absorption maximum in the active layer [80].

A similar effort enhanced light absorption by fabricating solar cells on structured

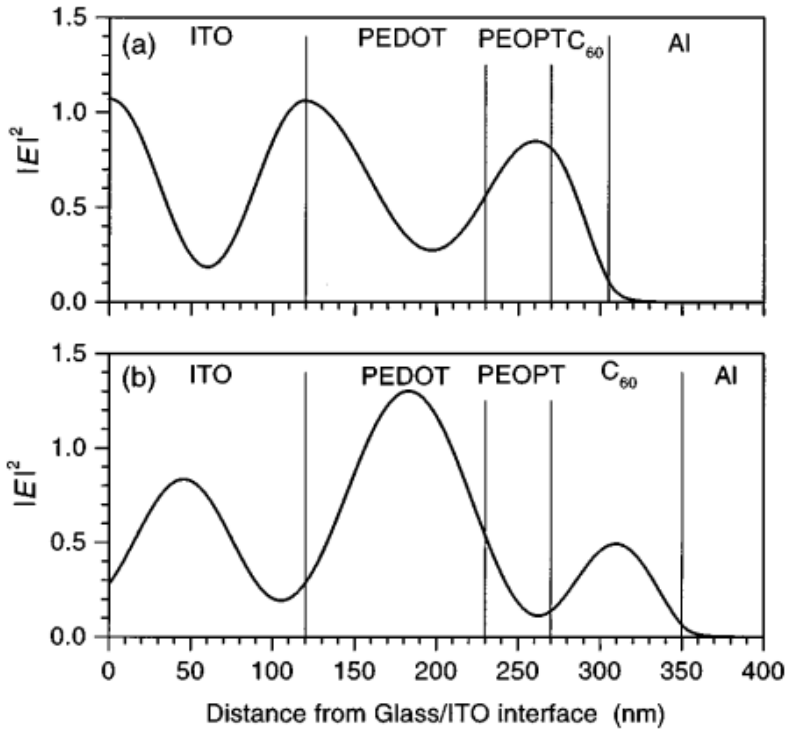

Figure 2-4: Optical field intensity modeling in organic photovoltaics. (a) The layer thicknesses in this device result in an optical field maximum at the interface between the active PEOPT and C_{60} semiconductor layers. Locating the interference maximum at this point improves the efficiency of the device. (b) Devices with a slightly thicker C_{60} layer have a minimum in the optical field located at the charge separation interface. After, Pettersson *et al.* [84].

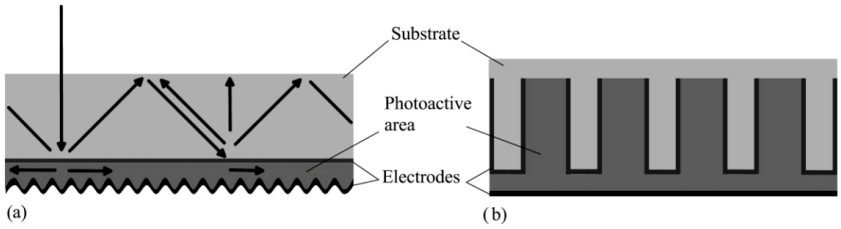

Figure 2-5: Schematic illustrations of two light trapping device architectures. (a) Patterning the electrode to form a diffraction grating is one method that has been employed to trap incident light in organic PV structures. The arrows represent theoretical pathways taken by the incident light in this structure. (b) Buried nanoelectrodes have also been used to increase the interaction distance between light and the organic PV active semiconductors. After Niggemann *et al.* [80].

substrates [81]. The substrate was structured to act as a prism reflecting the light through the active layers of the solar cell multiple times. Significant optical modeling is still needed to design optimized diffraction gratings and/or substrate shapes. This approach shows great potential as a way to separate the optical and electrical components of solar cells. However, typically structures can only be optimized for a single wavelength of incident light. The efficiency of these structures also depends on the angle of incidence of the solar radiation. Therefore, in practical applications, these devices would likely need to track the movement of the sun throughout the sky. However, the design of the diffraction gratings and substrate shapes is essentially independent of the layer thicknesses used in the actual conversion of light energy to electrical power. The solar cell can be designed first, and a diffraction grating optimized for that cell could be designed subsequently.

Metal Nanoclusters. Incorporating metal nanoclusters in devices has also been used as a method to increase the efficiency of organic photovoltaics. Several theories have been proposed to explain the increase in photocurrent observed when metal nanoparticles are added to a semiconducting layer. One theory proposes that the electric field is strengthened in the vicinity of the metal nanoclusters. The strength-

ened electric field increases absorption in the surrounding organic material leading to a greater photocurrent [85]. Alternatively, exciton plasmon modes in the metal clusters themselves could emit an electron leading to increased current [86].

Metal nanoclusters have been incorporated in many of the device architectures discussed above including dye-sensitized cells [82] and tandem cells where silver nanoclusters were used in between heterojunctions [83]. In this final demonstration the optical field close to the nanoclusters was found to have increased by up to a factor of 100 compared with the incident light intensity. While metal nanoclusters have yielded significant increases in field intensity, the nanoclusters are also a source of loss. Excitations can energy transfer to plasmon modes in the metal particles where they are likely dissipated and lost.

2.5 Achieving higher open-circuit voltages

The open-circuit voltage in organic PVs is also a major focus of current research efforts. There have been several reports attempting to empirically determine the origin of the open-circuit voltage. Others have attempted to derive models for the operation of devices from first principles.

It is generally accepted that the open-circuit voltage is in part determined by the energy levels of the donor and acceptor semiconductor layers. Several experimental studies have confirmed that the material energy levels play a role. A direct correlation between acceptor strength and open-circuit voltage in poly(*para*-phenylene vinylene) (MDMO-PPV)-based polymer/fullerene solar cells was reported [87, 88]. Similarly, the photovoltage in polythiophene-based polymer/fullerene solar cells was found to vary with oxidation potential of the donor conjugated polymer [89]. A study of 26 different bulk-heterojunction devices in the literature also indicated a linear relationship between the highest occupied molecular orbital (HOMO) of the polymer and the

V_{OC} [90]. These observations were used to increase the open-circuit voltage in solar cells based on poly(3-hexylthiophene) (P3HT) donor and a zinc oxide acceptor [91]. Tuning the band offset by substituting magnesium into the zinc oxide acceptor was found to result in an increase in the open-circuit voltage from 500 mV to 900 mV.

The work function of the contacts has also been observed to have an impact on the open-circuit voltage in some organic solar cells. For example, decreasing the work function of the polymeric contact material poly(3,4-ethylenedioxythiophene) (PEDOT) doped with poly-(styrenesulfonate) (PSS) was observed to decrease the open-circuit voltage in organic photovoltaics based on [6,6]-phenyl C_{61}-butyric acid methyl ester (PCBM) and poly(2-methoxy-5-(3',7'-dimethyloctyloxy)-*para*-phenylene (MDMO-PPV) [92]. The V_{OC} was also varied in small molecule organic photovoltaics by chemically modifying the work function of the indium tin oxide anode [93]. However, the contact work functions do not always impact the open-circuit voltage due to Fermi level pinning between the contacts and the organic semiconductor layers [94].

A numerical model was developed to predict the current-voltage curves of bilayer conjugated polymer photovoltaic devices accounting for charge photogeneration, charge transfer state recombination, drift and diffusion currents, and the injection and extraction of carriers at the electrodes [95]. The model suggested that the quantum efficiency of devices is primarily determined by a competition between charge pair dissociation and recombination. It was suggested that the charge pair dissociation rate is field dependent. The model indicated that the open-circuit voltage is primarily determined by the balancing of drift and diffusion currents. Consideration of space charge effects and electric field-induced drift current were needed to accurately predict the intensity dependence of open-circuit voltage.

Given that the open-circuit voltage is determined by a balancing of drift and diffusion currents, it is expected that the open-circuit voltage would depend on the rate of charge transfer state dissociation. Reducing recombination at the donor-

acceptor interface will increase carrier generation at that interface. This, in turn, would lead to an increase in the diffusion current, requiring a larger offsetting drift current at open-circuit. Therefore, the open-circuit voltage should increase when recombination is suppressed at the donor-acceptor interface.

Another model for the operation of molecular photovoltaic devices was developed by Nelson and colleagues [96, 97, 98]. Molecular PVs are model as a two-level system, connected to external contacts by chains of one or more charge transporting orbitals. The model captures the excitation of electrons by photon absorption using a generalized Planck equation and models electron transfer using Marcus theory [99]. Marcus theory is described in more detail in Chapter 4. The model finds that the current-voltage characteristics in organic PVs are dominated by the structure of the donor-acceptor interface including molecular sizes, orbital energy levels, and electron transfer rates. The model successfully reproduced a number of commonly observed features in current-voltage characteristics including a "kink" in the current-voltage curve close to open-circuit that is often observed when using materials with low mobilities. The model indicates that the open-circuit voltage is dominated by the acceptor-donor energy gap when recombination is important, and by the optical gap at which photon absorption occurs when recombination is insignificant. As in the earlier model, the open-circuit voltage is predicted to be a function of charge transfer state recombination at the donor-acceptor interface.

Greenham and colleagues have also developed a model to explain current-voltage characteristics in organic solar cells [100]. They found that by subtracting out the dark current, they were able to explain the intensity-dependent characteristics of the J-V curve. They argue that the open-circuit voltage should be understood as the voltage at which the opposite dark and light current contributions balance. By studying the light intensity and voltage dependence of these currents, they identified geminate recombination at the donor-acceptor interface as the dominant loss mechanism in

organic solar cells. Further, they measured the field dependence of this recombination and found it to be material dependent. In agreement with the earlier models, they find that open-circuit voltages in organic solar cells are limited by recombination at the donor-acceptor interface. They suggest that the primary route to improved photovoltaic materials is enhanced charge delocalization.

Starting from the Poisson equation and the basic continuity equations of holes and electrons, another group derived an analytical expression for the open-circuit voltage in organic planar heterojunction solar cells [101]. The model agrees that the V_{OC} is determined primarily by the diffusion of current away from the donor acceptor interface. The model is used to calculate the resistance at V_{OC} which in turn determines the fill factor. The slope of the illumination dependence of V_{OC} is used in the model to determine the dominant recombination mechanism. The model indicates that recombination in organic solar cells is dominated by geminate recombination at the donor-acceptor interface, consistent with the earlier studies.

The influence of the offset energies at the donor-acceptor interface on the open-circuit voltage was recently studied experimentally by measuring the maximum attainable value of V_{OC} for a range of donor-acceptor material pairs [102]. Maximum V_{OC} values were obtained for 14 different combinations of donor and acceptor materials by either reducing the temperature or increasing the light intensity until V_{OC} reached saturation. The maximum V_{OC} values were found to vary linearly with the interface offset energy and agreed well with an adapted version of the model formulated by Nelson [96, 97, 98]. It was suggested that many devices do not exhibit their maximum attainable V_{OC} at room temperature and 1 sun illumination due to recombination and high dark current. These results indicate that a high V_{OC} can be attained by increasing the energy offset between the donor and acceptor layers since large energy offsets result in lower dark current. However, large energy offsets can also inhibit electron transfer resulting in a reduction in J_{SC}. The results indicate a

trade-off may exist between V_{OC} and J_{SC}.

The importance of the device saturation dark current density (J_S) in determining the open-circuit voltage has also been discussed [103]. A series of devices were fabricated with different donor materials. The different donor materials exhibit varying intermolecular interaction strengths with fullerene acceptor materials. It was demonstrated that the V_{OC} values in organic photovoltaics show a strong inverse correlation with J_S. The intermolecular interactions between donor and acceptor molecules at the interface impacts the rate of exciton dissociation and charge transfer state recombination. Therefore, these interactions also impact V_{OC}.

While the details of each of the models described above differ, they all reach similar conclusions. The efforts to understand the origin of open-circuit voltage in organic solar cells via modeling agree that open-circuit voltage is at least partially dependent on charge transfer state recombination at the donor-acceptor interface. Reducing recombination is expected to increase the open-circuit voltage.

2.6 Conclusion

This chapter introduced organic photovoltaic devices and discussed the primary challenges limiting their efficiency. Organic photovoltaics have the potential to become an important electricity generation technology. Their compatibility with inexpensive, large-area manufacturing techniques makes them a particularly attractive solar cell technology. Inorganic thin film solar cells utilizing many of the same manufacturing technologies have rapidly achieved commercial scale in recent years. In order to successfully compete with conventional solar cell technologies (including thin film inorganic devices) and other electricity generation technologies, higher power efficiencies in organic solar cells must be achieved.

The power conversion efficiencies of organic photovoltaic devices have been lim-

ited by two primary challenges: (1) a trade-off between light absorption and exciton diffusion and (2) low open-circuit voltage due to charge recombination at the donor-acceptor interface. While several device structures have been demonstrated previously that successfully increase both the light absorption and exciton diffusion efficiencies, additional improvements are still needed. The origin of the open-circuit voltage in organic photovoltaics has been a subject of debate. Previous efforts to explain the origin of open-circuit voltage have been discussed above.

The next two chapters discuss two new device architectures that aim to overcome the challenges discussed above. Chapter 3 discusses organic PVs with an external light absorbing antenna. The anntenna in this device architecture decouples photon absorption and exciton dissociation in this device architecture; allowing these two processes to be optimized indepedently. Chapter 4 discusses organic PVs with a thin interfacial layer sandwiched between the donor and acceptor layers. The thin interfacial layer in this architecture creates a cascade energy structure at the exciton dissociation interface that reduces recombination at the donor-acceptor interface.

Chapter 3

Organic Solar Cells with External Antennas

This chapter discusses the design and optimization of organic photovoltaics (PVs) with an external light absorbing antenna. First, the device architecture is introduced. Next, we discuss the physics of energy transfer across a thin metal film, as illustrated in Figure 3-1a. We then formulate and solve a model that allows the calculation of the energy transfer efficiency in multilayer organic PV devices. The model gives insights into the ideal antenna material and antenna thickness. Next, we experimentally demonstrate several different antenna systems with varying characteristics. We fabricate devices with external antenna layers, illustrated in Figure 3-1b, and devices with resonant cavity antennas, illustrated in Figure 3-1c. Finally, the potential implications of these results and the future outlook of this device architecture are discussed.

3.1 Device architecture

As described in Chapter 2, the efficiency of organic photovoltaic devices is limited by a tradeoff between light absorption and exciton diffusion [104]. Overcoming this

tradeoff is critical to achieving high device efficiencies. Photosynthesis in plants and bacteria provide an example of how one might be able to overcome this bottleneck in organic solar cells. In photosynthesis, light absorption and exciton dissociation occur in distinct structures [49], as was discussed in Chapter 1 and illustrated in Figure 1-6. Incident solar radiation is first absorbed in light harvesting antenna complexes. The generated excitons are then exothermically guided to a different protein structure known as a reaction center. Exciton dissociation occurs in the reaction center.

In contrast to the energy transduction process in photosynthesis, in conventional organic photovoltaics the organic semiconductors must both absorb light and promote efficient charge extraction. The multiple roles required of the semiconductor layers in conventional organic solar cells significantly restricts the range of materials that can be deployed. The materials must possess a number of important characteristics including: (1) strong optical absorption capturing as much of the solar spectrum as possible, (2) efficient exciton transport throughout the bulk of the material, (3) optimal energy level alignment relative to the other semiconductor material used to allow for efficient exciton dissociation, and (4) sufficient charge carrier mobilities to allow efficient charge collection at the electrodes.

Taking the example of photosynthesis, we describe here a device architecture that decouples light absorption and exciton diffusion in organic PV via the addition of a light absorbing "antenna" external to the conventional charge generating layers, as illustrated in Figure 3-1b. As in photosynthesis, the charge generating semiconductor layers can absorb photons on their own, but they do not need to do it particularly well, as they are fed by an external antenna layer.

In this device architecture, energy transduction begins with photon absorption in the "antenna" layer. Radiation absorbed by the antenna is transferred into the charge generating layers via guided energy transfer across the thin metal cathode of the devices. Energy can be transferred radiatively into waveguide modes or non-

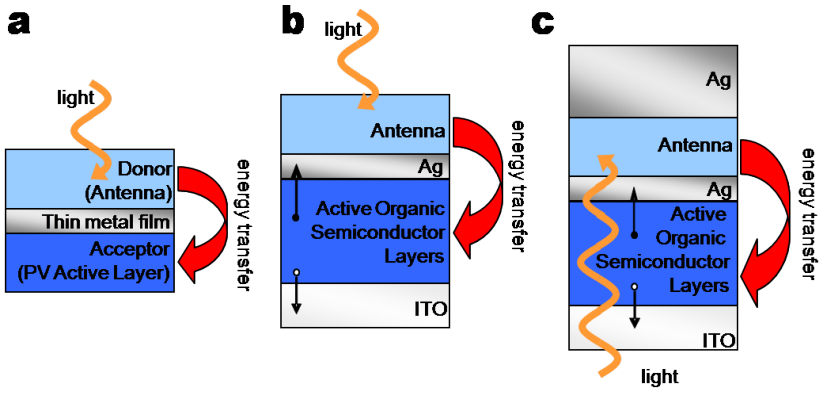

Figure 3-1: Organic photovoltaic devices with external antennas. (a) Conceptual schematic of energy transfer across a thin metal film, the critical physical process employed by this device architecture. (b) Schematic of the same energy transfer process being utilized by an organic photovoltaic cell with an external antenna. Energy absorbed in the antenna is transferred across the cathode to the photovoltaic active layers generating an exciton. The charges are then separated by the photovoltaic cell and collected at the electrodes. (c) Schematic of an organic PV with a resonant cavity antenna. The resonant cavity increases antenna absorption within the range where energy transfer is most efficient.

radiatively via surface plasmon polariton (SPP) modes in the interfacial thin silver contact. A particularly attractive feature of both of these guided mode energy transfer mechanisms is their propagation in the plane of the device, parallel to the exciton dissociation interface in the underlying organic solar cells. The dimensions of organic solar cells in this direction are on the order of 10^{-2} m, several orders longer than the thickness of the devices, on the order of 10^{-7} m. By redirecting the perpendicular solar radiation into parallel guided modes, the interaction distance between the incident radiation and the charge generating layers is significantly increased. The interaction distance is limited only by the distance that these modes travel at visible frequencies, typically several orders of magnitude longer than the thickness of the device. The large interaction distance between these modes and the PV layers results in efficient absorption of the guided radiation in the active semiconducting layers of the solar cell.

Once the energy is transferred to the charge generating layers, the energy trans-

duction process proceeds as in conventional organic solar cells; the excitons diffuse to the donor-acceptor interface where they are dissociated followed by collection of the free charges at the electrodes. By relying on the external antenna to absorb light, this new architecture has the potential to eliminate the tradeoff found in conventional organic solar cells between light absorption and exciton diffusion.

The architecture has several attractive features:

(1) Unlike the absorbing materials in conventional organic solar cells, the light absorbing materials in the antenna are not required to transport charge. New classes of materials may be deployed that have superior overlap with the solar spectrum. We will find below that ideal antenna materials will be optically active materials possessing both strong absorption and a high efficiency for photoluminescence (PL). A wide range of candidate materials possess these characteristics including strongly absorbing J-aggregate dyes, nanometallic particles, and quantum dots. Quantum dots and nanometallic particles have been utilized previously in the active layer of organic solar cells to increase absorption [83, 105]. However, their poor charge transport characteristics yielded poor device performance in these earlier efforts. It might also be possible to use photosynthetic antenna complexes such as phycobilisomes from cyanobacteria and red algae. Multiple materials can also be combined in the antenna to ensure broad overlap with the solar spectrum without degrading the electrical performance of the devices.

(2) Decoupling the light absorption and exciton diffusion in this architecture allows the charge separating PV cell to be optimized at a single peak wavelength corresponding to emission from the antenna. The charge generating layers no longer need to posess broad solar spectrum overlap. Materials can instead be selected primarily based on their electrical performance.

(3) Since the PV charge generating layers are not the only layers absorbing light, their thickness can be significantly reduced. The thickness of the charge generating

layers can be reduced to less than the exciton diffusion length, L_D, ensuring that all excitons are generated close to the donor-acceptor interface. With thin charge generating layers, the efficiency of exciton dissociation should approach unity [106]. Thin charge generating layers also ensure highly efficient charge collection.

External antennas require energy transfer across a thin metal contact, illustrated schematically in Figure 3-1a. Recently Andrew and Barnes investigated energy transfer from donor molecules to acceptor molecules on opposite sides of a metal film [107]. By exciting molecules on one side of the metal film and measuring photoluminescence from the film on the opposite side, they observed direct transfer of excitation energy between the molecules. Coupling was observed for metal films as thick as 120 nm. The energy transfer occurred primarily via surface plasmon polariton modes at the interfaces between the metal film and each dielectric material. We seek to use the same energy transfer mechanism in organic PVs with an external antenna.

The technical feasibility of this architecture depends on the efficiency of the energy transfer process. To assess the potential efficiency of the energy transfer process, we must first understand the physics of SPP energy transfer and SPP mediated energy transfer. Therefore, we proceed with a discussion of the physics of SPPs.

3.2 Physics of surface plasmon polariton energy transfer

Surface plasmon polaritons (SPPs) are a unique class of waves that exist at interfaces between a material with a positive dielectric constant and a material with a negative dielectric constant. They are most often studied at the interface between a dielectric (positive dielectric constant) and metal (negative dielectric constant). SPPs are comprised of a coupled oscillation of an electromagnetic field and surface charges at the interface between the two materials. The waves can propagate long

distances, often 1-10 μm, along the interface with a maximum field strength localized at the interface. The ability for SPPs to propagate over long distances makes them a particularly attractive energy transfer mechanism from the antenna to the charge generating layers in the architecture discussed in this chapter. The character of SPPs depends strongly on the characteristics of both the metal and dielectric material. The complex dielectric function of the dielectric material and the roughness of the metal determine the specific nature of SPPs at a given interface. The ability to control the structure of metals on the nanometer scale has recently generated significant interest in the application of SPPs to a wide range of fields including optics, sensors, medical imaging, microscopy, and data storage [108].

The existence of SPPs can be straightforwardly derived from Maxwell's equations with the application of appropriate boundary conditions. They are transverse magnetic in character. The existence of surface charge requires an electric field normal to the surface while propagation along the interface also requires an electric field in the propagation direction as illustrated in Figure 3-2a. The fields decay exponentially normal to the surface into both of the adjacent media, as illustrated in Figure 3-2b. The decay length in the metal is the classical skin depth. The bound, evanescent nature of the excitation restricts power from propagating away from the interface. However, the waves can propagate long distances along the interface because the modes are non-radiative.

The electromagnetic field of SPPs excite electron-hole pairs at the Fermi level of the metal. These electron-hole pairs subsequently relax producing phonons. Ultimately, SPPs are damped by electron-phonon collisions in the metal film. The propagation length of SPPs on a metal dielectric interface is given by [110]:

$$\delta_{SPP} = \frac{c}{\omega}\left(\frac{\epsilon_m + \epsilon_d}{\epsilon_m \epsilon_d}\right)^{3/2} \frac{(\epsilon_m)^2}{\epsilon_m} \tag{3.1}$$

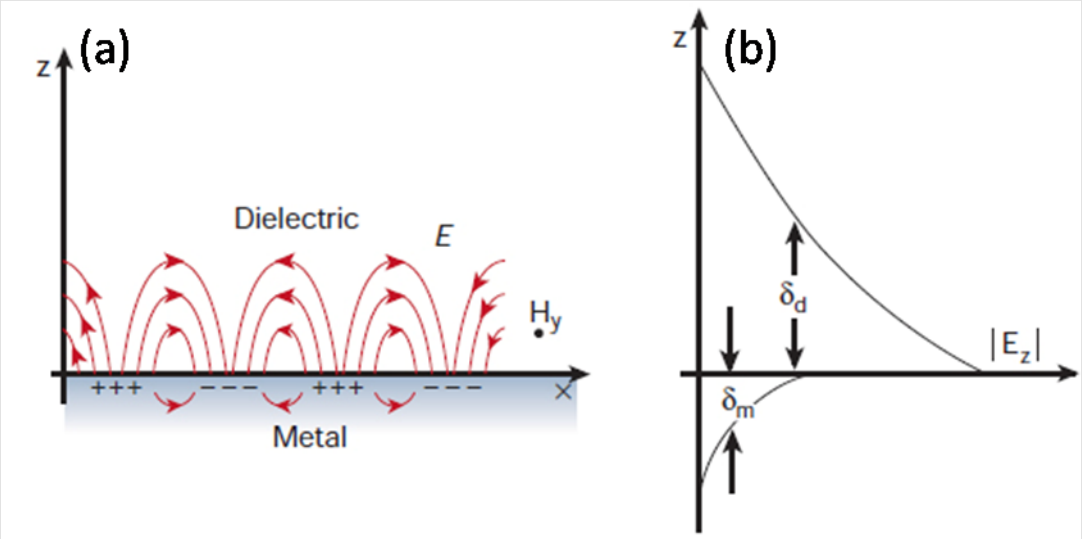

Figure 3-2: Surface plasmon polaritons (SPPs). (a) SPPs are transverse magnetic in character. SPPs are evanescent waves located at the interface between a material with a positive dielectric constant and a material with a negative dielectric constant (such as a metal). The existence of surface charge requires an electric field normal to the surface while propagation along the interface requires an electric field parallel to the surface. After Barnes *et al.* [109]. (b) The electric field associated with SPPs decays with the classical skin depth in the metal layer. The field also decays exponentially in the dielectric.

where ϵ_d and ϵ_m are the permittivities of the dielectric and metal layers, respectively.

For visible wavelengths, the internal damping of SPPs is least for the noble metals making silver an ideal contact metal to use on our devices. The propagation lengths for SPPs at a silver-air interface are typically tens of microns for visible wavelengths. The propagation lengths will be reduced at silver-dielectric interfaces and are reduced by silver roughness. However, we expect propagation distances of greater than 1 μm in our devices.

The frequency, ω, of SPP longitudinal oscillations is tied to the SPPs' in-plane wave vector magnitude, k_x, by the dispersion relation $\omega(k_x)$, described by:

$$\omega = ck_x \left(\frac{\epsilon_m \epsilon_d}{\epsilon_m + \epsilon_d} \right)^{-1/2} \tag{3.2}$$

This relation is plotted qualitatively in Figure 3-3. For comparison, the dispersion for photons in the dielectric medium and for a plasma oscillation in a free electron gas are plotted. The dispersion for photons in a dielectric are given by:

$$\omega_{photon} = \frac{ck_{photon}}{n_d} \tag{3.3}$$

where k_d is the photon wavevector and n_d is the refractive index of the dielectric medium. The dispersion for a plasma oscillation in a free electron gas is given by:

$$\omega_{plasma} = \left(\frac{\omega_p^2}{1 + \epsilon_d} \right)^{1/2} \tag{3.4}$$

where ω_p is the plasma frequency. The dispersion for plasma oscillations are independent of wave vector and thus appear as a horizontal line in Figure 3-3.

The polaritonic nature of SPPs is clearly illustrated in Figure 3-3; at low frequencies the SPP dispersion approaches that of photons in the dielectric material while at

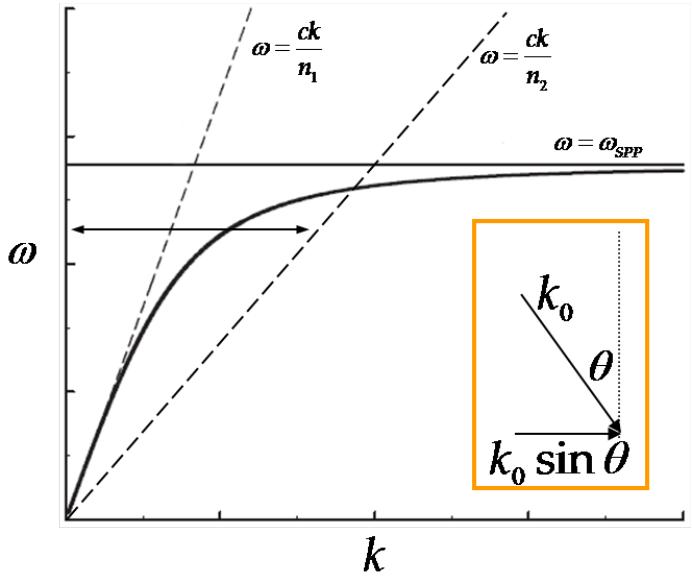

Figure 3-3: Dispersion relation for surface plasmon polaritons. The polaritonic nature of SPPs gives them hybrid characteristics between photons and bulk plasmons. However, in-plane momentum ($k_0 \sin\theta$) and energy must be conserved for coupling to occur. The dispersion relation for SPPs does not intersect that of the photon or plasmon. Therefore, conservation of in-plane momentum and energy are not possible and direct coupling does not occur. However, photons in a higher index medium (n_2) exhibit dispersion that does intersect that of the SPP so coupling is possible. The angle of incidence θ can be varied to match the in-plane momentum of the SPP and achieve coupling.

very high frequencies the SPP has the character of a plasma oscillation independent of wave vector. At low frequencies, additional momentum associated with the oscillating electrons in an SPP moves the dispersion to the right of the photon dispersion. Likewise, at high frequencies, the magnitude of electron oscillations in an SPP is always less than that of a pure plasma wave. The SPP dispersion does not intersect the dispersion for photons in the dielectric or the plasmon dispersion. Therefore, since energy and in-plane momentum must be conserved to scatter energy between SPPs and either photons or plasmons, it is impossible to scatter between an SPP and either a photon or plasmon without other interactions.

This explains why it is impossible to directly excite a plasmon from air. However, as suggested by the second photon dispersion line with a higher index of refraction in Figure 3-3, it is possible to excite SPPs using an alternative experimental configuration known as the Kretschmann geometry [111]. In this geometry, a layer of another dielectric medium with a higher index of refraction is placed adjacent to the metal/dielectric pair where the SPP is supported. This is illustrated in Figure 3-4 where the second dielectric has been placed on the opposite side of the metal film. Light in the dielectric with the higher index of refraction can couple to the SPP mode under the condition of total internal reflection, where an evanescent photon permeates the multilayered structure. For a given energy, or ω, one can adjust the angle of incidence in the second dielectric medium to access all of the wave vectors to the left of the second photon line in Figure 3-3. Where the dispersion relations intersect, the system is in plasmon resonance and energy can be coupled between the two states.

The discussion above yields an important conclusion. For a given wavelength it is only possible for photons with a specific angle of incidence to excite plasmons. This does not appear very practical for solar cells. However, for the device architecture described in this chapter we are primarily interested in coupling between excitons in the antenna layer and plasmons. Exciton-plasmon coupling is similar to that between

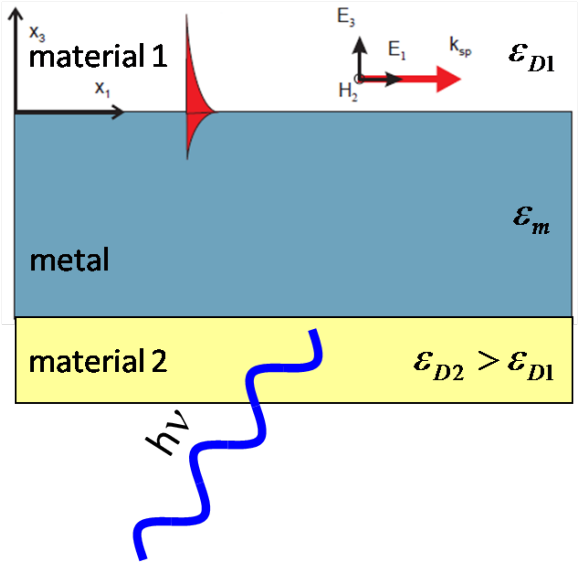

Figure 3-4: Kretschmann geometry for exciting surface plasmon polaritons. In this geometry, light is incident through higher refractive index material 2. The interface between material 1 and the metal can support SPPs. The evanescent wave in material 2 permeates through the thin metal layer when the angle of incidence is greater than the angle of total internal reflection, allowing scattering with SPPs.

an exciton and a photon. However, the interaction is between the electric field of the radiative dipole at an excited molecule and the electric field of the plasmon.

The oscillating electric field of the radiative dipole associated with an exciton can be damped by several mechanisms. First, the exciton can non-radiatively decay into phonons. However, this non-radiative decay is minimized in materials with high photoluminescence efficiency. Second, the exciton can emit photons into free space. This process can be minimized in a multilayer device stack consisting of both metals and dielectric materials. The rate of photon emission, given by Fermi's golden rule, depends on the photonic mode density. Near a metal film, such as the contacts in an organic PV stack, the photonic mode density drops dramatically as visible light is strongly absorbed by free charges in the metal. Third, excitons can also radiate into dielectric waveguide modes in the the antenna/PV stack. Many of these modes exist within the active charge generating layers in our device structure so this damping mechanism will aid energy transfer from the antenna. Photons in waveguide modes

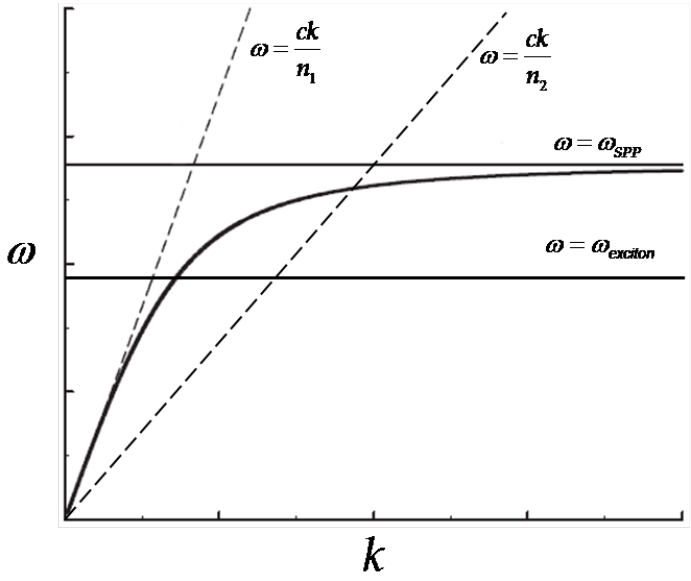

Figure 3-5: Near field dispersion for excitons in a light absorbing antenna. Unlike photons, excitons can couple to photons and SPPs due to their broad range of accessible wavevectors in the near field. The dipole coupling rate depends on the photonic mode density.

interact with the charge generating layers identically to incident light. Finally, as indicated above, the exciton can non-radiatively energy transfer into surface plasmon polariton modes at the adjacent metal surface.

The theoretical basis for dipole coupling to modes in a multilayer stack has been described in detail elsewhere [112] and agrees well with experiment [113]. The near field of the dipole is composed of an infinite sum of plane waves containing components of a large range of wavevectors. Thus, the near field of the dipole can be approximated as having a horizontal line dispersion relation. This dispersion relation for the dipole associated with the exciton allows direct coupling with photon, waveguide, and plasmon modes throughout the multilayer device stack, as illustrated in Figure 3-5. The relative efficiency of coupling to each mode depends on its mode density as given by Fermi's golden rule [114]. High efficiency energy transfer from excited molecules (excitons) to SPP modes has been demonstrated before in metallic slabs [115] and thin films [107].

We expect SPP modes to be a particularly effective energy transfer mechanism due to their long range propagation parallel to the exciton dissociation interface in organic PVs. Therefore, we seek to design structures that favor this mode of energy transfer. In order to do this we need to develop a model for energy transfer in multiple layer organic semiconductor structures. The next section describes our work developing such a model.

3.3 Modeling energy transfer in organic solar cells

The potential of the architecture described in this chapter to improve organic photovoltaic device efficiency depends on achieving as high an energy transfer efficiency as possible. Understanding the energy transfer from the antenna to the semiconductor layers in this architecture is critical. Therefore, we model energy transfer within a multilayer organic solar cell device stack. As discussed above, we seek to design device structures with enhanced energy transfer via surface plasmon polariton modes in the cathode contact and via radiation into waveguide modes.

The traditional approach to considering near field energy transfer phenomena and photonic mode density in thin multilayer stacks relies on the dipole model of Chance, Prock, and Silbey (CPS) [112]. In CPS theory an exciton within the organic device is modeled as a point dipole whose electric field is described by dyadic Greens functions. The model simulates classical damping of an oscillating charge distribution near or within a multilayer dielectric and metal stack. The technique calculates the dipole lifetime and the wavevector distribution of its decay. However, the CPS technique does not directly describe interlayer energy transfer, and, in many cases, a quantitative understanding of interlayer energy transfer using CPS theory has not been possible. Instead, it has been common to couple the exact CPS model with a quantum mechanical model that compares the probability of exciton decay as a function of

wavevector to the various non-radiative and radiative modes of the multilayer stack [116]. Such hybrid approaches have been used, for example, to calculate the fraction of photons emitted by an OLED in a specific viewing direction [117, 118], but they suffer from complexity and are innately approximate.

In our work, we eliminate the need for the quantum mechanical appendage to CPS by analytically determining the Poynting vector, P, throughout the multilayer stack [119]. The derivation of the extension to CPS has been described elsewhere [119] and is beyond the scope of this thesis. For each radiating dipole, the total energy transfer to the active charge generating PV layers is found by calculating ΔP across the PV layers. In addition to the total energy transfer, the model allows the study of the wavevector dependence of energy transfer from the antenna to the active semiconducting layers in the PV.

The energy transfer model also quantifies losses in the silver layers and losses to free space photons and can be used to optimize the thickness of layers throughout the device. Before utilizing the model to design organic PVs with external antennas, we first demonstrate the accuracy of the model by (i) calculating the spatial profile of Förster energy transfer [120] within a thin film consisting of a mixture of donor and acceptor molecules and (ii) calculating the efficiency of SPP-mediated energy transfer across a thin silver film. Elsewhere, we have also used the model to calculate the angular emission profile and the radiative output of a typical organic light emitting diode (OLED) [119].

3.3.1 Förster energy transfer

We first demonstrate the accuracy of the model by modeling Förster energy transfer. Förster energy transfer occurs when the evanescent near field of a donor dipole couples with the evanescent near field of an acceptor molecule [120]. Since the near fields of both dipoles decay as $1/R^3$, the overall rate of energy transfer decays like $1/R^6$. In

addition, if the donor is to transfer energy E, it is necessary that the acceptor possess an allowed transition to a state of energy E above the ground state. Although no real photon is emitted in Förster transfer, it is common to express this latter requirement in terms of the overlap between the absorption spectrum of the acceptor and the emission spectrum of the donor.

In Figure 3-6a, we show the energy transfer spectrum from an excited aluminum tris(8-hydroxyquinoline) (Alq_3) molecule. In this plot, the excited molecule is located at the origin. The excited molecule is embedded within an infinite film containing 1% of the acceptor copper phthalocyanine (CuPc) in the donor Alq_3. Since the absorption of CuPc overlaps the Alq_3 fluorescence spectrum, we expect Förster energy transfer from Alq_3 to CuPc. The rate of energy transfer is plotted as a function of u, the component of the wavevector parallel to the surface ($k_{\parallel}$) normalized by the magnitude of the wavevector in the dipole layer (k_0). As expected for evanescent coupling, the spectrum is dominated by short range energy transfer through modes with large $k_{\parallel}$. The z dependence of the normalized energy transfer rate is shown in Figure 3-6b. In cylindrical coordinates, the typical $1/R^6$ dependence of the energy transfer rate, b_{ET}, becomes

$$\frac{1}{b_0}\int du\,\Re\left(\int dA\frac{dS_{z,j}^{\perp,\parallel *}}{dz}\right)=\frac{b_{ET}\left(z\right)}{b_0}=\int_0^{\infty} rdr\int_0^{2\pi} d\phi\rho\frac{R_0^6}{\left(r^2+z^2\right)^3}=\rho\frac{\pi}{2}\frac{R_0^6}{z^4} \quad (3.5)$$

where R_0 is the Förster radius, a measure of the strength of the coupling, and ρ is the density of acceptor molecules. Thus, we expect the rate of Förster transfer to decay as $1/z^4$. Indeed, this is consistent with the model result as illustrated in Figure 3-6b. The Förster radius is calculated to be $R_0 = 38$ Å.

This calculation demonstrates that the model can be used to determine whether Förster transfer is enhanced in complex planar structures [121].

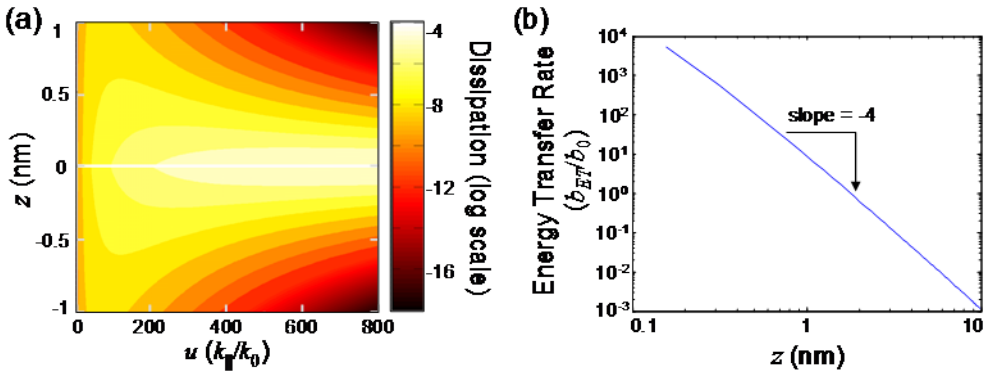

Figure 3-6: Förster energy transfer as a function of position. (a) Förster energy transfer as a function of position z, normalized to the surface parallel wavevector. The excited molecule is embedded within an infinite film of 1% CuPc in Alq_3. The dipole is located at $r = z = 0$ and the emission wavelength is $\lambda = 535$ nm. Bright features correspond to faster energy transfer. (b) The z dependence shows a $1/z^4$ power law consistent with Equation 3.5 and a Förster radius of $R_0 = 38$ Å. At $\lambda = 535$ nm, the dielectric constants for CuPc and Alq_3 are: $\epsilon = 1.908 + 0.265i$ and $\epsilon = 2.962$, respectively.

3.3.2 Energy transfer across a thin metal film

Next, as an example of layer-to-layer dipole energy transfer, we have calculated the emission spectrum of the structure experimentally studied by Andrew and Barnes [107]. This structure is formed on a glass substrate by first spin coating a 60 nm thick donor film of polymethylmethacrylate (PMMA) doped with 4% Alq_3 by weight, then thermally evaporating a 60 nm thick silver film, and finally spin coating a 60 nm thick acceptor PMMA film doped with 1.6% rhodamine-6G (R6G) by weight. The samples are pumped by a laser on the donor side at a wavelength of $\lambda = 408$ nm. The excitation approximately corresponds to the Alg_3 absorption maximum and R6G absorption minimum. During photoexcitation the photoluminescent spectrum is recorded on the acceptor side of the sample.

In the calculation, we integrate the contribution of dipoles throughout the donor and acceptor films. However, when integrating over dipoles throughout the films the result is found to be similar to the case where the dipoles are located in two thin strips at the center of each PMMA film. The quantum yields (q) of the dipoles are taken

to be 25% [122, 123] and (95±1.5)% [124] for Alq_3 and R6G molecules, respectively. Figure 3-7 shows the energy absorption in the silver and R6G-doped PMMA layers as a function of the normalized surface-parallel wavevector, u. The wavelength used for this calculation is $\lambda = 535$ nm. The SPP peak at $u \approx 1.1$ dominates the absorption and is strongly evident in both the silver and the acceptor films. Thus, we conclude that the energy transfer to the R6G molecules occurs mainly via this SPP mode. The coupling to SPP modes is best for perpendicular dipoles. Parallel dipoles outcouple better to the air where the energy is lost. Radiative modes have normalized surface-parallel wavevectors smaller than $u = 0.67$. Parallel wavevectors between $u = 0.67$ and $u = 1$ are guided in the glass and PMMA. (Note that the refractive index of PMMA is only slightly lower than that of glass.) The magnitude of radiated power directly from Alq_3 is low due to the thick silver layer. Thus, the measured light emission from this structure is dominated by the R6G emission, which in turn gains its energy predominantly via SPP-assisted energy transfer from the Alq_3 dipoles. For completeness, we note that the Alq_3 dipoles also radiate into the glass substrate, as indicated by the blue curves in Figure 3-7. The radiated power in the glass substrate is about 2000 times larger than the power radiated into the air on the acceptor side.

The spectral distribution of the outcoupled energy fraction with respect to the total dipole energy is shown in Figure 3-8. It compares well with the experimental data given in Figure 2(b) of Andrew and Barnes [107]. Calculation of the emission spectra is done by multiplying the out-coupling fractions at each wavelength by the normalized intrinsic emission spectra extracted from Figure 1(d) of Andrew and Barnes [107]. We also calculate the total energy transfer efficiency by normalizing to the energy of an Alq_3 dipole. Figure 3-8 shows an exponential decrease in the transfer efficiency as the silver thickness is increased. The maximum transfer efficiency is approximately 6%. Energy transfer can be enhanced by increasing the concentration of R6G molecules in the PMMA layer. Relative to Förster transfer between point

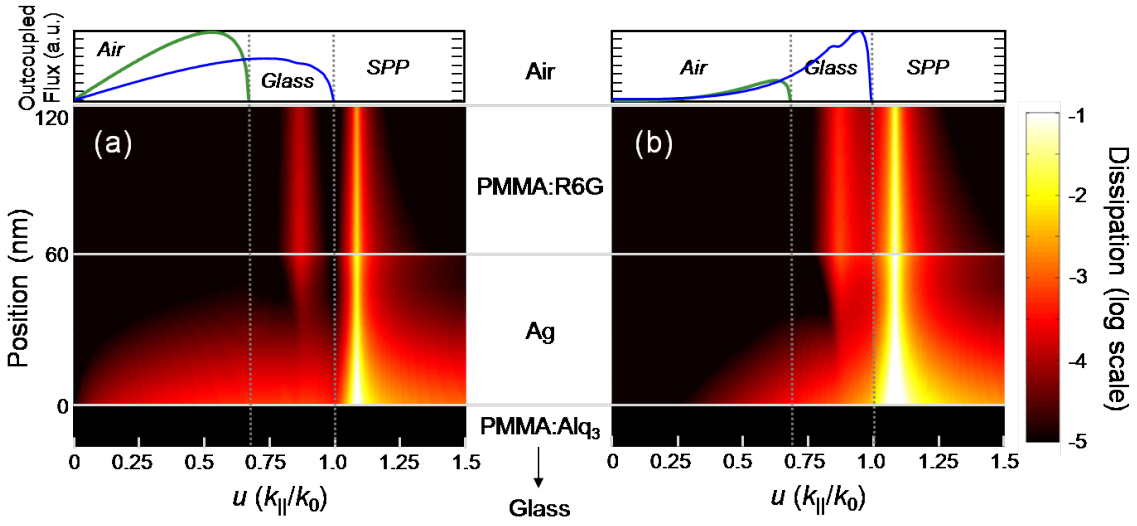

Figure 3-7: Spectral distribution of energy transfer across a thin film. (a) Absorption of parallel dipole energy as a function of position and normalized surface-parallel wavevector. The dipole is located at the middle of the PMMA:Alq_3 layer and the emission wavelength is $\lambda = 535$ nm. The green and blue curves show the outcoupled energy flux from the PMMA:R6G-air and PMMA:Alq_3-glass interfaces, respectively. The blue curve is rescaled by 1/2000 to share the same y-axis with the green curve. (b) Same as part (a) but for perpendicular dipoles. Perpendicular dashed lines divide the flux into air-outcoupled and glass-waveguided portions. Dielectric constants for PMMA and R6G were extracted from Andrew and Barnes [107].

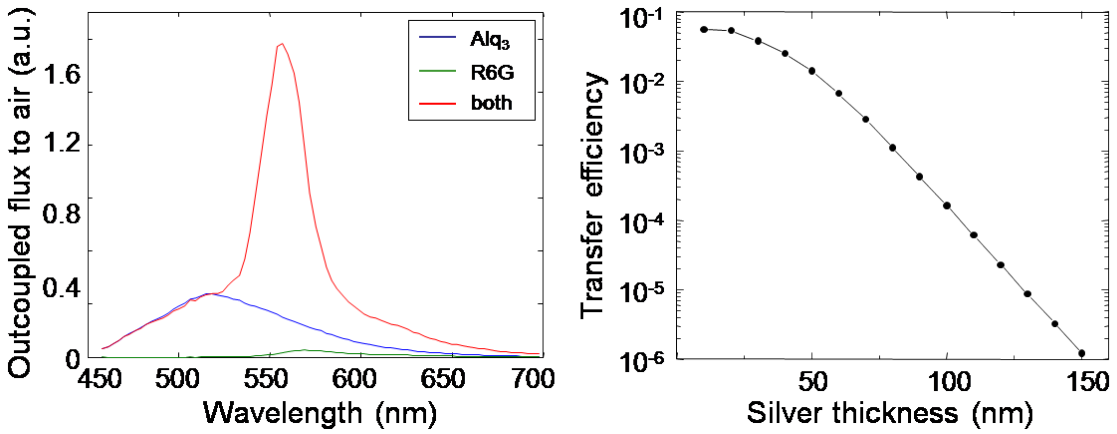

Figure 3-8: Energy transfer efficiency across a thin film. (a) The calculated ratio of emitted power to the total dipole energy for the structure of Andrew and Barnes [107] The data is shown for samples without the R6G acceptor (PMMA:Alq_3/Ag/PMMA) (blue curve), samples without the Alq_3 donor (PMMA/Ag/PMMA:R6G) (green curve), and samples containing both Alq_3 and R6G (PMMA:Alq_3/Ag/PMMA:R6G) (red curve). The silver layer thickness is 60 nm. The R6G absorption and PL spectra of R6G and Alq_3 are extracted from Fig. 1(d) of Andrew and Barnes [107]. (b) The energy transfer efficiency, which is the ratio of the energy absorbed by the R6G-doped PMMA layer to the total Alq_3 dipole energy as a function of silver thickness.

dipoles, mediation by the SPP enables energy transfer over much longer distances [107]. The limitation for SPP-mediated energy transfer is typically the decay length of the evanescent SPP field in the donor and acceptor dielectrics. This may be on the order of 100 nm, significantly longer than the typical Förster radius for point dipoles of < 5nm.

The model indicates that energy transfer depends on both the location and the orientation of the exciton in the antenna. Exciton dipoles oriented perpendicular and parallel to the SPP interface couple into SPP modes with different efficiencies. The PL efficiency of the antenna is also critical for energy transfer. While energy transfer from the antenna to SPPs does not involve emitting an actual photon, the process is proportional to the quantum yield of the antenna material. Finally, the efficiency of energy transfer from the antenna to the active charge generating layers in the underlying organic PV also depends on the light absorption of the active PV layers

at the energy transfer wavelength. The PV semiconducting layers must compete with other SPP decay mechanisms.

The ability of the model formulated above to calculate the efficiency of SPP-mediated energy transfer across a thin silver film allows us to predict the performance of organic photovoltaics with an external antenna layer. In the sections that follow, we utilize the model to design structures that promote energy transfer from an external antenna to the active charge generating layers in the underlying PV.

3.4 Devices with external antennas

In this section, we demonstrate devices with an external antenna layer. We first employ (Alq_3) as the antenna material. Next, we experimentally measure the energy transfer efficiency from the antenna to the PV active layers by fabricate devices with tetrakis(pentafluorophenyl)porphyrin (H_2TFPP) as the antenna layer.

3.4.1 Devices with Alq_3 antennas

As indicated above, we first employ Alq_3 as the antenna material. Alq_3 is a well studied material that has been used extensively in organic light emitting diodes (OLEDs). Alq_3's optical properties, including absorption and photoluminescence, have been thoroughly studied making it an ideal material to use as an antenna in the first demonstration of organic photovoltaic devices with an external antenna.

Modeling results We first model our initial prototype structure, consisting of a conventional small molecule organic bilayer heterojunction solar cell with one additional layer fabricated on top. As illustrated in Figure 3-9, the device structure is glass/Ag (400 Å)/copper phthalocyanine (CuPc, 180 Å)/CuPc:3,4,9,10 perylenetetracarboxylic bisbenzimidazole (PTCBI, 1:1, 180 Å)/PTCBI (180 Å)/bathocuproine

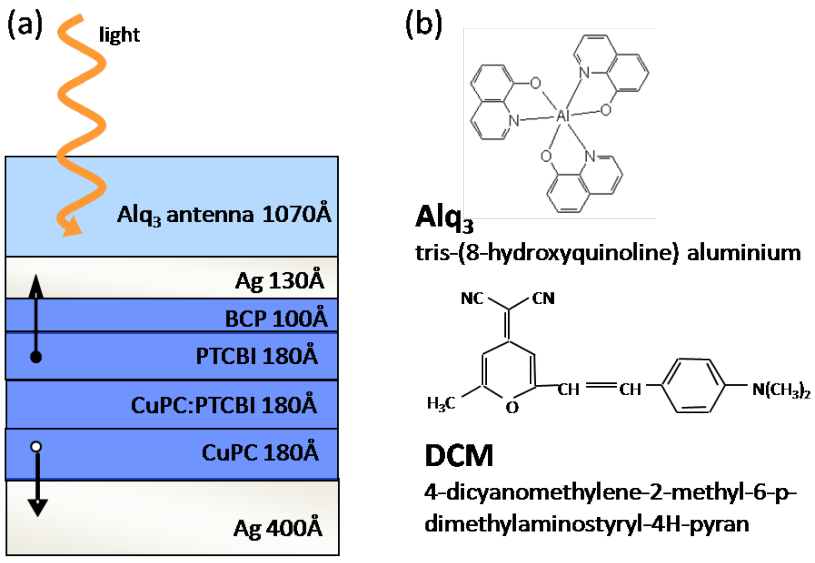

Figure 3-9: Device structure for photovoltaics with an Alq_3 antenna. (a) The device structure fabricated to test the performance of an Alq_3 antenna layer. The device is illuminated from the antenna side of the device. (b) The antenna materials used in this section. Alq_3 is a material commonly used in organic light emitting diodes. DCM is a common laser dye.

(BCP, 100 Å)/Ag (130 Å)/Alq_3 (1070 Å). For the purposes of modeling, each material is described by its wavelength dependent index of refraction and extinction coefficient. The indices of refraction and extinction coefficients of all modeled thin films were directly measured using a spectrophotometer (Aquila Instruments, nkd8000).

The coupling probability density of antenna excitons is shown in Figure 3-10 as a function of distance to the antenna-silver layer interface and the parallel component of the wavevector, u, normalized by the wavevector of an unconfined photon in the antenna layer. Normalized wavevectors with $u < 1$ correspond to radiative modes; $u > 1$ corresponds to non-radiative energy transfer. As discussed above, the energy coupling is dependent on the transition dipole orientation with respect to the plane of the interface. Therefore, we consider the cases of perpendicular (Figure 3-10a) and parallel (Figure 3-10b) oriented dipoles separately. At a given dipole distance, integration of the energy dissipation across wavevectors u yields unity. An isotropic

film can be approximated as possessing 1/3 perpendicular and 2/3 parallel oriented transition dipoles.

The modeling results illustrated in Figure 3-10 indicate that the probability of coupling is greatest for perpendicularly oriented dipoles into modes with $u > 1$, corresponding to SPPs. Coupling to dielectric waveguide modes with $u < 1$ is strongest for dipoles oriented parallel to the Ag-antenna interface.

One distinct SPP mode is evident in the calculations of exciton decay in this device with a normalized propagation constant of $u = 1.8$, corresponding to localization at the antenna-silver interface. A second mode with much weaker overlap with antenna excitons is also visible at $u = 1.1$, corresponding to localization at the glass-silver interface. Coupling to SPPs is especially strong approaching the thin silver electrode. For dipoles oriented parallel to the interface, both dielectric waveguide and SPP modes are significant. Radiation into dielectric waveguide modes is dominant far from the antenna-silver interface.

Total energy transfer as a function of dipole location and orientation is shown in Figure 3-11. For these calculations, we assume that the Alq_3 antenna is doped with a randomly-oriented fluorescent dye with a free space photoluminescence (PL) efficiency of 70% and an emission wavelength of $\lambda = 615$ nm where CuPc absorbs strongly. In this PV stack, the average efficiency of energy transfer to the PV is 52% over the thickness of the antenna layer. We find that energy transfer occurs predominantly via Förster coupling to the photovoltaic, mediated by the non-radiative SPP mode localized at the silver cathode. If the silver electrode separating the PV and antenna is thick, the SPP is confined to either the antenna or the PV. When the cathode is thin, the SPP mode extends into both the antenna and PV, and can mediate the transfer of energy. Consequently, the efficiency of energy transfer is maximized for thinner top silver contacts. In Figure 3-11, we observe that energy coupling via SPPs

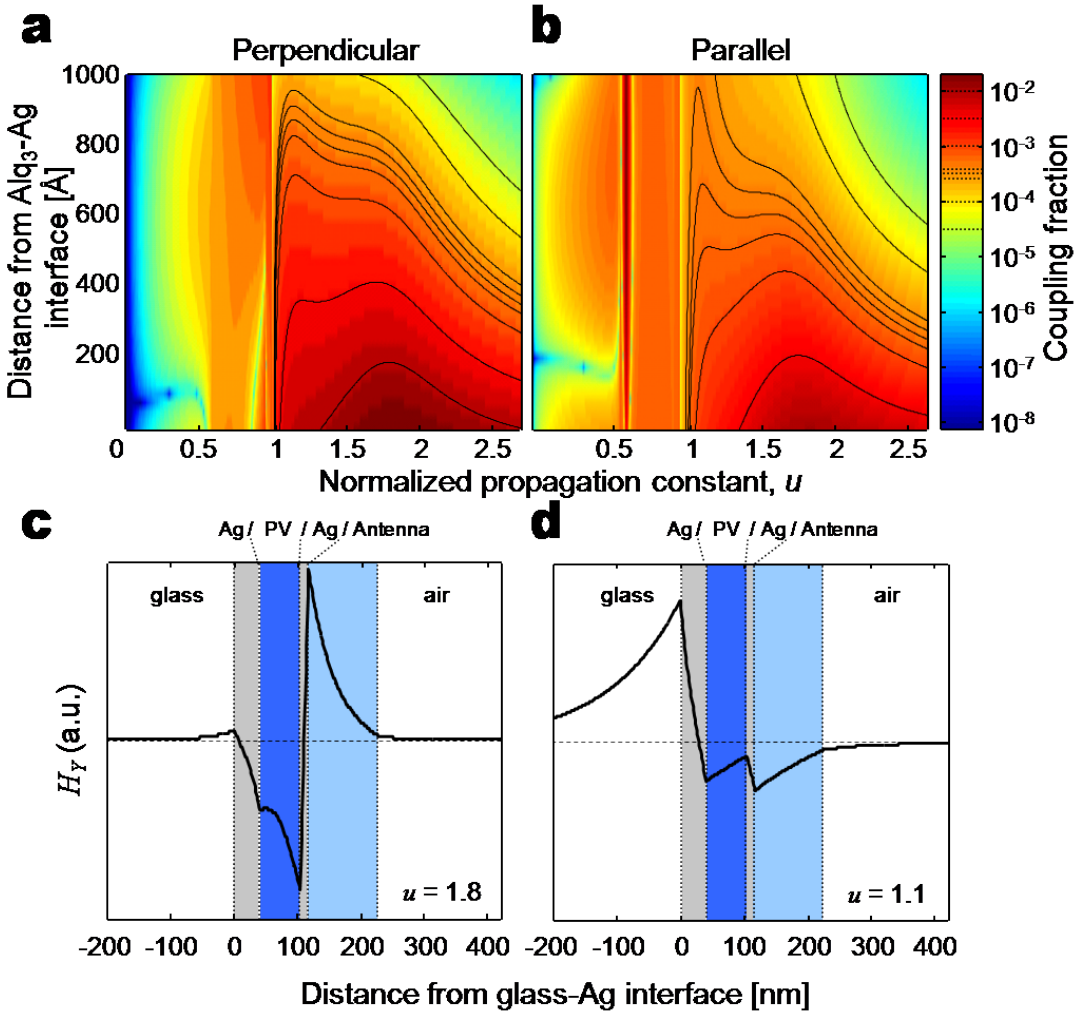

Figure 3-10: Modeled energy transfer in an organic photovoltaic with a light absorbing antenna. (a) Coupling fraction for perpendicular oriented dipoles with respect to the device plane. Note that coupling fractions are plotted on a logarithmic scale. Contours are added (for $u > 1$ only, dotted lines on color bar) to emphasize peaks in coupling fraction at $u \approx 1.8$ and $u \approx 1.1$. (b) Same as part (a) except for parallel oriented dipoles. (c) The transverse magnetic (H_y) mode profile at $u = 1.8$ confirms that the SPP is localized at the antenna/photovoltaic interface and has significant overlap with the photovoltaic active semiconductor layers. (d) The SPP peak at $u = 1.1$ is localized at the glass/photovoltaic interface. The mode profiles were calculated by artificially setting absorption losses to zero in each layer and calculating the stationary states of the multilayer stack.

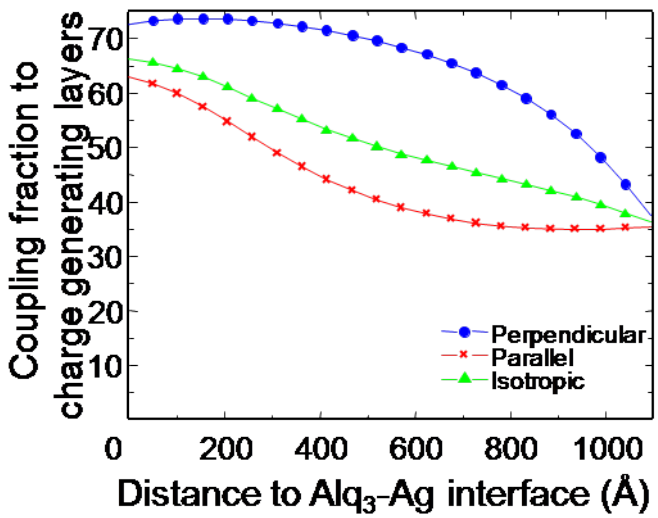

Figure 3-11: Coupling fraction for energy transfer from antenna to organic layers. Coupling is strongest for perpendicularly oriented dipoles located close to the Alq_3/Ag interface due to their stronger emission into SPP modes. Over the first 1000 Å, the mean exciton coupling fraction to the organic layers is 52% for an isotropic distribution of dipoles.

effectively increases the length of Förster energy transfer to ∼1000 Å.

Experimental results. We fabricate the PV with an external antenna modeled above. The organic materials were purified by vacuum thermal sublimation prior to device fabrication. All materials were deposited by thermal evaporation at a pressure of $< 10^{-6}$ Torr. All active device areas were 0.01 cm^2. The device structure, identical to the device modeled above, is glass/Ag(400 Å)/CuPc(180 Å)/CuPc:PTCBI(1:1, 180 Å)/PTCBI(180 Å)/ BCP(100 Å)/Ag(130 Å)/Alq_3 (1070 Å).

As discussed above, the modeling results indicate that the magnitude of energy transfer is expected to be approximately proportional to the free space PL efficiency of the antenna layer. Therefore, to isolate the impact of the antenna while avoiding interference effects due to changes in device structure we fabricate identical photovoltaic cells with antennas of varying PL efficiency. The PL efficiency of Alq_3 can be varied by molecular doping [123]. We vary the photoluminescence efficiency by fabricating antenna layers comprised of an isotropic mixture of Alq_3 and either the quenching ma-

terial CuPc or the laser dye 4-dicyanomethylene-2-methyl-6-(p-dimethylaminostyryl)-4H-pyran (DCM) co-deposited at a ratio of 100:1. At these doping ratios, the absorption of the antenna is not significantly changed. However, the PL efficiencies of the co-deposited films were measured to be ∼0% and 75% with CuPc and DCM, respectively. The PL efficiencies were measured relative to Alq_3, asuming the PL efficiency of Alq_3 is 25% [123].

Comparing the performance of these devices allows us to isolate the photocurrent originating from light absorbed in the antenna. Devices with an antenna whose PL has been quenched by CuPc should exhibit negligible energy transfer from the antenna. We also fabricate devices with no antenna layer.

External quantum efficiency measurements were made using a xenon lamp with a monochromator, chopped at $f = 90$ Hz, and measured using a lock-in amplifier. Light intensity was measured with a calibrated silicon photodiode. The external quantum efficiencies (EQE) of these devices as a function of wavelength are shown in Figure 3-12. At wavelengths where Alq_3 is transparent, the devices are nearly identical, indicating that interference effects do not cause differences in quantum efficiency. However, over the region of 350 nm $< \lambda <$ 450 nm, where Alq_3 absorption is the strongest, the devices with functioning antenna layers exhibit increased quantum efficiency.

The increase in external quantum efficiency, $\Delta\eta_{EQE}$, originates in sequential completion of three processes:

$$\Delta\eta_{EQE} = \eta_{ABS-Antenna} \times \eta_{EnergyTransfer} \times \eta_{IQE} \tag{3.6}$$

where $\eta_{ABS-Antenna}$ is the normalized absorption in the antenna, $\eta_{EnergyTransfer}$ is the energy transfer efficiency across the silver electrode, and η_{IQE} is the internal quantum efficiency of the artificial reaction center. We calculate absorption in the

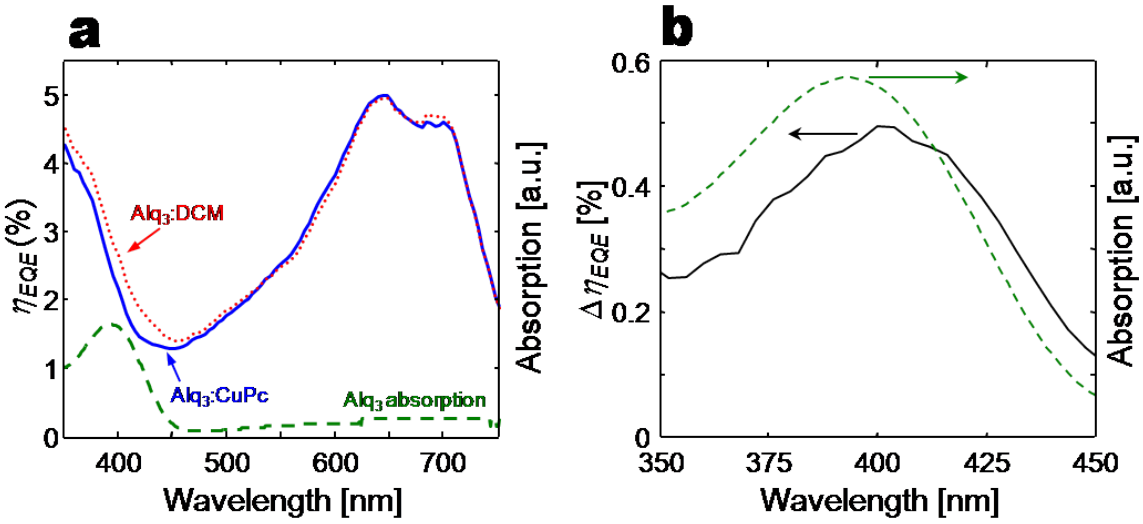

Figure 3-12: External quantum efficiency (EQE) for photovoltaic devices with an Alq_3 antenna. (a) Devices with external Alq_3 functional antenna layers (dotted line) exhibit an increase in external quantum efficiency over the wavelength range where Alq_3 absorption occurs (dashed line). The photocurrent spectra are identical outside the spectral range where Alq_3 absorbs. (b) The change in external quantum efficiency correlates well with Alq_3 absorption.

antenna layer and find $\eta_{ABS-Antenna} = 24\%$ for all antenna compositions. We have measured reflection and transmission to calculate total absorption in the device with an Alq_3:CuPc antenna at the measured fluorescence maximum of DCM at $\lambda = 615$ nm and calculate η_{IQE} =5%. These values result in a total energy coupling efficiency across the silver film of $\eta_{EnergyTransfer} = 46\%$, similar to the predicted value of 52%.

Despite achieving an energy transfer efficiency of 46%, the overall enhancement in EQE due to the antenna layer is limited by the low absorption in the antenna layer. The modeling results discussed above indicate that the SPP mode extends deeply into both dielectric layers on either side of the silver cathode, extending the range of energy transfer up to ∼1000 Å. In order to realize the benefits of the antenna architecture, sufficient light must be absorbed within this distance from the cathode. Efficient SPP-mediated energy transfer also requires materials with high PL efficiency. Unfortunately, the PL efficiency of highly absorptive organic semiconductors is typically diminished by intermolecular energy transfer known as concentration quenching.

3.4.2 Measurement of energy transfer efficiency

To reduce the uncertainties in the measurement of $\eta_{EnergyTransfer}$, we fabricate an organic superlattice photodetector with an antenna. Organic superlattice photodetectors consist of thin alternating donor and acceptor semiconducting layers. The layers are made thin enough to eliminate all losses due to exciton diffusion. Every exciton generated is separated. Under an applied bias, all of the separated charges are swept out of the device efficiently and the devices exhibit an internal quantum efficiency close to 100% [106, 125]. For the purposes of calculating the energy transfer efficiency from an antenna, we assume $\eta_{IQE} = 100\%$ which gives a lower bound for $\eta_{EnergyTransfer}$. This structure should enhance $\eta_{EnergyTransfer}$, since it allows thicker CuPc layers while maintaining a high η_{IQE}, thereby increasing the absorption of SPPs in the charge generating layers.

For the measurement of energy transfer efficiency we select the antenna material tetrakis(pentafluorophenyl)porphyrin (H_2TFPP). It is selected for its combination of moderate PL efficiency (η_{PL} = 2-3%) and high absorption coefficient (α = 106 cm^{-1} at λ = 400 nm) that allows nearly 100% of incident radiation to be absorbed within the ∼100 nm range of SPP-mediated energy transfer. We fabricate four H_2TFPP antennas with varying η_{PL} by blending H_2TFPP with different concentrations of CBP, as illustrated in Figure 3-13. The addition of CBP reduces concentration quenching. To eliminate energy transfer altogether, additional devices were fabricated with non-functioning antennas comprised of H_2TFPP codeposited with 3.5% of CuPc.

EQE measurements were made at a reverse bias of 3.5 V. The measured absorption and PL efficiency of the H_2TFPP antenna is used to determine $\eta_{EnergyTransfer}$ from the increase in external quantum efficiency, $\Delta\eta_{EQE}$ as given by

$$\eta_{EnergyTransfer} = \frac{\Delta\eta_{EQE}}{\eta_{ABS}\eta_{PL}} \tag{3.7}$$

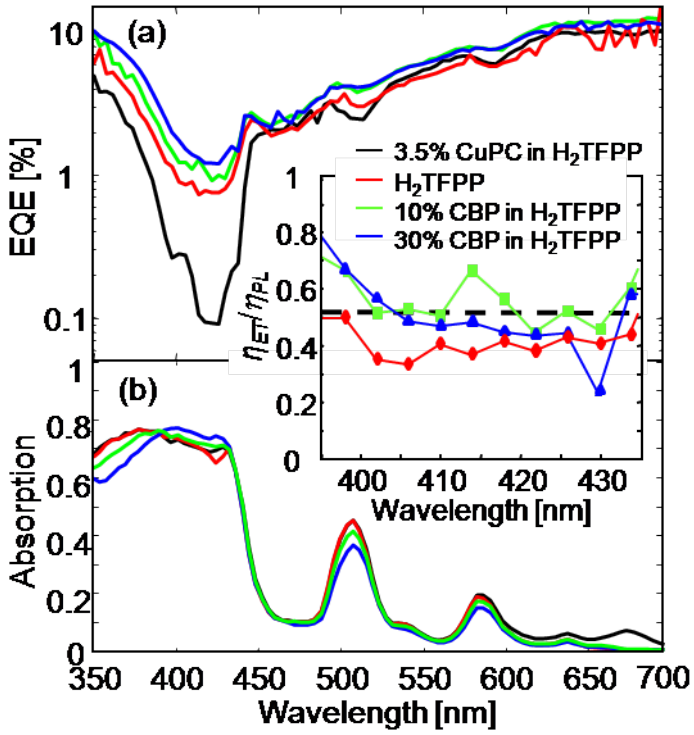

Figure 3-13: Experimental measurement of energy transfer efficiency using superlattice photodetectors. (a) Measurement of external quantum efficiency (EQE) of devices with different antenna compositions: 3.5% CuPc in H_2TFPP, PL = 0% (solid); 100% H_2TFPP, PL = 2.4±0.2% (long dashed); 90:10 H_2TFPP:CBP PL = 2.5±0.3% (short dashed); 70:30 H_2TFPP:CBP PL = 3.4±0.3% (dotted). (b) Absorption spectra of different antenna layers on glass. Inset: Calculation of energy transfer efficiency normalized by the η_{PL} of the various antennas yields $\eta_{EnergyTransfer} = 51\pm10\%$.

Using the quenched antenna as the baseline, and noting that the absorption of H_2FTPP is $\eta_{ABS} = 75\%$ for $\lambda = 450$ nm, we obtain $\eta_{EnergyTransfer} = 51\pm10\%$, as illustrated in the inset of Figure 3-13. Note that the overall change in quantum efficiency remains small in this device due to the weak η_{PL} of H_2TFPP.

The peak efficiency of SPP-mediated energy transfer in previous studies [107] was approximately $\eta_{EnergyTransfer} = 5\%$ [125], too small for most applications. The nearly order of magnitude improvement in this work is due to reductions in the thickness of the interfacial silver layer and increasing the SPP absorption in the organic semiconductors. The organic semiconductors must compete with SPP loss in the silver layer. It may be possible to increase the quantum efficiency of an antenna

further by optimizing the orientation and position of luminescent antenna excitons with respect to the thin Ag cathode.

3.5 Devices with resonant cavity antennas

Despite measuring an energy transfer efficiency as high as 51±10%, the absolute increases in device performance demonstrated in the previous section were small due to weak antenna absorption or weak antenna PL efficiency. The ideal antenna material would possess both strong light absorption and high PL efficiency. Unfortunately, materials with both of these characteristics are difficult to find. Therefore, to exploit less absorptive materials with high η_{PL}, we modify the device architecture, enclosing the antenna within a resonant cavity. The resonant antenna cavity boosts the absorption in the antenna without significantly impacting the antenna material's PL efficiency. The absorption in the antenna layer is increased dramatically by tuning the cavity to the absorption peak of the antenna material. Off resonance the antenna acts as a mirror, but near the resonant wavelength, the antenna absorption is significantly enhanced, and energy is fed back into the PV cell via SPP-mediated energy transfer.

With the introduction of a resonant cavity antenna, we change the direction of illumination from the cathode to the anode side of the device. In the earlier devices light passed through the antenna before passing through to the active PV layers. If the antenna absorbed all of the light, a true decoupling between light absorption and exciton diffusion would be achieved in these devices. However, upon further consideration, it is likely more appropriate to illuminate the devices from the anode allowing the incident radiation to pass through the active PV layers before reaching the antenna. In this configuration, the light that would have been absorbed directly by the PV is still absorbed directly. The antenna enhances absorption in those regions

of the solar spectrum where the organic PV materials absorb weakly.

In the next sections we demonstrate PV devices with resonant cavity antennas. We first demonstrate devices using the same antenna material as above, Alq_3. Then, we demonstrate devices with tetraphenylnapthacene (rubrene) serving as the light absorbing material. Rubrene's absorption is an ideal match for the primary absorption gap found in conventional organic solar cells based on donor material CuPc and acceptor material C_{60}.

3.5.1 Devices with Alq_3 resonant cavity antennas

Next, we build devices with Alq_3 resonant cavity antennas. We model the energy transfer efficiency in these devices to determine the optimal antenna thickness. We then fabricate and characterize devices with Alq_3 resonant cavity antennas.

Modeling Results. We model devices with the following structure: glass/ITO (1600 Å)/CuPc (200 Å)/C60 (200 Å)/BCP (85 Å)/Ag (200 Å)/Alq_3 (x Å)/Ag (600 Å), as illustrated in Figure 3-14a. To find the optimal antenna thickness, we model absorption in the multilayer stack using a transfer matrix formulation [70]. We find that a 700 Åthick Alq_3 film tunes the cavity close to the $\lambda = 400$ nm absorption peak of Alq_3 resulting in the greatest absorption enhancement. The absorption in the tuned Alq_3 resonant cavity antenna is illustrated in Figure 3-14b.

The spectral dependence of energy transfer in devices with an Alq_3 resonant cavity antenna is shown in Figures 3-15a and 3-15b for dipoles oriented perpendicular and parallel to the interfaces, respectively. As in the previous modeling results, the energy transfer rate is plotted against the component of the wavevector parallel to each interface normalized by the wavevector magnitude in the antenna, u. Again, normalized wavevectors with $u < 1$ correspond to radiative modes while those with $u > 1$ correspond to non-radiative energy transfer. We locate the dipole in the middle

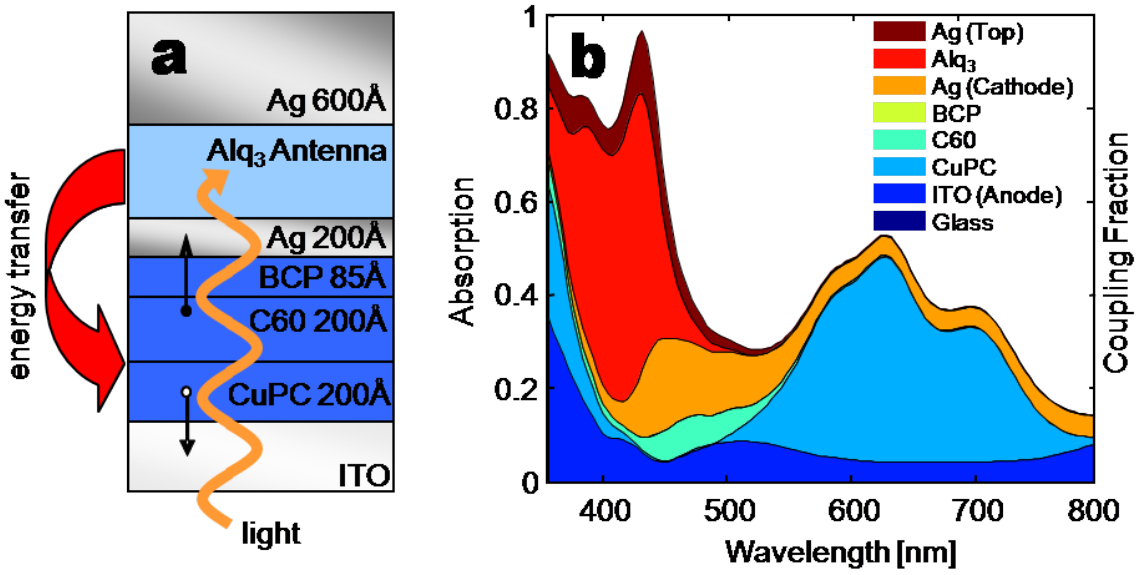

Figure 3-14: Device structure and absorption for photovoltaics with an Alq_3 resonant cavity antenna. (a) Device structure with a resonant antenna cavity. Light is incident from the substrate side of this device. Incident light first passes through the organic photovoltaic device. A portion of the light that is not absorbed by the organic PV directly is absorbed in the antenna. (b) Absorption in all device layers with illumination from glass side and an Alq_3-based antenna thickness of 700 Å. The tuned cavity results in significantly increased absorption in the antenna layer.

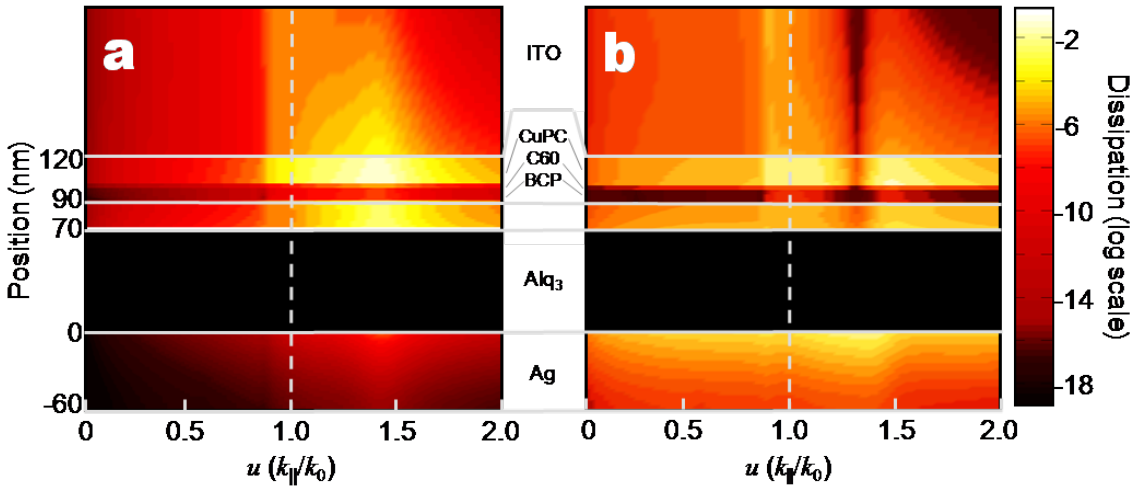

Figure 3-15: The spectral dependence of energy transfer with a resonant cavity antenna is shown in (a) and (b) for dipoles oriented perpendicular and parallel to the interfaces, respectively. Coupling is greatest for perpendicularly oriented dipoles into modes with $u > 1$, corresponding to surface plasmon polaritons (SPPs). Coupling to dielectric waveguide modes with $u < 1$ is also strong for dipoles oriented parallel to the Ag-antenna interface.

of the antenna layer for these calculations.

In resonant cavity devices utilizing Alq_3 as the antenna material, we find that energy transfer occurs predominantly via non-radiative coupling, mediated by SPP modes with $u > 1$ localized at the silver cathode. For parallel dipoles, energy transfer via waveguide modes with $u < 1$ is also observed. Loss in the silver layers is significant but is minimized by reducing the thickness of the silver cathode. Coupling is strongest to the CuPc semiconductor layer.

Total energy transfer as a function of dipole location is shown in Figure 3-16. Including PL efficiency losses, the average efficiency of energy transfer to the PV layers is 40% over the thickness of the antenna layer for an isotropic distribution of dipoles. The free space PL efficiency of excitons in the antenna was assumed to be 70% at $\lambda = 615$ nm. This assumption is consistent with our selection of antenna materials described below. The peak energy transfer efficiency near the silver cathode is found to be 53%. The average energy transfer efficiency is reduced slightly by the addition

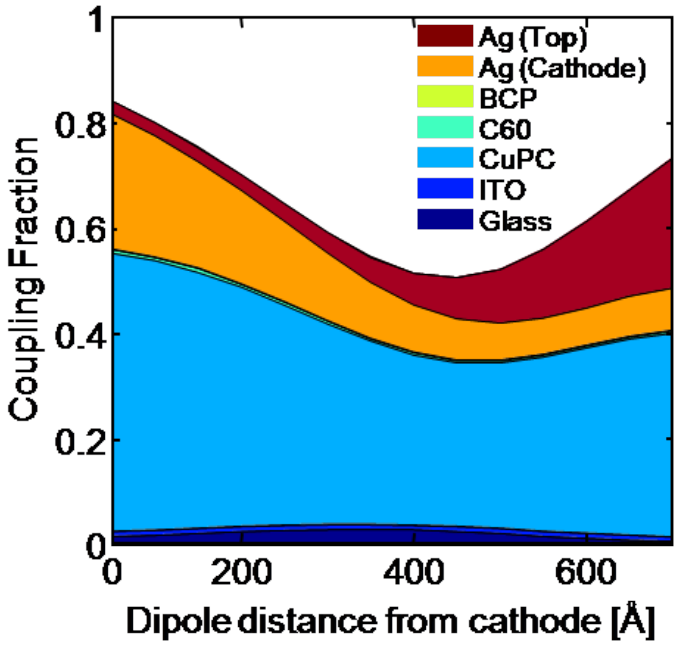

Figure 3-16: Dipole location dependence of energy transfer to photovoltaic device layers. The coupling fraction to organic layers throughout the device is illustrated as a function of the dipole distance from Alq_3-Ag interface. Over the thickness of the antenna, the mean exciton coupling fraction to the organic layers is 40% for an isotropic distribution of dipoles.

of the silver layer forming the top of the resonant antenna cavity. While the average energy transfer efficiency in these devices is lower than the devices demonstrated above without resonant antenna cavities, the overall impact to device performance is expected to be higher due to the significant increase in absorption in the antenna due to the formation of the cavity.

Experimental Results. Next, we again fabricate devices with resonant cavity antennas. As before, we fabricate identical charge generation structures with antennas of varying PL efficiency to isolate photocurrent contributed by absorption in the antenna layer. Fabricated devices with resonant antenna cavities have the following structure: glass/ITO (1600 Å)/CuPc (200 Å)/C60 (30 Å)/BCP (85 Å)/Ag (200 Å)/antenna (700 Å)/Ag (600 Å). As before, the Alq_3-based antennas consist of isotropic mixtures

of Alq_3 and either 1% of the quenching material CuPc or 1% of the laser dye DCM. To highlight the Alq_3-based antenna effect the C_{60} layer in each device was reduced to a thickness of 30 Å. This modification allowed us to fully characterize the operation of the antenna. The devices are illuminated from the glass side.

The external quantum efficiencies of devices with an Alq_3 resonant cavity antenna as a function of wavelength are shown in Figure 3-17 and compared to the reflectivity of the antenna cavity. Off-resonance, the devices with the antenna cavity performed slightly better than devices with no cavity. We found that these differences where due to higher reflectivity with a resonant cavity relative to the silver contact used otherwise. However, this difference is artificial as fabricating a thicker silver cathode on devices without antennas increases the performance slightly. To remove differences due to the lower cathode reflectivity in the absence of an antenna, in Figure 3-17 we scaled the performance of the antenna-less devices up by 16% across the spectrum to match the cavity reflectivity at $\lambda > 550$nm.

In the region 375 nm $< \lambda <$ 475 nm, where the cavity is tuned to Alq_3 absorption, the devices with functioning antennas exhibit increased quantum efficiency of up to 200% compared to those with non-functioning antennas. The peak increase in external quantum efficiency is approximately 80% for devices with external light absorbing antennas compared to those without. The energy transfer efficiency is estimated by summing the photocurrent for the devices with non-functioning antennas and the antenna absorption multiplied by a scalar representing the energy transfer efficiency. The efficiency of energy transfer from the resonant cavity in these devices is found to be 46%. This is slightly higher than the predicted energy transfer efficiency of 40% in these devices. The difference between the modeled and measured efficiencies of energy transfer are likely a result of the slightly rough nature of silver contacts fabricated on top of other organic semiconductor layers.

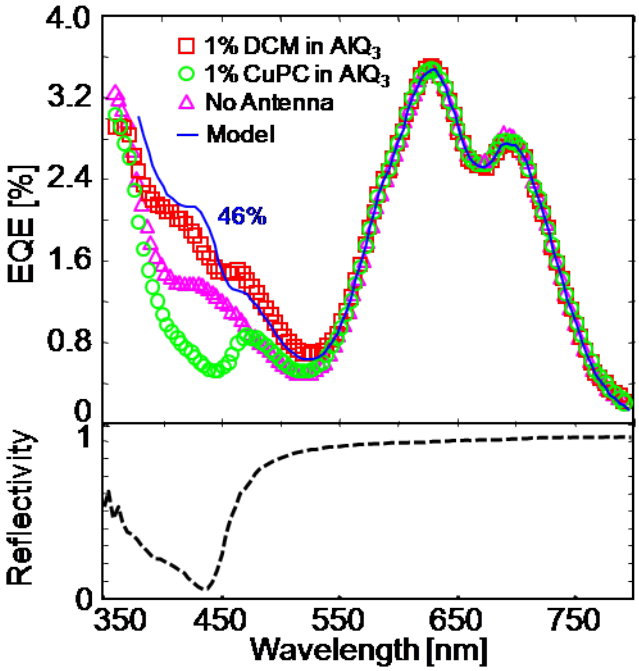

Figure 3-17: External quantum efficiency (EQE) for devices with an Alq_3 resonant cavity antenna. Devices with a functional Alq_3-based resonant antenna cavity exhibit an increase in EQE over the wavelength range where Alq_3 absorption occurs and cavity reflectivity decreases. Functional antennas employ the laser dye DCM whereas nonfunctional antennas employ the quencher CuPc. The functional antenna shows a significant performance enhancement versus both the quenched antenna and devices fabricated without any antenna. The model discussed in the text indicates an energy transfer efficiency of approximately 46%.

3.5.2 Devices with rubrene resonant cavity antennas

Small-molecule organic PVs based on copper phthalocyanine and fullerene are characterized by an absorption gap between the phthalocyanine Q and Soret bands, 475 nm $< \lambda <$ 575 nm. Alq_3, with an absorption peak near 400 nm is not an ideal antenna material to fill this gap. Therefore, next we seek to select a new antenna material that will boost the performance of a phthalocyanine-based PV by exploiting efficient SPP-mediated energy transfer. Tetraphenylnapthacene (rubrene), a common organic light emitting device material, has an absorption coefficient of $\sim 10^4$ cm^{-1} at $\lambda = 550$ nm. Using rubrene as a Förster energy transfer donor for the laser dye 4-(dicyanomethylene)-2-t-butyl-6-(1,1,7,7-tetramethyljulolidyl-9-enyl)-4H-pyran-(DCJTB), yields $\eta_{PL} = 90 \pm 10\%$. This material combination is particularly well-suited to enhance the performance of a $CuPc/C_{60}$-based solar cell.

Modeling Results. As before, we calculate the expected optical absorption in each layer using a transfer matrix method to tune the rubrene resonant cavity antenna structure. A 1250 Åthick film of 30% rubrene and 2% DCJTB in transparent carbazole biphenyl (CBP) tunes the cavity close to the $\lambda = 500$ nm absorption peak of rubrene. Figure 3-18 illustrates the absorption throughout the PV device with a tuned rubrene resonant antenna cavity. The tuned cavity results in significantly increased absorption in the antenna layer. Unfortunately, the resonant antenna cavity impacts the electric field throughout the device. Therefore, while absorption is increased in the antenna layer, the direct absorption in the active semiconducting layers in the PV decreases slightly. In order to improve overall device performance, the absorption and energy transfer in the antenna will have to overcome these losses relative to devices with no antenna.

While rubrene's absorption peaks ultimately determine the strength of absorption in the resonant cavity antenna with different antenna thicknesses, modifying the

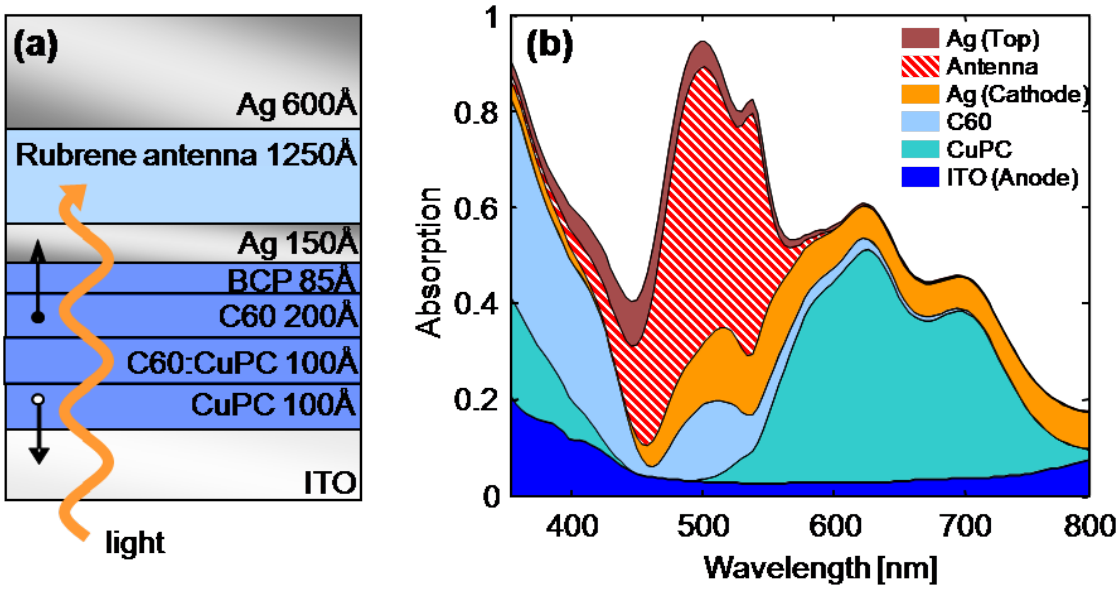

Figure 3-18: Device structure and absorption for photovoltaics with a rubrene resonant cavity antenna. (a) Device structure with a rubrene resonant antenna cavity. (b) Calculated absorption within devices with a rubrene resonant cavity antenna with illumination from the glass side. The tuned cavity yields significantly increased absorption in the antenna layer.

antenna thickness does yield some flexibility in tuning the antenna's absorption to a specific absorption gap in the underlying solar cell. The flexibility in tuning the antenna should make this technique applicable to a wide range of solar cell material combinations.

We again model energy transfer within a multilayer organic PV stack. We assume $\eta_{PL} = 90\%$ at $\lambda = 650$ nm. The wavevector dependence of energy transfer from the antenna to the PV is shown in Figure 3-19a. The energy transfer is plotted against the component of the wavevector parallel to each interface normalized by the wavevector magnitude in the antenna, u. Normalized wavevectors with $u < 1$ correspond to radiative modes while those with $u > 1$ correspond to non-radiative energy transfer. Once again, for these calculations, the dipole is located in the middle of the antenna layer. Also as before, we find energy transfer occurs predominantly via non-radiative coupling, mediated by SPP modes with $u > 1$.

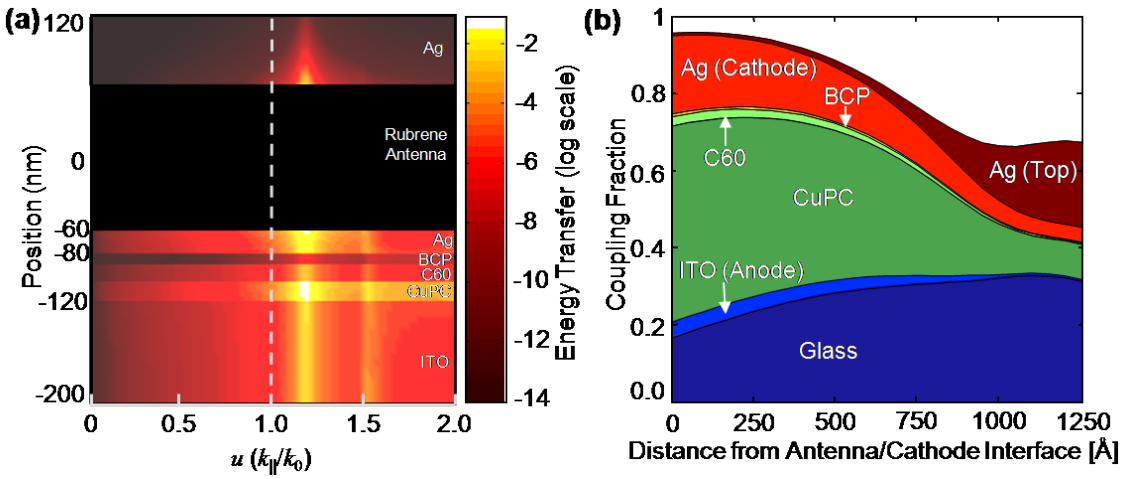

Figure 3-19: Energy transfer in organic photovoltaics with a rubrene resonant antenna cavity. (a) The normalized in-plane wavevector (u) dependence of energy transfer throughout the resonant cavity devices is shown for dipoles oriented perpendicular to the antenna/cathode interface. The parallel geometry is similar. Coupling is greatest for dipoles into modes with $u > 1$, corresponding to surface plasmon polaritons (SPPs). (b) The modeled dipole coupling fraction to each layer in the photovoltaic stack as a function of the dipole distance from the antenna/cathode interface. Coupling to the CuPc and C_{60} layers results in photocurrent.

Finally, we model the dipole coupling efficiency to each layer in the PV stack as a function of the dipole distance from the antenna/cathode interface, as illustrated in Figure 3-19b. Near the cathode, $\eta_{ET} = 54\%$. However, the efficiency decreases beyond ~85 nm. Averaged over the entire antenna thickness, $\eta_{ET} = 31\%$.

Experimental Results. We fabricate devices with rubrene-based resonant cavity antennas tuned specifically to the absorption gap in conventional C_{60}/CuPc PV cells. We compare rubrene/DCJTB antenna devices to control devices without an antenna and to devices with quenched antennas. The quenched antennas were fabricated with 2% of the quenching material CuPc instead of DCJTB in the host rubrene. The external quantum efficiencies of these devices as a function of wavelength are shown in Figure 3-20 and compared to the reflectivity of the antenna cavity. Devices with functional external rubrene-based antenna layers exhibit an increase in EQE over

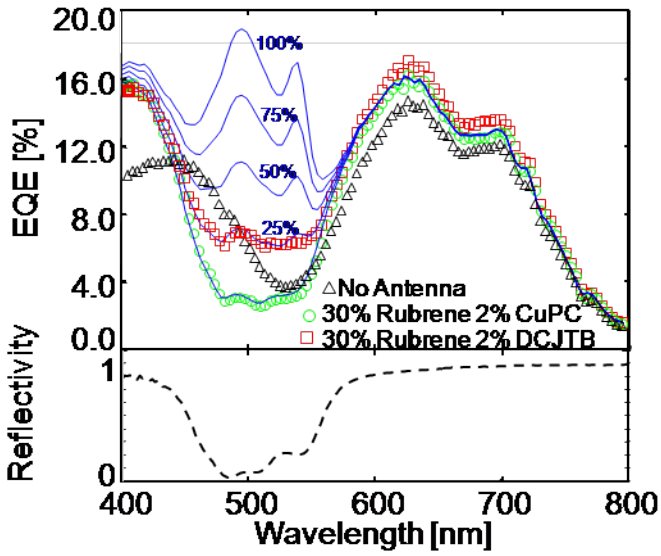

Figure 3-20: External quantum efficiency (EQE) for devices with a rubrene resonant antenna cavity. Devices with a functional external rubrene-based antenna exhibit an increase in EQE over the wavelength range where rubrene absorption occurs and the cavity reflectivity decreases. Functional antennas employ the laser dye DCJTB whereas nonfunctional antennas employ the quencher CuPc. The functional antenna shows a significant performance enhancement versus both the quenched antenna and devices fabricated without any antenna. Comparison with modeling indicates that the energy transfer efficiency is approximately 25%. We also show the expected EQE for energy transfer efficiencies of 0%, 50%, and 75%.

the wavelength range where rubrene absorption occurs and the cavity reflectivity decreases. The antennas fill in the absorption gap in the underlying solar cells. The functional antenna devices show a significant performance enhancement relative to both the quenched antenna and devices fabricated without any antenna.

The absorption of the antenna (from Figure 3-18) and the internal quantum efficiency at the PL maximum of DCJTB, $\eta_{IQE} = 30\pm10\%$ at $\lambda = 640$ nm, is used to determine $\eta_{EnergyTransfer}$ in these devices. We find the energy transfer efficiency from the antenna is $25\pm10\%$, consistent with the calculated result of $\eta_{ET} = 31\%$ in Figure 3-19b. Figure 3-20 also shows the expected EQE for energy transfer efficiencies of 0%, 50%, and 75%. As illustrated in the figure, with improved energy transfer, the quantum efficiency in the spectral gap between the semiconductors' absorption peaks

could be significantly improved. The absorption modeling also demonstrates that the improved quantum efficiency outside the region where the resonant cavity absorbs is due to reflectivity changes that modify the electric field profile within the device.

3.6 Outlook for this device architecture

On the basis of the results described in this chapter, we anticipate that the addition of external antennas onto thin film organic photovoltaics provides a flexible route towards achieving high efficiency devices. Fabricated devices exhibit energy coupling of 30-50%, demonstrating that plasmon mediated coupling is a viable method of transferring energy from the external antenna into the charge generating layers. While the introduction of the antenna necessarily adds a step into the energy transduction process, the anntenna decouples photon absorption and exciton dissociation; these two processes can be optimized indepedently, increasing device design flexibility.

The device architecture discussed in this chapter has two primary advantages:

1. The PV charge generating layers are freed from optical absorption constraints. This offers the opportunity to design PVs on the basis of high internal quantum efficiency, low series resistance, and high stability, negating the necessity for disordered bulk heterojunctions and thick resistive layers to achieve high external quantum efficiencies. Also, with a more sophisticated antenna design, the PVs could be optimized for a single wavelength: the antenna energy transfer wavelength.

2. Since the optically absorbent material in the antenna does not need to conduct excitons or charges, new materials are possible for light absorption in organic PVs, including J-aggregates and quantum dots. Antenna materials should be selected for high optical absorption and photoluminescence efficiency. Resonant cavity antennas are one route to achieving high absorption in the antenna,

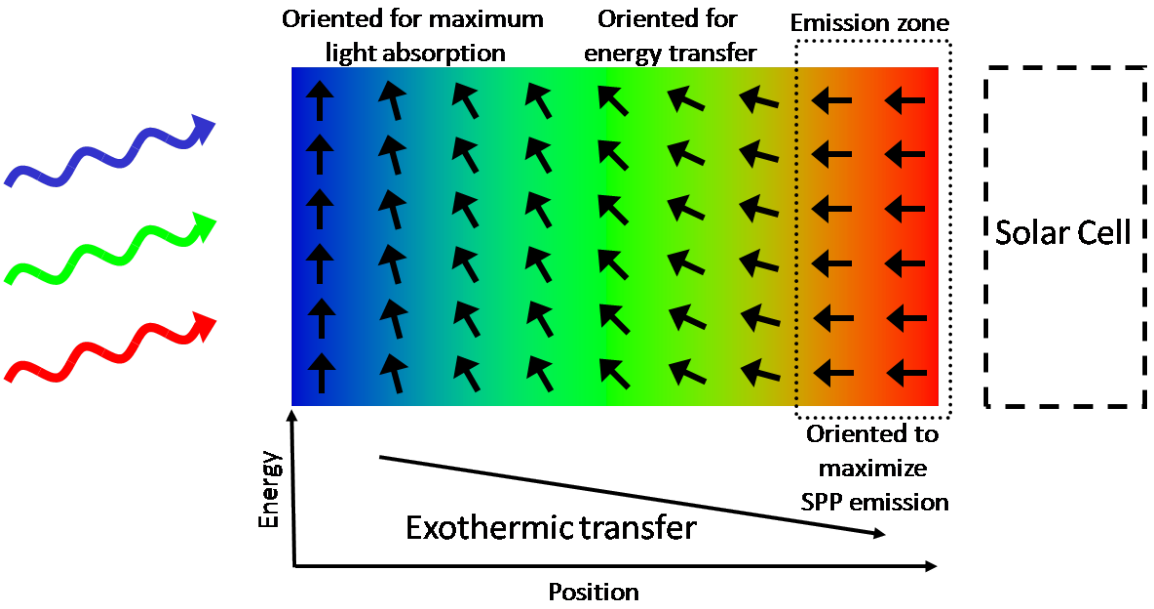

Figure 3-21: Idealized antenna design. The ideal antenna would likely employ multiple absorbing materials to achieve maximum absorption across the visible spectrum. The materials could also be selected to exothermically transfer absorbed energy towards an "emission zone" close to the silver cathode. SPP mediated energy transfer to the active organic PV layers is most efficient near the silver cathode. Molecular alignment could also be used to maximize the efficiency of energy transfer from the antenna.

indicating that antenna structural design could yield further efficiency improvements. Antennas could include multiple materials or material orientations such as that illustrated in Figure 3-21 to maximize antenna absorption or to focus antenna emission near the metal film where it is most efficient.

Antennas can be successfully employed with organic solar cells in spectral regions where the absorption fraction of the PV cell drops below $\eta_{EnergyTransfer}$. We expect this method to be most effective for organic PVs that exhibit weak absorption in some spectral regions. We have demonstrated an efficiency improvement for CuPc/C_{60} devices which exhibit weak absorption over the wavelength range 475 nm $< \lambda <$ 575 nm. However, this technique for improving the efficiency of organic solar cells is also applicable to other organic solar cell material pairs as the resonant antenna cavity can be tuned across the solar spectrum. Further improving the efficiency of energy

transfer through judicious selection of cathode structures or antenna materials could further expand the effectiveness of this device architecture.

Finally, the external light absorbing antenna concept discussed in this chapter can also be used with inorganic solar cells. External organic semiconductor light absorbing antennas can be used to concentrate light on an inorganic solar cell without the need for expensive optics or mechanical tracking. We demonstrate the use of this concept in devices known as luminescent solar concentrators (LSCs) in Appendix A.

Chapter 4

Organic Solar Cells with Interfacial Layers

This chapter discusses the design of organic photovoltaics (PVs) with a thin interfacial layer sandwiched between the donor and acceptor layers, as illustrated in Figure 4-1.

First, the device architecture is introduced. Recombination of charges immediately following dissociation from excitons represents a major loss mechanism in organic photovoltaics. The thin interfacial layer in this architecture creates a cascade energy structure at the exciton dissociation interface that reduces this recombination. To place this device architecture in context, the physics of exciton dissociation and charge transfer state recombination are discussed.

Next, we demonstrate devices exhibiting increased efficiency due to the addition of an interfacial layer. We study how the energy level alignment of the interfacial layer impacts recombination and develop criteria for optimal interface material design and selection. We quantify the optimal thickness of the added interfacial layer by fabricating devices with a range of different interfacial layer thicknesses. Devices with too thin an interfacial layer exhibit limited improvements in charge collection due to partial layer coverage. Devices with an interfacial layer that is too thick suffer

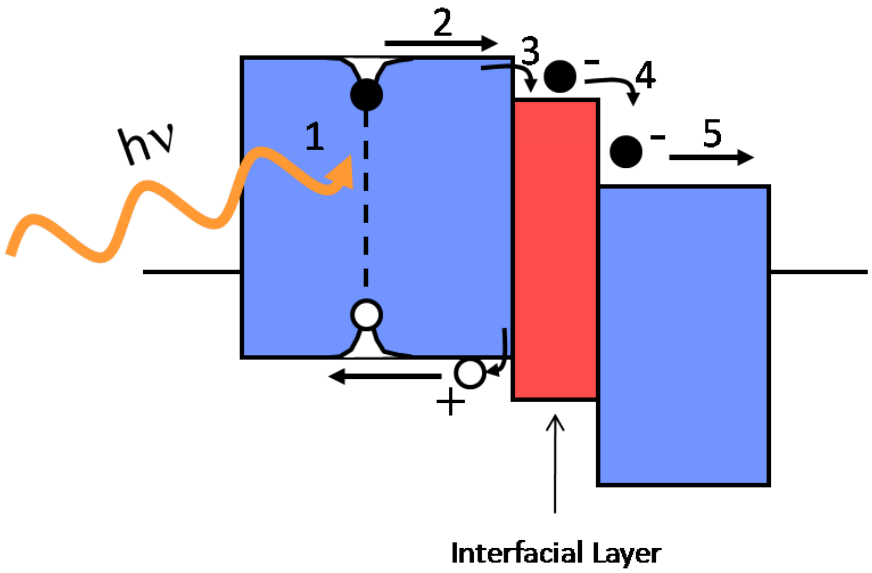

Figure 4-1: Energy level schematic of an organic photovoltaic with an interfacial layer. The interfacial layer creates a cascade energy structure at the interface between the two organic semiconductor layers. This energy cascade reduces recombination losses leading to higher efficiency. Photosynthesis uses a similar multistep electron cascade dissociation architecture.

from carrier transport problems in the interfacial layer. Determining the optimal interfacial layer thickness gives greater insight into the physical mechanism of charge carrier recombination at the exciton dissociation interface in organic PVs.

Finally, the potential implications of these results and the future outlook of this device architecture are discussed.

4.1 Device architecture

As discussed in Chapter 2, recombination of separated charges at the exciton dissociation interface in organic PVs represents a major loss mechanism. Reducing these losses promises increases in both open-circuit voltage (V_{OC}) and short-circuit current (J_{SC}) leading to higher power conversion efficiencies. In photosynthesis, exciton dissociation is accomplished by an electron transfer cascade utilizing several molecules, as discussed in Chapter 1 and illustrated in Figure 1-7. The electron transfer cascade

quickly separates the charges yielding highly efficient exciton dissociation.

Taking the example of photosynthesis, we insert a thin interfacial layer between the donor and acceptor layers to destabilize the charge transfer state populated immediately after exciton dissociation. As illustrated in Figure 4-1, the interfacial layer in this device architecture is selected such that the material's lowest unoccupied molecular orbital (LUMO) and highest occupied molecular orbital (HOMO) energy levels are between the corresponding LUMO and HOMO energy levels of the donor and acceptor materials respectively. The thin interfacial layer creates a cascade energy structure at the exciton dissociation interface.

In this architecture, the energy transduction process begins with the generation of excitons by light absorption in either the donor or acceptor material. The excitons then diffuse to the interface between the donor and acceptor layers as in conventional organic solar cells and dissociate rapidly and populate a charge transfer (CT) state across the interface. In contrast to conventional organic photovoltaic devices, the charges in the CT state are rapidly separated by the energy cascade structure. Once the CT state is spatially separated, the ability for the separated charges to recombine is significantly reduced. The physics of the exciton dissociation process is discussed in more detail in the next section. Finally, the separated charges are collected at the electrodes.

In addition to reducing the recombination of photogenerated charges, the interfacial layer also reduces the recombination of injected charges, leading to a reduction in dark current. The interfacial layer creates an energy barrier in the middle of the device and injected electrons are unable to recombine with injected holes at the donor-acceptor interface. A reduction in dark current is expected to yield an increase in open-circuit voltage.

Previously, additional layers have been introduced between the anode and the donor material in organic PVs in order to reduce dark current and increase the open-

circuit voltage. The added layer at the anode in these devices has been referred to in the literature as either a "buffer" or "electron blocking" layer. Kinoshita *et al.* inserted a layer of molybdenum trioxide (MoO_3) adjacent to the indium-tin-oxide (ITO) anode in solar cells based on tetraphenylporphine and C_{60} [126]. The addition of the MoO_3 layer increased the open-circuit voltage from 0.57 V to 0.97 V and the power conversion efficiency increased from 1.25% to 1.88%. However, the short-circuit current density and fill factor were unchanged in these devices. The MoO_3 layer was found to have changed the effective work function at the contact. The enhanced performance was explained by the suppression of Fermi level pinning at the anode. Similarly, Li *et al.* demonstrated enhanced efficiency for SnPc/C_{60} solar cells with an electron blocking layer at the anode consisting of either MoO_3 or boron subphthalocyanine chloride (SubPc) [127]. The addition of an electron blocking layer in these devices was found to increase the open-circuit voltage from 0.16 V to as high as 0.42 V with a 30 nm layer. However, most of the open-circuit voltage increase was achieved with electron blocking layers as thin as 2 nm. Devices with an electron blocking layer also exhibited increases in fill factor and short-circuit current. The increased short-circuit current was due to absorption in the electron blocking layer. The devices were thin enough that excitons generated in the electron blocking layer could still reach the donor-acceptor interface and dissociate. The efficiency of fully dissociating photogenerated excitons was not shown to have been improved in either of these earlier efforts.

The addition of an interfacial layer at the donor-acceptor interface has also been demonstrated previously. However, earlier studies have not demonstrated improvements in the efficiency of exciton dissociation and charge transfer state separation. Several studies have demonstrated increases in short-circuit current with no change in open-circuit voltage.

Hiramoto *et al.* demonstrated three layer organic PV devices based on metal-

free phthalocyanine and two different n-type perylene layers [128]. While the devices have a similar energy cascade structure as the device architecture introduced earlier in this chapter, the interfacial layer was 10-20 nm. As will be discussed later in this chapter, this is likely too thick to enhance the separation of charge transfer states. The device enhancement observed was due to the addition of a second exciton dissociation interface in the device. The efficiency of forming excitons in the middle layer was enhanced since excitons were always formed close to one of the dissociation interfaces. They reported no enhancement for interfacial layer thicknesses less than 10 nm. The introduction of an interfacial layer in these devices did not increase the open-circuit voltage.

Triyana *et al.* inserted a PTCDI layer in an organic solar cell consisting of CuPc and PTCBI [129]. However, the thickness of the interfacial layer, 18 nm, was too thick to enhance charge transfer state separation. Devices with a PTCDI interfacial layer exhibited increased current due to absorption in the PTCDI layer. The efficiency of dissociation was not enhanced for excitons originating in the donor or acceptor layers. The open-circuit voltage was unchanged with the addition of the interfacial layer in these devices.

Zhang *et al.* demonstrated devices with three active semiconducting layers [130]. They fabricated devices consisting of m-MTDATA, CuPc, and C_{60}. The thickness of the CuPc layer was varied from 20 nm to 90 nm. These devices exhibited increased short-circuit current compared to devices fabricated with m-MTDATA and CuPc or CuPc and C_{60}. As in the studies discussed above, the increase in performance was due to increased absorption and the introduction of two different exciton dissociation interfaces. CuPc was demonstrated to be capable of bipolar carrier transport. The open-circuit voltage did not increase in the three layer devices.

Similarly, Dai *et al.* fabricated three layer devices utilizing zinc phthalocyanine (ZnPc), lead phthalocyanine (PbPc), and C_{60} [131]. The interfacial layer was 20 nm

thick in these devices. PbPc extended the absorption into the near-infrared in these devices resulting in a higher short-circuit current. However, no change in V_{OC} was exhibited.

Yang *et al.* demonstrated devices utilizing two donor materials, CuPc and SnPc, in parallel with acceptor C_{60} [132]. SnPc was introduced to broaden the spectral sensitivity of the devices into the infrared. The morphology of the devices was controlled with organic vapor phase deposition to ensure that simultaneous contact between CuPc and C_{60} and between SnPc and C_{60} was maintained. In these devices excitons generated in CuPc were dissociated at the CuPc/C_{60} interface while excitons generated in SnPc were dissociated at the SnPc/C_{60} interface. The potential cascade energy structure (CuPc/SnPc/C_{60}) was not utilized to enhance exciton dissociation. Devices exhibited increase short-circuit current consistent with higher absorption. The open-circuit voltage was unchanged.

In general, the interfacial layers in the efforts discussed above have been too thick to enhance the efficiency of charge transfer state separation. When an enhancement in short-circuit current has been observed, the increase was due to absorption in the interfacial layer.

Open-circuit voltage increases have also been demonstrated with the addition of an interfacial layer between the donor and acceptor semiconductors. However, in these studies the short-circuit current did not change or decreased with the addition of an interfacial layer.

Sista *et al.* demonstrated devices with CuPc sandwiched between tetraceno[2,3-*b*]thiophene (TT) and C_{60} [133]. The interfacial layer thickness was varied from 2 nm to 13 nm. The open-circuit voltage increased from 0.31 V to 0.56 V with an 8 nm CuPc interfacial layer. However, the short-circuit current decreased slightly in these devices. The decrease in short-circuit current density indicates that the efficiency of exciton dissociation and charge transfer state separation was likely decreased in these

devices. Primarily due to the increase in open-circuit voltage and a slight increase in fill factor, the power conversion efficiency increased from 0.78% to 1.54% with a 13 nm interfacial layer. The short-circuit current increased slightly with increasing interfacial layer thickness due to absorption in the interfacial layer. However, the short-circuit current never reached the same magnitude as in devices with no interfacial layer.

Kinoshita *et al.* fabricated similar devices utilizing CuPc as the interfacial layer between donor material pentacene and acceptor material C_{60} [134]. The thickness of the interfacial layer was varied between 0 nm and 10 nm. The interfacial layer increased the open-circuit voltage from 0.38 V to 0.47 V. This change was attributed to the larger HOMO level of CuPc (5.1 eV) compared to pentacene (5.0 eV). The short-circuit current was found to remain constant for thin interfacial layers with thickness less than approximately 2 nm. However, the short-circuit current decreased as the interfacial layer thickness was increased beyond 2 nm. Measurements of external quantum efficiency indicated that devices exhibited increased performance in regions where the interfacial layer absorbs light and slightly decreased performance elsewhere. These changes offset each other with thin interfacial layers, explaining the steady short-circuit current with thin interfacial layers. As the interfacial layer thickness increased, the performance decrease attributed to donor and acceptor absorption grew larger than the increased absorption in the interfacial layer, resulting in a reduction in short-circuit current. The optimal thickness for the interfacial layer was found to be approximately 2 nm.

In all of the previous studies discussed above, the addition of an interfacial layer successfully increased open-circuit voltage or short-circuit current but not both. However, while the study discussed above by Kinoshita *et al.* focused primarily on CuPc as the interfacial material, they also reported a single data point using ZnPc as the interfacial layer. They reasoned that ZnPc was superior to CuPc as an interfacial layer because ZnPc exhibits an increased excited state lifetime. Devices with a 2 nm

ZnPc interfacial layer sandwiched between pentacene and C_{60} exhibited increases in both short-circuit current density and open-circuit voltage. J_{SC} increased from 8.02 mA/cm^2 to 8.75 mA/cm^2 while the V_{OC} increased from 0.38 V to 0.43 V. This is the only report that we are aware of that achieved simultaneous increases in both solar cell parameters. The power conversion efficiency for devices with a 2 nm ZnPc interfacial layer increased from approximately 1.8% to 2%. Unfortunately, EQE measurements for devices with a ZnPc interfacial layer were not reported. Therefore, it is not known from where the increased current originated. The authors imply the improvement in the short-circuit current is likely due to absorption by the interfacial layer while the dissociation of excitons originating in pentacene is kept the same. There is no evidence that either the efficiency of exciton dissociation or the efficiency of separting charge transfer states was increased in these devices.

The previous efforts to add an interfacial layer in organic PVs appear to have suffered from poor materials selection. The interfacial layer thickness in many of the previous devices was also too thick to enhance the separation of the charge transfer state. We seek to add a thin interfacial layer to organic solar cells to enhance the dissociation of excitons into free charges by suppressing the recombination of charges populating the charge transfer state at the donor-acceptor interface. The technical feasibility of this architecture depends on the physics of exciton dissociation and charge transfer state recombination. Therefore, we proceed with a discussion of the physics of these processes in the next section

4.2 Physics of exciton dissociation and charge transfer state recombination

The physics of exciton dissociation and charge transfer state recombination motivate adding a thin interfacial layer to organic heterojunction photovoltaic devices. In this

section, we briefly review the primary physical mechanisms for these processes.

In conventional, inorganic crystalline semiconductors, charge separation upon photoexcitation is not a concern. In those materials, carrier photoproduction is a direct process; free charge carriers are produced immediately upon light absorption. In contrast, photoexcitation in organic semiconductors does not form free charge carriers. Strong carrier localization in organic semiconductor materials prevents excited electrons and holes from escaping from their common Coulomb potential well before thermalization. The excited carriers are trapped by localized states and form Coulombically bound geminate pairs rather than free charges. These electron-hole pairs, also known as excitons, are the primary product of photoexcitation in disordered organic semiconductors. Once created, excitons can recombine or dissociate into free carriers. These processes are described by the Onsager theory of geminate recombination. Using Onsager theory [135], the probability that a thermalized charge pair will escape geminate recombination in the presence of an external electric field, F, is given by [68]:

$$f(r,\theta) = \exp(-A)\exp(-B)\sum_{m=0}^{\infty}\sum_{n=0}^{\infty}\frac{A^m}{m!}\frac{B^{m+n}}{(m+n)!} \tag{4.1}$$

$$A = \frac{q^2}{4\pi\epsilon\epsilon_0 rkT} \tag{4.2}$$

$$B = \frac{qFr}{2kT}(1 + cos\theta) \tag{4.3}$$

where ϵ is the dielectric constant of the disordered organic medium, r is the initial separation distance between the oppositely charged carriers, θ is the angle between the radius vector r and the applied field vector F, and $f(r,\theta)$ is the probability that the charge pair will dissociate as a function of the separation distance and the angle between the external field and the radius vector connecting the electron with the parent ion.

Figure 4-2 illustrates the dissociation probabilities of excitons generated with varying applied electric fields. In this figure, a positive charge is fixed at the origin. At a given field strength, the probability of dissociation is illustrated as a function of initial electron position in both x and y. The applied field is oriented in the x direction. As illustrated, the probability of dissociation is strongly dependent on the electric field strength. Photogenerated excitons in disordered solids are typically confined to a single molecule. Therefore, the initial separation is on the order of 1-2 nm. The typical electric field strength in an organic semiconductor device can be approximated as $E = \frac{V}{d}$ where a typical voltage is 0.5 V and thickness is on the order of 50 nm. Using these values, the field strength is found to be approximately 10^5 V/cm. Figure 4-2, illustrates that with an external field strength of $F = 10^5$ V/cm excitons have a very low probability of dissociation. Even with an applied field strength of $F = 10^6$ V/cm excitons would be unlikely to dissociate efficiently. Unfortunately, this indicates that the applied field strength alone is not strong enough to dissociate excitons into free charges effectively in organic solar cells. Photogenerated excitons instead will typically be lost to recombination.

As discussed in Chapter 2, the challenge of dissociating excitons in disordered organic materials requires the use of a donor-acceptor heterojunction device architecture. If photogenerated excitons reach the interface between the donor and acceptor layers before recombining, the energy level offset between the two materials can promote dissociation via electron transfer. Immediately following electron transfer a charge transfer (CT) state is formed that consists of the electron on an acceptor molecule at the interface and the hole on a donor molecule at the interface. Unfortunately, as discussed below, these two carriers are still partially bound in the CT state.

Electron transfer at the donor-acceptor interface is energetically favorable if the charge transfer state energy is lower than the energy of the exciton in both the donor

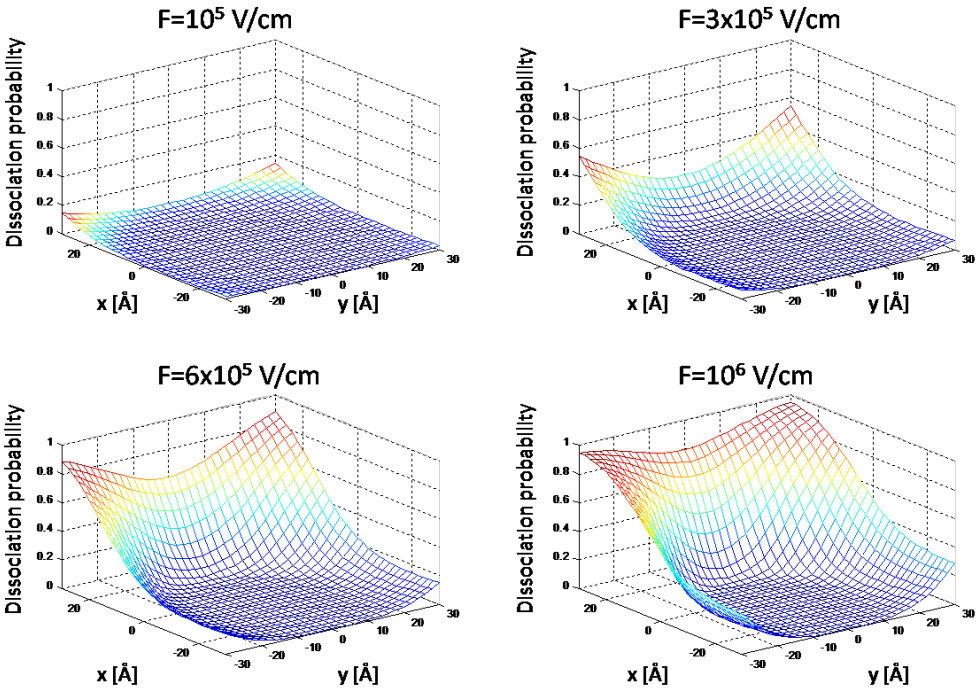

Figure 4-2: Electric field dependence of exciton dissociation. The probability of exciton dissociation is strongly dependent on the electric field strength. The probability of exciton dissociation is plotted as a function of the initial electron position in both x and y for field strengths F of 10^5, 3x10^5, 6x10^5, and 10^6 V/cm respectively. In these plots, a positive charge is assumed fixed at the origin. The applied field is oriented in the x direction. Photogenerated excitons in disordered solids are typically confined to a single molecule. Excitons in these materials are characterized by an initial separation on the order of 1-2 nm.

and acceptor layers. If this condition is not met, exciton transfer from donor to the acceptor (or vice versa) to the lowest energy state is favored. If the charge transfer state is not the lowest energy state at the donor-acceptor interface, the device is unlikely to operate as an efficient solar cell. Electron transfer to a charge transfer state is the critical first step in exciton dissociation.

The process of exciton dissociation via electron transfer from an excited donor molecule to an acceptor molecule to form a charge transfer state can be derived from Fermi's Golden Rule [136]:

$$k_{if} = \frac{2\pi}{\hbar} \left| \langle \psi_i \left| V \right| \psi_f \rangle \right|^2 \rho(E_f) \tag{4.4}$$

where $\langle \psi_i \left| V \right| \psi_f \rangle$ corresponds to the electronic coupling matrix element between states i and f under application of a perturbation V, and $\rho(E_f)$ is the density of final states.

The electron transfer mechanism described here is driven primarily by vibrational motions. The transition occurs so rapidly that the nuclei of the atoms involved can be considered to be stationary during the transition. Therefore, the Franck-Condon approximation can be used and the electron transfer equation can be factored into an electronic and a vibrational contribution:

$$k_{if} = \frac{2\pi}{\hbar} \left| V_{if} \right|^2 (FCWD) \tag{4.5}$$

where $V_{if} = \langle \psi_i \left| V \right| \psi_f \rangle$ is the electronic coupling matrix element and FCWD denotes the Franck-Condon-weighted density of states. Assuming that all the vibrational modes are classical ($\hbar\omega_i < k_B T$) as is true at high temperatures, the FCWD obeys a standard Arrhenius type equation [136]:

$$FCWD = \sqrt{\frac{1}{4\pi k_B T \lambda}} \exp \frac{-(\Delta G^0 + \lambda)^2}{4\lambda k_B T} \tag{4.6}$$

where λ corresponds to the "reorganization" energy, ΔG^0 is the Gibbs free energy or driving force for the reaction, k_B is the Boltzmann constant, and T is the temperature. Using this expression for the density of states, the electron transfer rate takes the form of the semiclassical Marcus theory expression [137]:

$$k_{if} = |V_{if}|^2 \sqrt{\frac{\pi}{\lambda k_B T \hbar^2}} \exp \frac{-(\Delta G^0 + \lambda)^2}{4\lambda k_B T} \tag{4.7}$$

The expression for the rate of electron transfer, Equation 4.7, indicates a number of important features of electron transfer reactions. First, as discussed in [136], a complete understanding of exciton dissociation requires detailed knowledge of the driving force for dissociation (ΔG^0), the electronic coupling between the initial and final state, and the reorganization energy (λ). Quantifying the driving force for dissociation, while still an active area of research, is fairly well understood. Indeed, as discussed below, several groups have now directly measured the energy of the charge transfer state at the donor-acceptor interface in some systems. This energy can be subtracted from the energy of the initial exciton state to approximate the energy difference driving dissociation. Even when direct measurement of the charge transfer state energy is not possible, the energy can be estimated as the difference between the LUMO level of the acceptor and the HOMO level of the donor minus a term corresponding to the Coulomb attraction between the two charges. Mathematically, this is given as [136]:

$$\Delta G^0 = E^{D+} + E^{A-} - E^{D*} - E^A + E_{cb} \tag{4.8}$$

$$\Delta E_{cb} = \sum_D \sum_A \frac{q_D q_A}{\epsilon_s r_{DA}} \tag{4.9}$$

where E^{D*} and E^{D+} represent the total energies of the isolated donor in the equilibrium geometries of the lowest excited state and of the cationic state respectively, E^A and E^{A-} represent the total energies of the isolated acceptor in the equilibrium

geometries of the ground state and of the anionic state respectively, q_D and q_A correspond to the atomic charges on the donor and the acceptor respectively, r_{DA} is the charge transfer state separation distance, and ϵ_s is the static dielectric constant of the medium.

Unfortunately, the electronic coupling between molecules in a solid state, thin film device is difficult to measure given current experimental tools. The electronic coupling matrix element is determined, in part, by the overlap of the initial state and final state wavefunctions. Therefore, the electronic coupling term can be impacted by the specific alignment of molecules at the donor-acceptor interface. In many cases, the quantities are also impacted by conformational changes that occur when different molecules are brought into close proximity as at the donor-acceptor interface in organic PV. Calculations of electronic coupling between molecules typically require quantum chemical calculations [138]. Much attention has been given to estimating the electronic couplings associated with electron transfer reactions in organic materials [139]. Rates of recombination and charge transfer state separation are sensitive to the extent of the wavefunctions of the electron and hole on either side of the junction [140].

The reorganization energy is also difficult to measure experimentally. The reorganization energy consists of both intramolecular and intermolecular components. The intramolecular component corresponds to changes in the geometry of individual molecules before and after electron transfer. The intermolecular component refers to changes in the polarization of the surrounding molecules before and after the change in state. The intramolecular component of the reorganization energy can be estimated using density functional theory calculations [141]. The intermolecular component of the reorganization energy is difficult to calculate in nonpolar systems. However, the reorganization energy is expected to be relatively consistent for all organic semiconductor materials. Therefore, it is unlikely to change dramatically with

the introduction of an interfacial layer.

4.2.1 Electron transfer calculations

One calculation of particular relevance to small molecule organic solar cells was reported by Yi *et al.* [141, 136]. They calculated electron transfer and charge recombination rates at the donor-acceptor interface in pentacene/C_{60} solar cells [141]. They performed calculations for several pentacene/C_{60} spatial configurations, corresponding to different interface morphologies. For example, the pentacene chain can be oriented perpendicular or parallel to the C_{60} molecule. The intermolecular distance, lateral displacement along the pentacene chain, and the pentacene rotation angle with respect to the C_{60} molecule can also be varied. As discussed above, in performing these calculations three quantities are critical: (i) the electronic coupling between states, (ii) the reorganization energy, and (iii) the total change in energy between the initial and final state. The results of the calculations confirmed that the electronic coupling between states is dependent on the molecular configuration; the morphology at the donor-acceptor interface is likely to have a significant impact on the rates of exciton dissociation and recombination. The calculations also yielded an exponential dependence on intermolecular distance: as the distance between the molecules increases, the electronic coupling, corresponding to the molecules' wavefunction overlap, decreases. The authors estimated the overall reorganization energy to be approximately 0.5 eV and calculated the rates for electron transfer and charge recombination. The results of these calculations are illustrated in Figure 4-3 [141]. As illustrated, the charge recombination rates are consistently lower than charge transfer rates for this material system. Also, both the charge transfer and the charge recombination rates fall quickly as the intermolecular distance d_i is increased.

Brédas and colleagues have also calculated the electron transfer and charge re-

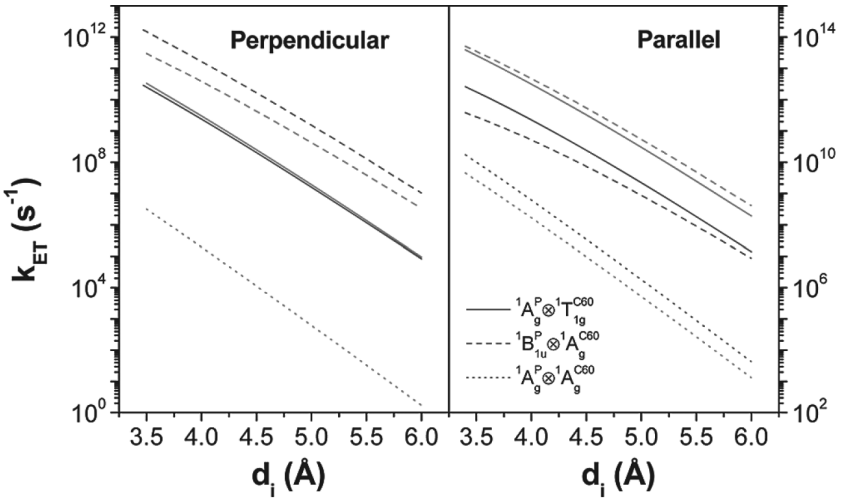

Figure 4-3: Charge transfer and charge recombination rates in pentacene/C_{60} solar cells. The rates of charge transfer from excitons to charge transfer states in pentacene/C_{60} solar cells are illustrated for parallel and perpendicular molecular configurations as a function of intermolecular distance d_i. (Solid and dashed lines correspond to charge transfer.) Charge recombination rates from charge transfer states to the ground state are also illustrated. (Dotted lines correspond to charge recombination.) Charge recombination rates are consistently lower than charge transfer rates for this material system. Adapted from [141].

combination rates at the donor-acceptor interface in a dimer of phthalocyanine (Pc) and perylene bisimide (PTCDI) [136]. The calculations indicate that while the rate of electron transfer is consistently higher than the rate of charge recombination, this difference was sensitive to the dielectric constant of the medium. The ratio of the dissociation rate constant to the recombination rate constant, k_{dis}/k_{rec}, was found to vary from 45 at $\epsilon = 3$ to 2.5 at $\epsilon = 5$. Charge recombination becomes more important as the polarity of the medium is increased. The results also indicated very different values for the electronic coupling, V_{if}, for exciton dissociation and charge recombination. V_{if} was calculated to be 447 cm^{-1} for exciton dissociation and 1600 cm^{-1} for charge recombination at $\epsilon = 3$. The results confirm that the electronic coupling terms can make important contributions to rates of exciton dissociation and charge recombination.

However, the calculations also indicate that charge transfer states at the donor-acceptor interface are often strongly bound due to Coulomb attraction between the two charges [136, 141]. The binding energy for the charge transfer states is calculated to be several tenths of an electron volt, far larger than kT. Exciton dissociation occurs rapidly and efficiently. However, the charges then become trapped in bound charge transfer states. The calculations indicate that organic solar cells fabricated from pentacene/C_{60} and Pc/PTCDI should not be capable of efficiently separating photogenerated excitons.

4.2.2 Experimental studies of exciton dissociation

Exciton dissociation and the separation of charge transfer states in organic solar cells has also been studied experimentally. Initial exciton dissociation to populate a charge transfer state has been shown to occur rapidly, on the order of 10-50 fs, in a variety of material systems [142, 143, 144]. However, the separation of the charge transfer state is not well understood. Recently the Coulomb binding energies of charge transfer

excitons were measured using time-resolved two-photon photoemission spectroscopy [41]. Coulomb binding energies of up to 0.43 eV, far larger than kT, were measured for CT excitons formed on a crystalline pentacene surface.

The theoretical calculations and experimental results discussed above indicate that the initial separation of charges after exciton dissociation would have to be very large in organic heterojunction solar cells to overcome Coulomb binding. The theory of exciton dissociation discussed above does not support a sufficient initial separation of the charges. Therefore, charge transfer states formed after the initial dissociation of an exciton are predicted to predominantly decay by non-radiative recombination or light emission. However, efficient charge separation has been demonstrated in a variety of electronic devices, including devices fabricated using the materials discussed in the theoretical calculations above [145].

There have been several attempts to quantify the efficiency of charge separation. A total efficiency of charge transfer and separation of 78% was measured in a copolymer blend using time-correlated single photon counting (TCSPC) [146]. A charge transfer state dissociation efficiency of 60% was calculated in a polymer blend solar cell by formulating a model for device operation based on Onsager's theory [147]. A similar model indicated that at open-circuit voltage nearly all photogenerated charge carriers are lost to recombination [148]. The illumination intensity dependence of the photocurrent indicated negligible recombination in a bulk heterojunction solar cell comprised of poly-3(hexylthiophene) (P3HT) and methanofullerene (PCBM) [149]. Finally, bulk heterojunction devices exhibiting near 100% internal quantum efficiency were recently demonstrated [66].

Interfacial charge transfer states have also been probed directly in bulk heterojunction solar cells using Fourier-transform photocurrent spectroscopy (FTPS) [150]. Features in the absorption spectra of polymer-fullerene blends were identified that were inaccessible in the spectra of both the materials individually. These below-

gap absorption features were only found for blends and were modulated by changing the morphology and relative material concentrations in the blend. These absorption bands were also found in the external quantum efficiency spectrum for these devices, indicating that directly photoexcited charge transfer states can dissociate to form free charges, contributing to photocurrent [42]. Furthermore, the V_{OC} for a series of polymer-PCBM solar cells was found to scale linearly with the charge transfer state energy. The photophysics of below-gap excitations of polymer-fullerene solar cells were also recently described [43]. Efficient generation of free charges following below-gap, charge transfer state excitation was demonstrated. Finally, charge transfer states have also been studied via photoluminescence (PL) [44] and electroluminescence measurements (EL) [45]. PL measurements indicated that the binding energy of charge transfer states in MDMO-PPV/PCBM solar cells is approximately 130 meV [44]. EL measurements were found to be a simple and efficient way to characterize the energetics of the CT states in some material systems [45]. The V_{OC} under solar illumination was found to vary linearly with the CT state EL peak position in a number of different polymer bulk heterojunction solar cells.

4.2.3 Proposed mechanisms for charge transfer state separation

Several mechanisms have been proposed that might explain the separation of the bound polaron pairs at the donor-acceptor interface into free carriers that has been observed experimentally. First, interface dipoles between the donor and acceptor layers in polymer solar cells could play a role in dissociating charge transfer states [37]. Immediately after the initial electron transfer from the exciton state, an effective energy barrier for the hole could be formed on the polymer chain nearest to the interface due to zero-point oscillation of the hole on the donor polymer chain. When the hole is transferred to the next polymer chain away from the donor-acceptor interface this

barrier separates the two Coulombically bound charges, reducing the probability of geminate recombination. Unfortunately, this explanation is dependent on a specific molecular morphology at the donor-acceptor interface and may not be widely applicable. This model has also been criticized [38] since it requires that the hole effective mass along the polymer chain be less than one tenth the rest mass of an electron, a condition that is unrealistic in organic semiconductor materials. The theory also fails to explain efficient exciton dissociation in devices comprising small molecules as both donor and acceptor materials.

Peumans and Forrest [38] propose an explanation for efficient exciton dissociation based on the Onsager model. They suggest that the donor-acceptor interface confines the electron and hole to the layer in which they reside. This confinement limits recombination since the volume available for electron-hole recombination is reduced relative to that described in the original Onsager theory. Furthermore, the donor-acceptor interface orients the charge transfer state, favoring charge separation perpendicular to the interface plane. Finally, if the materials at the interface have different carrier mobilities, they suggest that that charge in the material with the greater mobility will sample a far larger volume of space prior to the opposite charge reaching the interface where it can recombine. It was suggested that these features of the donor-acceptor interface in organic PVs explain the observations of higher efficiency exciton dissociation and charge transfer state separation than might otherwise be expected.

It has also been proposed that impurity doping in organic solar cells focuses the voltage drop across the devices at the donor-acceptor interface [39]. Unidentified impurities were found to significantly increase the performance of bilayer devices. It was proposed that dopants in each layer could yield a strong electric field at the exciton dissociation interface. As discussed above, the dissociation probability of excitons increases with field strength. Modifying the electric field across the exciton separation interface via semiconductor doping could reduce recombination of charge

transfer states.

Janssen and colleagues have pointed to the possible role of disorder [40]. They study the evolution of the charge transfer state using transient absorption spectroscopy. The dynamic behavior of the charge transfer state can be studied by monitoring changes in the absorption band of the materials in the spectral region where the charge transfer state absorbs. They propose that molecular disorder and defects at the donor-acceptor interface create energetic disorder among different local sites in the bulk. The energetic disorder causes carriers to migrate away from the interface to sites of lower local energy. The migration of carriers to sites of lower energy, enabled by disorder, compensates for the Coulomb attraction and allows for efficient recombination.

Finally, the separation of the charge transfer state populated immediately following exciton dissociation could occur prior to the thermalization of the polaron pair. The excess energy associated with the exciton state could assist in the separation of charge transfer states [41]. Similarly, it has been suggested that changes in local polarization of the medium prior to relaxation could promote charge transfer state separation [151]. Similar models have been suggested to explain exciton dissociation in conjugated polymers [152]. In polymers, it has been suggested that excess photon energy above the exciton energy is converted into the vibrational heat bath of a polymer segment. This excess vibrational energy could give the carriers sufficient energy to dissociate fully. The field and temperature dependence of carrier photogeneration in conjugated polymers has been demonstrated to be consistent with this model [153]. Correlation has also been observed in polythiophene/PCBM blends between the free energy difference for exciton dissociation and the efficiency of charge separation using transient absorption spectroscopy [154]. These results are consistent with the theory of hot exciton dissociation.

It is not yet clear which of the mechanisms discussed above may contribute to

the charge transfer state separation that has been observed experimentally in organic photovoltaics. However, while some charges are separated fully in organic solar cells, recombination of the charges populating interfacial charge transfer states remains a major loss mechanism. In the device architecture demonstrated in this chapter, excitons dissociate to form charge transfer states at the donor-interfacial layer or acceptor-interfacial layer interfaces. However, when the interfacial layer is thin, charge transfer state dissociation is promoted as the charge on the interfacial layer is immediately adjacent to lower energy states in either the donor (hole) or acceptor (electron) layers. The charge on the interfacial layer rapidly electron transfers to the other semiconductor layer, populating a more spatially extended charge transfer state across the interfacial layer. The Coulombic binding between the two charges is reduced in this second extended charge transfer state. The reduced binding energy between the charges is expected to suppress charge recombination. Therefore, we expect the efficiency of separating excitons originating in both the donor and acceptor layers to increase. In the next section, we fabricate devices to test the impact of adding an interfacial layer to organic solar cells.

4.3 Devices with interfacial layers

We add a thin interfacial layer to organic solar cells based on two different donor-acceptor heterojunctions. First, we fabricate devices utilizing 4,4',4"-tris-(2-methylphenyl phenylamino) triphenylamine (m-MTDATA) and 3,4,9,10-perylenetetracarboxylic bis-benzimidazole (PTCBI) as the donor and acceptor materials, respectively. m-MTDATA and PTCBI do not form a high performance organic solar cell. However, the wide band gap of m-MTDATA allows us to clearly identify the impact of adding an interfacial layer. m-MTDATA's wide electronic bandgap ensures we achieve a cascade energy level alignment for excitons generated in both the donor and acceptor

layers, despite significant uncertainty in LUMO energy levels. These devices serve as a proof of concept for the device architecture. Second, we add an interfacial layer to organic solar cells using the donor material CuPc and the acceptor material C_{60}. CuPc and C_{60} are two of the most common organic semiconductor solar cell materials.

In the experimental sections that follow all organic materials were purified by vacuum thermal sublimation prior to use and all materials were deposited by thermal evaporation at $\sim 10^{-6}$ Torr. All active device areas were 0.02 cm^2. Current density-voltage ($J-V$) characteristics for devices with and without an interfacial layer were measured under 1 sun AM1.5G illumination (1000 W/m^2) using a solar simulator (Newport Oriel Model 91191). The illumination intensity at the devices was calibrated using a broadband power meter. External quantum efficiency (EQE) measurements were made using a xenon lamp with a monochromator, chopped at $f = 90$ Hz, and measured using a lock-in amplifier. Light intensity was measured with a calibrated silicon photodiode.

4.3.1 m-MTDATA/PTCBI devices with an interfacial layer

LUMO levels in organic semiconductors are notoriously difficult to measure with accuracy; uncertainties in LUMO measurements are often 0.5 eV or higher [155]. Unfortunately, in state-of-the-art organic solar cells, the difference between donor and acceptor LUMO levels is only ~ 0.5 eV. Therefore, it would be difficult in these devices to have certainty regarding the energy cascade at the interface with an interfacial layer. In order to prove the concept of using an interfacial layer, we first fabricate devices employing a wide band gap donor material. The large gap between the LUMO levels of the donor and acceptor layers allows us to choose an interfacial layer that we know will create the desired energy cascade for all excitons, despite the uncertainties in LUMO levels.

We fabricate devices utilizing m-MTDATA (HOMO = 5.1$\pm$0.15 eV; LUMO =

2.0±0.5 eV) [156] and PTCBI (HOMO = 6.2±0.15 eV; LUMO = 3.6±0.5 eV) [157] as the donor and acceptor materials, respectively. m-MTDATA's wide bandgap prevents it from absorbing solar radiation effectively. Therefore, it is not an attractive solar cell material. However, m-MTDATA has commonly been used in organic light emitting diodes making it a well studied material and a good candidate for the initial proof of concept devices. m-MTDATA's wide bandgap ensures we achieve the desired interfacial energy cascade between the donor and acceptor materials for all photogenerated exciton even with significant uncertainty in the LUMO energy levels. To achieve the desired energy cascade between m-MTDATA and PTCBI we desire a material with a LUMO level between 2.0 eV and 3.6 eV and a HOMO level between 5.1 eV and 6.2 eV. The dye material tetraphenylnapthacene (rubrene) (HOMO = 5.36±0.15 eV; LUMO = 3.15±0.5 eV) [158], the same dye material we used in the previous chapter, has the correct energy level alignment. The energy level diagram for these devices is illustrated in Figure 4-4.

We fabricate devices with the following structure: glass/indium tin oxide (ITO, 160 nm)/m-MTDATA (25 nm)/rubrene (x nm)/PTCBI (25 nm)/bathocuproine (BCP, 9 nm)/Ag (60 nm). The rubrene interfacial layer thickness is varied 0.5 nm $< x <$ 10 nm. We also fabricate devices with no interfacial layer as a control. We model absorption in these devices using a transfer matrix formulation [70] and find the thin interfacial layers utilized here have a negligible impact on the electric field distribution within these devices. Changes in absorption in the donor and acceptor layers are negligible.

Current density-voltage curves for m-MTDATA/PTCBI solar cells with different rubrene interfacial layer thicknesses are illustrated in Figure 4-5. Devices with no interfacial layer exhibit a short-circuit current density, J_{SC}, of 0.19 mA/cm^2, an open-circuit voltage, V_{OC}, of 0.51 V, and a fill factor, FF, of 0.34. The power conversion efficiency of the control devices is calculated to be 0.033%. When a thin interfacial

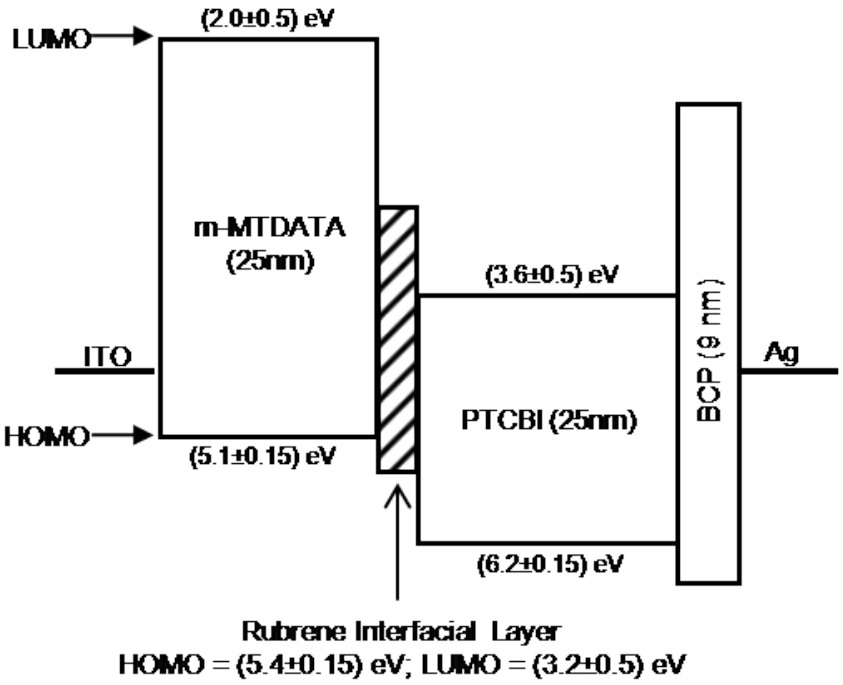

Figure 4-4: Device structure for m-MTDATA/PTCBI solar cells with an interfacial layer. Rubrene is employed as the interfacial layer between wide-bandgap donor material m-MTDATA and acceptor material PTCBI. The device structure is: glass/indium tin oxide (ITO, 160 nm)/m-MTDATA (25 nm)/rubrene (x nm)/PTCBI (25 nm)/bathocuproine (BCP, 9 nm)/Ag (60 nm). The rubrene interfacial layer thickness is varied 0.5 nm $< x <$ 10 nm. Energy levels are available in the literature [156, 157, 158].

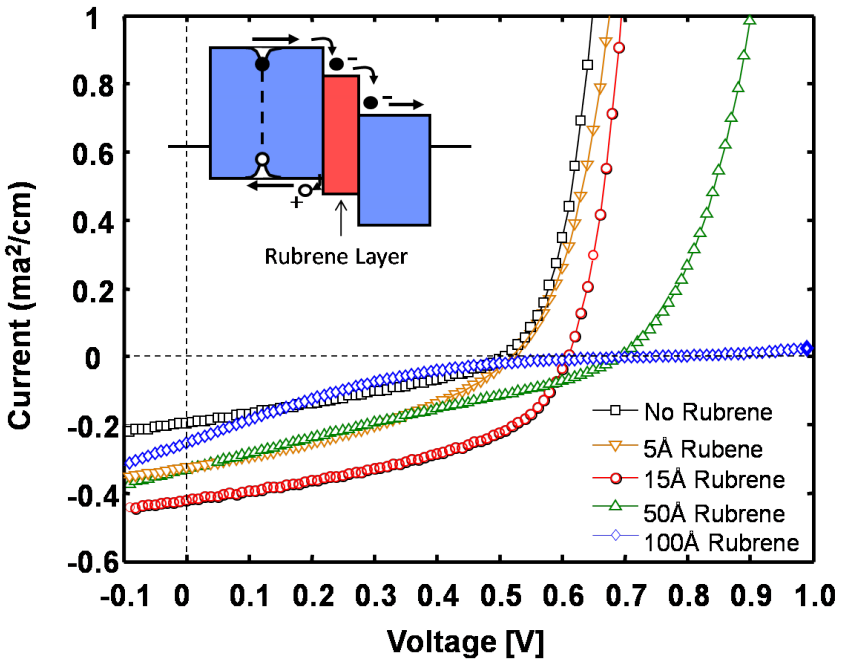

Figure 4-5: Current density-voltage (J-V) characteristics for m-MTDATA/PTCBI solar cells with an interfacial layer. Devices with thin interfacial layers exhibit increases in both short-circuit current and open-circuit voltage. As the interfacial layer thickness increases, the open-circuit voltage continues to increase but the short-circuit current decreases. The shape of the curves indicate series resistance becomes significant as the interfacial layer thickness increases.

layer of rubrene is introduced the J_{SC}, V_{OC}, and FF all increase. Devices with a 1.5 nm rubrene layer exhibit $J_{SC} = 0.41$ mA/cm^2, $V_{OC} = 0.61$, and $FF = 0.45$. The photocurrent increases 126% compared to the control devices, a remarkable increase given the relatively small change to the device structure. The power conversion efficiency for devices with a 1.5 nm thick rubrene interfacial layer is calculated to be 0.112%, representing a 239% improvement over the control devices.

As the thickness of the interfacial layer is increased beyond 1.5 nm, the V_{OC} continues to increase linearly, as illustrated in Figure 4-6. However, the J_{SC} and FF both decrease as the thickness of the rubrene interfacial layer increases beyond 1.5 nm. As a result, the power conversion efficiency also decreases. The optimal thickness for a rubrene interfacial layer sandwiched between m-MTDATA and PTCBI is found to

be ∼1.5 nm. This layer thickness corresponds to approximately one monolayer of the interfacial material. Unfortunately, the interfacial layer is likely to be discontinuous for thin layers. Therefore, we are likely not improving the performance of the device uniformly throughout its area. We have not measured the spatial performance of the device. However, it might be possible to achieve even higher increases in performance with a continuous thin interfacial layer.

Next, we measure the external quantum efficiency (EQE) of m-MTDATA/PTCBI solar cells with a thin rubrene interfacial layer. EQE measurements enable us to identify the origin of the the short-circuit current enhancement identified in the J-V characteristics. Figure 4-7 shows the EQE for devices with three different rubrene thicknesses as a function of wavelength. The control device EQE is characterized by two primary absorption peaks. PTCBI absorbs broadly in the region 450 nm $< \lambda <$ 700 nm while m-MTDATA absorption is characterized by a well defined peak 325 nm $< \lambda <$ 400 nm. The orthogonal absorption spectrums of these materials enables us to straightforwardly identify the origin of the short-circuit current improvement.

As illustrated in Figure 4-7, with a 1.5 nm rubrene interfacial layer the photocurrent is enhanced for excitons generated in both m-MTDATA and PTCBI. However, the rubrene interfacial layer also absorbs a portion of the incident light. Rubrene exhibits three closely spaced absorption peaks in the region 450 nm $< \lambda <$ 550 nm. These features are easily discerned in the EQE data for devices with a 10 nm interfacial layer. However, rubrene does not absorb in the region 325 nm $< \lambda <$ 400 nm where m-MTDATA absorbs most strongly. Similarly, rubrene does not absorb at wavelengths $\lambda >$ 600nm. PTCBI absorption extends into the region $\lambda >$ 600nm. Figure 4-7 shows an increase in EQE across the entire visible spectrum, despite rubrene absorbing only over the region 450 nm $< \lambda <$ 550 nm. The quantum efficiencies associated with only PTCBI absorption ($\lambda >$ 600nm) and m-MTDATA absorption (325 nm $< \lambda <$ 400 nm) also increase. This indicates that the increased performance

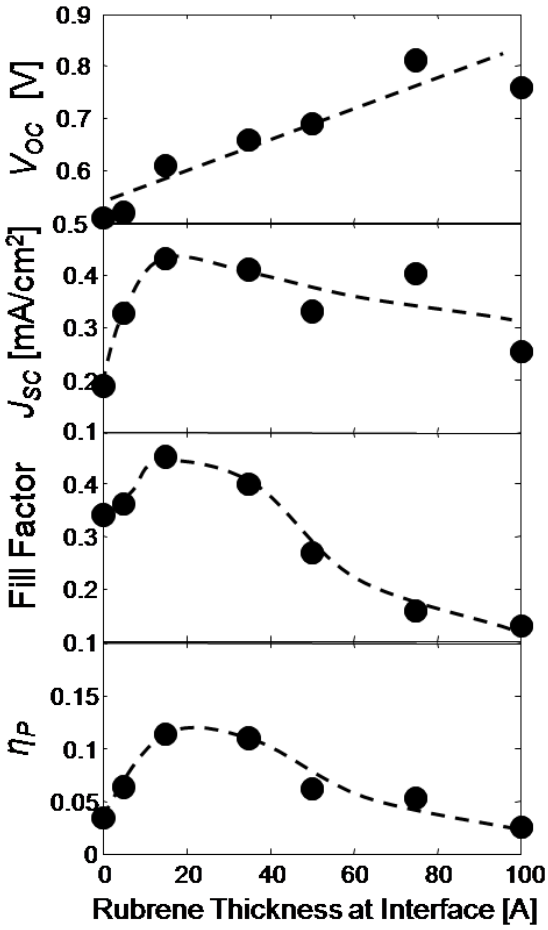

Figure 4-6: Performance parameters of m-MTDATA/PTCBI solar cells with an interfacial layer as a function of interfacial layer thickness. The V_{OC} increases linearly with interfacial layer thickness. The J_{SC} is observed to more than double with thin interfacial layers. However, J_{SC} decreases as the interfacial layer is further increased. The fill factor also increases with thin interfacial layers. The fill factor decreases for devices with a thick interfacial layer. The power conversion efficiency, η_P, increases for thin interfacial layers but then decreases as the interfacial thickness increases further.

is not simply due to light absorption in the rubrene layer. The EQE increases for excitons originating in both the donor and acceptor layers.

However, similar to the trends observed in the J-V characteristics above, as the thickness is increased further, the short-circuit current enhancement falls. When a 10 nm interfacial layer is introduced, the EQE associated with PTCBI returns to the same level found for devices with no interfacial layer while the EQE for excitons generated in m-MTDATA falls to below that for the control device. The differences in the reduction in performance with a thick interfacial layer is likely explained by the different charge carrier mobilities in rubrene. As the thickness of the interfacial layer is increased, excitons separate across either the donor-interfacial layer or acceptor-interfacial layer interfaces. With thick interfacial layers, the charge transfer state is not impacted by the energy cascade structure. The charge on the interfacial layer does not immediately see the lower energy state in the opposite semiconductor material from where it originated. Therefore, the charge transfer state must separate as usual followed by carrier diffusion through first the interfacial layer and then the opposite semiconductor. Relatively high hole mobilities have been measured in rubrene thin films [159]. Therefore, holes originating from excitons in the PTCBI acceptor layer can likely reach the donor layer without significant recombination. Electrons originating from excitons in the m-MTDATA donor layer are likely not transported through thick rubrene interfacial layers efficiently, leading to lower performance on that side of the device.

We isolate the contributions to EQE from each of the three light absorbing materials by scaling the absorption for each material within the devices to fit the EQE data. Figure 4-8 illustrates the modeling results for a typical m-MTDATA/PTCBI device. In order to fit the EQE curves we selected a single fit parameter for each layer, corresponding to the efficiency of exciton dissociation in each layer. A unique set of the three fit parameters (one for each layer) fit the dataa best in each case.

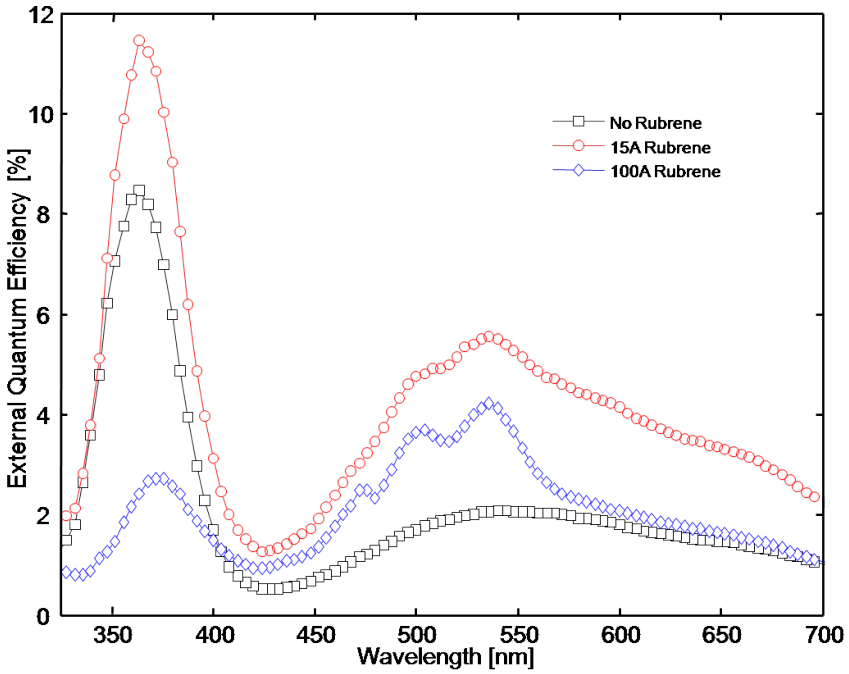

Figure 4-7: External quantum efficiency (EQE) for m-MTDATA/PTCBI devices with an interfacial layer. The control device EQE (black squares) is characterized by two primary absorption peaks. PTCBI absorbs broadly in the region 450 nm $< \lambda <$ 700 nm while m-MTDATA absorption is characterized by a well defined peak 325 nm $< \lambda <$ 400 nm. The orthogonal absorption spectrums of these materials enables the identification of the origin of the short-circuit current improvement. With a 1.5 nm rubrene interfacial layer (red circles) the photocurrent is enhanced for excitons generated in both m-MTDATA and PTCBI. Rubrene absorption in the range 450 nm $< \lambda <$ 550 nm is apparent in devices with a 10 nm interfacial layer (blue diamonds).

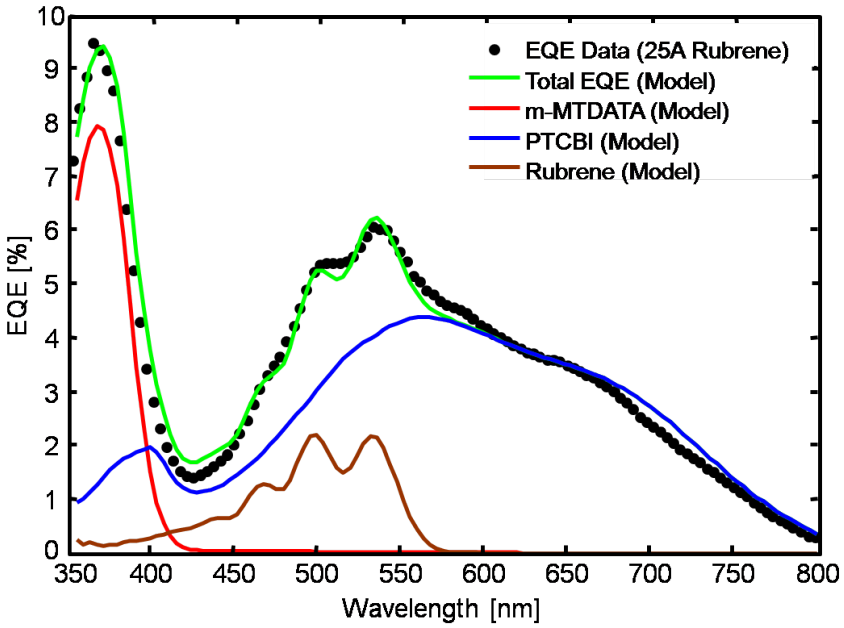

Figure 4-8: Identification of the donor and acceptor layer contributions to external quantum efficiecy (EQE) in m-MTDATA/PTCBI devices with an interfacial layer. The black dots represent EQE data for m-MTDATA/PTCBI solar cells with a 25 Årubrene interfacial layer. The contributions to EQE originating from excitons in m-MTDATA (red line), PTCBI (blue line), and rubrene (brown line) are illustrated. The sum of the three individual contributions, representing the total EQE, is illustrated by the green line. The model achieves a good fit to the device data. Separately, we have performed the same analysis illustrated here for all of the devices fabricated with a rubrene interfacial layer.

The unique fit to the measured EQE curves indicates that the model is successful at separating the EQE contributions for excitons generated in each layer.

Figure 4-9 plots the maximum EQE contributions from the m-MTDATA donor layer and the PTCBI acceptor layer as a function of the thickness of the interfacial layer. The efficiency of exciton dissociation and charge transfer state separation is greatest with an interfacial thickness of approximately 1.5 nm. Relative to the control devices, the maximum EQE in the m-MTDATA layer increased from 2.0% to 4.3% with a 1.5 nm thick interfacial layer. Likewise, the maximum EQE in the PTCBI layer increased from 7.3% to 10.1% with a 1.5 nm thick interfacial layer. As the thickness of the interfacial layer is increased beyond 1.5 nm, the maximum EQE decreases in

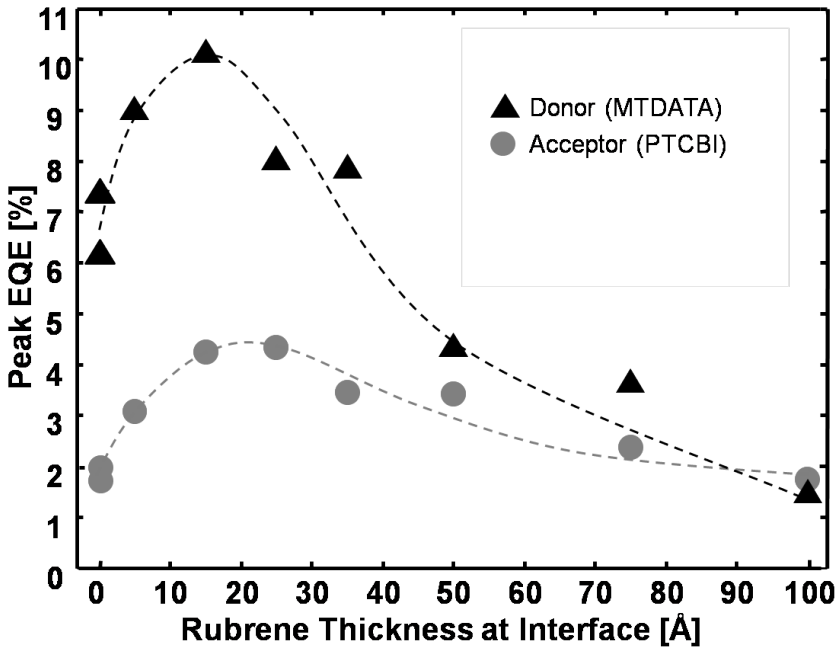

Figure 4-9: Interfacial layer thickness dependence of donor and acceptor contributions to external quantum efficiency (EQE) in m-MTDATA/PTCBI devices. Following the model methodology discussed in the text, the maximum EQE contributions from the m-MTDATA donor (black triangles) and PTCBI acceptor (silver circles) layers are plotted as a function of interfacial layer thickness. The efficiency of dissociating excitons from both layers is enhanced with thin rubrene interfacial layer thicknesses. The dashed lines serve as a guide to the eye.

both the donor and acceptor layers, as expected from the J-V characteristics. The maximum EQE for excitons originating in the m-MTDATA and PTCBI layers falls to 1.7% and 1.4% respectively with a 10 nm rubrene interfacial layer.

The results of adding an interfacial layer to m-MTDATA/PTCBI solar cells appear promising. Introducing a rubrene interfacial layer increases the power conversion efficiency by up to 239% compared to devices without an interfacial layer. The results match the theory developed above and indicate that a cascade energy structure at the donor-acceptor interface can facilitate separation of the charge transfer state formed immediately following exciton dissociation. Ultimately, devices comprised of m-MTDATA and PTCBI as the donor and acceptor materials respectively are poor solar cells. Even with the dramatic efficiency improvement achieved here, the per-

formance of these devices is unimpressive. The wide bandgap nature of m-MTDATA yields poor overlap with the solar spectrum. Therefore, we next seek to apply this concept to standard organic solar cells.

4.3.2 CuPc/C_{60} devices with an interfacial layer

To demonstrate that the interfacial layer architecture can successfully be applied to higher performance organic solars cells we next add an interfacial layer to a conventional copper phthalocyanine (CuPc)-fullerene (C_{60}) heterojunction solar cell. Organic PVs based on CuPc and C_{60}, common in the literature, are among the best small-molecule devices demonstrated to date [64]. We fabricate devices with the structure illustrated in Figure 4-10. The energy levels for CuPc (HOMO = 5.2±0.15 eV; LUMO = 3.4±0.5 eV) and C_{60} (HOMO = 6.4±0.15 eV; LUMO = 4.0±0.5 eV) are found in the literature [160, 161, 162]. We concentrate on two interfacial layer materials: chloro aluminum phthalocyanine (ClAlPC; HOMO = 5.40.15 eV; LUMO = 3.70.5 eV) and titanium oxide phthalocyanine (TiOPC; HOMO = 5.7±0.15 eV; LUMO = 3.9±0.5 eV).

The device structures fabricated are the following: indium tin oxide (ITO) (160 nm)/CuPc (20 nm)/ClAlPC or TiOPC (x nm)/C_{60} (40 nm)/BCP (9 nm)/Ag (60 nm), where the thickness of the interfacial layer is varied 1 nm $< x <$ 4.5 nm. Figure 4-10 illustrates the energy level alignments for these devices. As before, the interfacial layer materials have been selected to create an energy cascade structure at the charge separation interface for excitons originating in both the donor and acceptor layers.

The J-V characteristics for devices with a ClAlPC interfacial layer are shown in Figure 4-11. There are two important changes as the thickness of the interfacial layer is increased. First, as the thickness of the interfacial layer is increased, the open-circuit voltage (V_{OC}) under illumination increases linearly from 0.43 V with no interfacial

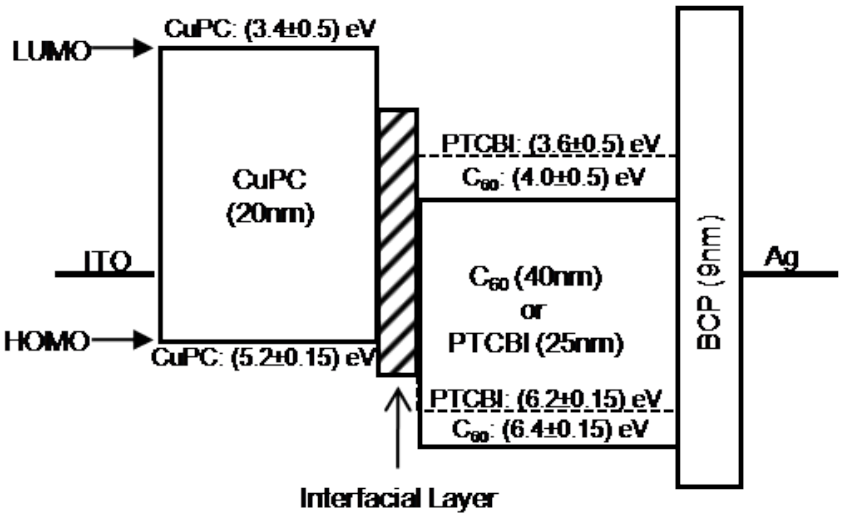

Figure 4-10: Energy level schematic for CuPc/C_{60} and CuPc/PTCBI devices with an interfacial layer. Thin interfacial layers of either ClAlPC or TiOPC are inserted between the donor and acceptor semiconductor layers to provide a multistep electron transfer cascade for exciton dissociation. The interfacial layer destablizes charge transfer states at the donor-acceptor interface.

layer to 0.57 V with a 4.5 nm interfacial layer. This effect has been demonstrated previously [127] and is believed to be due to a reduction in charge recombination with a corresponding decrease in dark current. Second, devices with an interfacial layer exhibit an increase in photocurrent from 4.4 mA/cm^2 to 5.9 mA/cm^2 with the introduction of a 1.5 nm interfacial layer. The photocurrent then decreases as the interfacial layer thickness is increased. The power conversion efficiency of the CuPc/C_{60} PVs increases from 1.10% for the control device with no interfacial layer to 1.64% with a 1.5 nm interfacial layer, decreasing to 1.53% for a 4.5 nm interfacial layer.

The EQE as a function of wavelength for devices with a ClAlPC interfacial layer is shown in Figure 4-12a. CuPc and C_{60} absorb light in distinct portions of the visible spectrum; C_{60} dominates the absorption of the device in the range 380 nm $< \lambda <$ 550 nm while CuPc dominates the absorption in the range 550 nm $< \lambda <$ 700 nm. ClAlPC absorbs primarily in the range 700 nm $< \lambda <$ 800 nm. Therefore, as

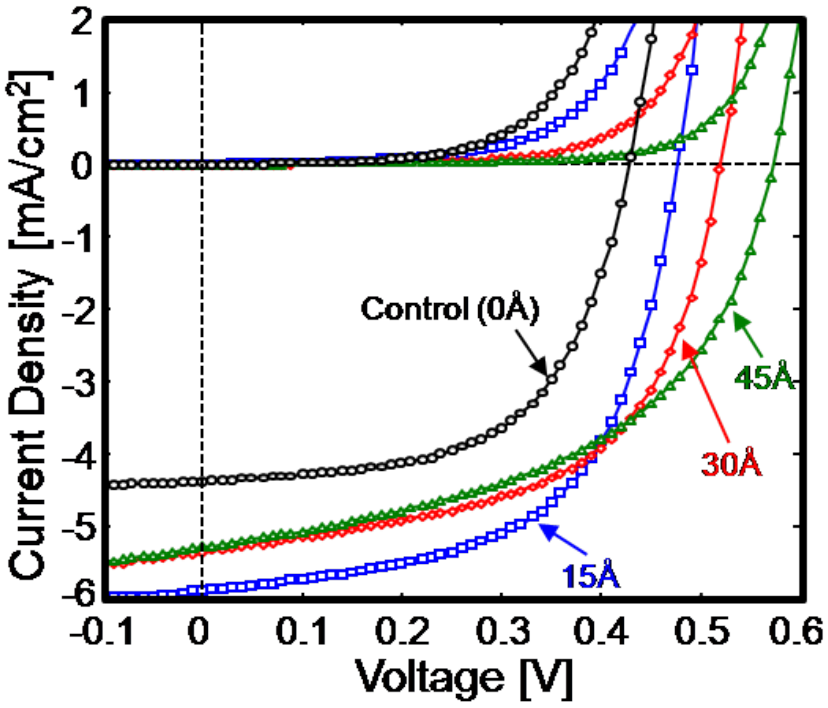

Figure 4-11: Current density-voltage (J-V) characteristics for CuPc/C_{60} devices with ClAlPC interfacial layers. The control devices (black circles) have no interfacial layer. The insertion of a thin 1.5 nm interfacial layer (blue squares) increases the short-circuit current and the open-circuit voltage. As the thickness of the interfacial layer is further increased to 3 nm (red diamonds) and 4.5 nm (green triangles) the open-circuit voltage increases but the short-circuit current decreases.

before, the EQE measurements can be used to understand the origin of the device performance improvements upon insertion of the thin layer of ClAlPC. The effect observed here is for very thin interfacial layers and any change in light absorption in the donor and acceptor layers is negligible.

The EQE spectrum demonstrates that the improvement in J_{SC} observed in the current-voltage characteristics was primarily due to increased EQE from excitons generated in C_{60}. The EQE associated with C_{60} absorption (380 nm $< \lambda <$ 550 nm) increases from 28% at $\lambda = 452$ nm with no interfacial layer to 45% at $\lambda = 452$ nm with a 1.5 nm interfacial layer. As the thickness of the interfacial layer increases further, the EQE associated with C_{60} absorption decreases. The EQE associated with CuPc absorption decreases slightly with the introduction of an interfacial layer. Finally, the observed peak in EQE in the range 700 nm $< \lambda <$ 800 nm is due to direct absorption by the ClAlPC layer [163].

The EQE versus interfacial layer thickness for devices with ClAlPC and TiOPC interfacial layers at selected wavelengths is shown in Figure 4-12b. $\lambda = 452$ nm corresponds to C_{60} absorption while $\lambda = 624$ nm corresponds to CuPc absorption. TiOPC has similar energy levels to ClAlPC and TiOPC interfacial layers yield similar efficiency trends when added to CuPc/C_{60} solar cells. The optimal interfacial layer thickness is found to be approximately 1.5 nm for both materials. However, the CuPc performance does not appear to be improved using these interfacial layer materials. As described above, LUMO measurements typically have high uncertainty. Unfortunately, this means we cannot know with certainty that the devices fabricated here actually have the desired energy cascade for excitons originating in the CuPc layer. This likely explains the lack of improvement in the CuPc EQE. Alternatively, it is possible that poor electron mobility in the interfacial layer accounts for the lack of improvement in charge generation from CuPc excitons. However, this explanation is unlikely given no increase in performance is found even for very thin interfacial

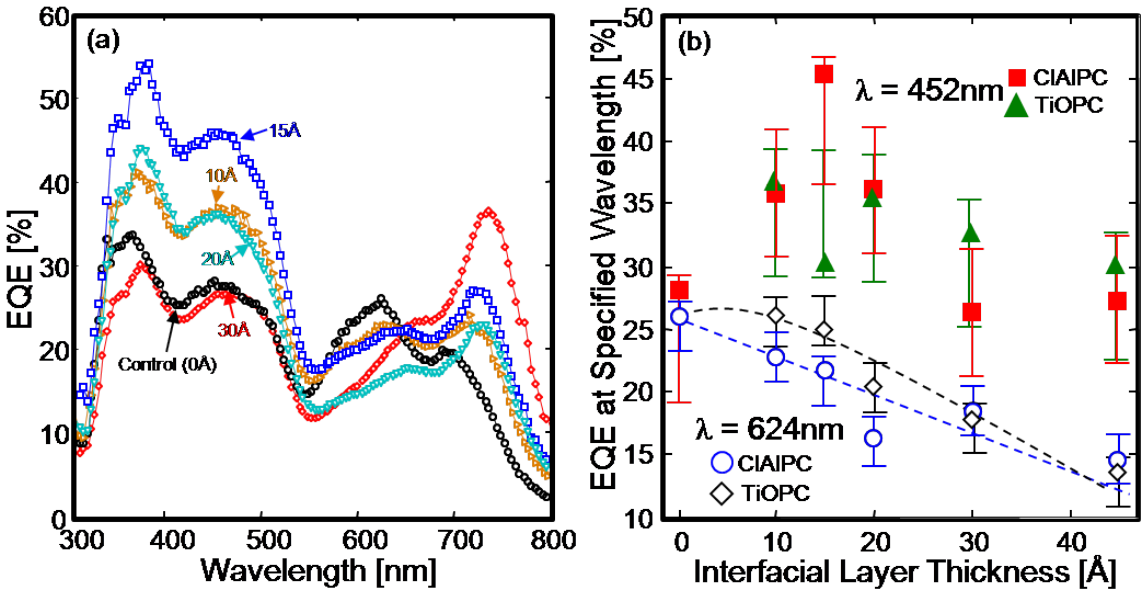

Figure 4-12: External quantum efficiency (EQE) of CuPc/C_{60} devices with an interfacial layer. (a) External quantum efficiency versus wavelength in devices with and without ClAlPC interfacial layers. (b) External quantum efficiency versus interfacial layer thickness for devices with ClAlPC and TiOPC interfacial layers at selected wavelengths. λ = 452 nm corresponds to C_{60} absorption while λ = 624 nm corresponds to CuPc absorption. The error bars are determined by comparing the efficiency of a pool of CuPc/C_{60} control devices to a CuPc/C_{60} control device grown together with each test device. The dashed lines serve as a guide to the eye.

layers.

4.3.3 CuPc/PTCBI devices with an interfacial layer

Finally, we further test the generality of the multistep interface substituting PTCBI (HOMO = 6.2±0.15 eV; LUMO = 3.6±0.5 eV) for C_{60} as the acceptor material. PTCBI is another material that is often utilized in organic solar cell devices with CuPc. We fabricate devices with the following structure: glass/ITO (160 nm)/CuPc (20 nm)/ClAlPC (0 nm or 1.5 nm)/PTCBI (40 nm)/BCP (9 nm)/Ag (60 nm). PTCBI has similar energy levels as C_{60}. Therefore, we expect to observe a similar increase in performance with a ClAlPC interfacial layer.

Figure 4-13a illustrates the current density-voltage characteristics for devices with

and without a ClAlPC interfacial layer. A 1.5 nm ClAlPC interfacial layer is found to enhance both the short-circuit current and the open-circuit voltage. The interfacial layer increases the short-circuit current density from 2.6 mA/cm^2 to 3.7 mA/cm^2 and the open-circuit voltage increases from 0.41 V to 0.46 V.

Figure 4-13b illustrates the impact on EQE of the interfacial layer in these devices. Unfortunately, there is no apparent benefit to the efficiency of charge generation from CuPc or PTCBI excitons. The increased performance observed in Figure 4-13a appears to have originated from direct absorption in the interfacial layer. This result is striking because the HOMO levels of PTCBI and C_{60} are similar. A similar interfacial cascade energy level alignment was created with ClAlPC in devices with C_{60}. However, while the energy level alignment yielded a significant increase in the efficiency of separating excitons originating in C_{60}, there is no apparent increase in the efficiency of separating excitons generated in PTCBI.

4.4 Discussion of results

There are several possible explanations for why the efficiency of separating the charge transfer states formed upon exciton dissociation is not always enhanced. First, the LUMO energy alignment in these devices could be different. If the PTCBI LUMO is higher than that of the ClAlPC interfacial layer, electrons would preferentially transfer to the interfacial layer. The PTCBI layer would then impose a barrier to electron collection, and significant charge could become trapped in the ClAlPC layer. Indeed, the LUMO values given in the literature for ClAlPC (3.7±0.5 eV) and PTCBI (3.6±0.5 eV) indicate that this could be the correct explanation. However, as indicated, there is typically significant uncertainty in LUMO measurements so we cannot know with certainty that this is the correct explanation.

Another possible explanation is that a cascade interfacial energy gradient alone

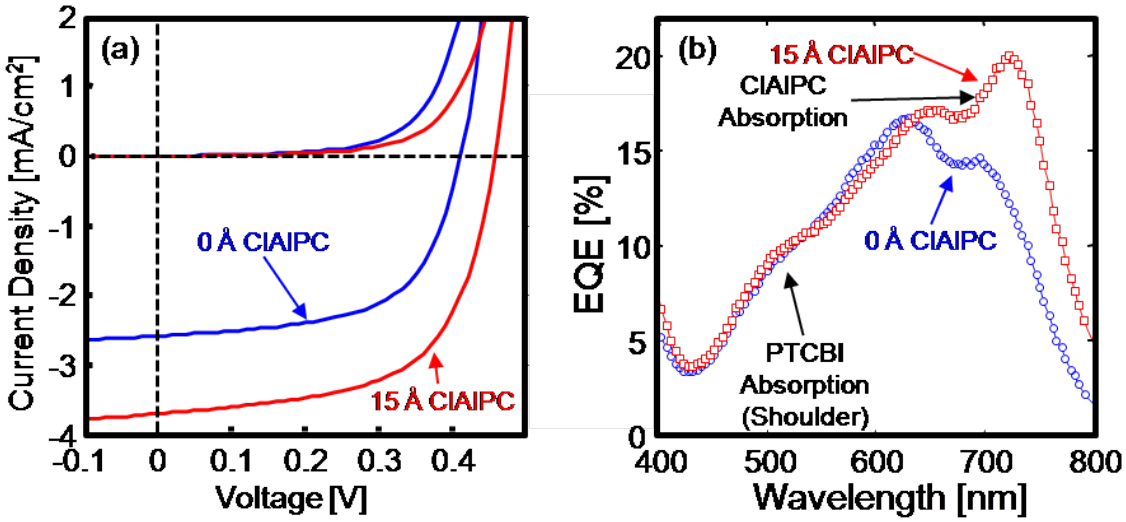

Figure 4-13: Characterization of CuPc/PTCBI devices with an interfacial layer. (a) Current density-voltage characteristics for CuPc/PTCBI based solar cells with and without a 1.5 nm ClAlPC interfacial layer. (b) EQE versus wavelength for CuPc/PTCBI devices with and without a 1.5 nm ClAlPC interfacial layer. Although PTCBI and C_{60} exhibit similar energy levels, the interfacial layer does not improve the dissociation of excitons originating in PTCBI (indicated by the absorption shoulder at $\lambda \approx 500$nm). The observed improvements at $\lambda \approx 700$nm are due to direct absorption by ClAlPC.

is insufficient to guarantee a decrease in charge transfer state recombination. The rates for electron transfer and charge transfer state recombination also depend on the electronic coupling between states. The electronic coupling depends on the specific wavefunction overlap and, therefore, the morphology of the interface. It is possible that the ClAlPC interfacial layer disrupts the morphology at the donor-acceptor interface differently with C_{60} and PTCBI. If ClAlPC only minimally disrupts the morphology of the CuPc/PTCBI interface, the rate of charge transfer state recombination may not decrease significantly.

Finally, as discussed earlier in this chapter, it is possible that bound charge transfer states are not always formed. Instead, excitons may dissociate via a "hot" process where the excess energy of the exciton state aids dissociation of the charges prior to themalization and population of a charge transfer state. If a hot exciton dissociation process dominates, charge separation may already be very efficient. Therefore, introducing an interfacial layer may not decrease recombination in some devices.

4.5 Outlook for this device architecture

The results described in this chapter indicate that introducing thin interfacial layers between the donor and acceptor semiconductor layers in organic solar cells can reduce interfacial recombination and enhance device performance. Planar heterojunction organic solar cells with thin interfacial layers exhibit enhanced short-circuit current density, J_{SC}, and open-circuit voltage, V_{OC}.

The trends in V_{OC} indicate the interfacial layer is successful in reducing the recombination of injected charge. Injected charges no longer reach the donor acceptor interface where they can readily recombine. The charges may instead collect adjacent to the interfacial layer and contribute to the enhancement of the electric field at the interface. This potential electric field enhancement could enhance the open-circuit

voltage further and may also enhance exciton dissociation.

The increase in J_{SC} indicates that the interfacial layer also reduces the rate of recombination of coulombically bound charges immediately upon exciton dissociation at the donor-acceptor interface. Reducing the rate of recombination allows these charges to escape more efficiently, contributing to higher current and greater power generation. The interfacial layer reduces recombination by destabilizing the charge transfer state. After formation of the charge transfer state, the charges undergo a second electron transfer reaction to a more spatially separated charge transfer state consisting of one charge on the donor layer and the other charge on the acceptor layer. The interfacial layer spatially separates the two charges. The charges in this second, more spatially separated, charge transfer state are less coulombically bound and are therefore less likely to recombine. We found the optimal interfacial layer thickness to be approximately 1.5 nm in solar cells based on m-MTDATA and PTCBI and solar cells comprised of CuPc and C_{60}.

However, while we have demonstrated improved performance in several different devices and using several different interfacial layers, the introduction of an interfacial layer does not always aid exciton dissociation. The interfacial layers employed above did not improve the efficiency of dissociating CuPc excitons in CuPc/C_{60} solar cells. The interfacial layer also did not improve the efficiency dissociating PTCBI excitons in CuPc/PTCBI devices. A number of hypothesis are described above for why performance enhancements were not observed. The introduction of thin interfacial layers may prove to be an important probe of the physics of exciton separation in organic PV cells.

While the introduction of interfacial layers successfully increased the performance of some solar cells, unfortunately, the physics of exciton dissociation remain unclear. It is known that organic solar cells require an interface to efficiently dissociate tightly bound excitons [63]. But it is now evident that charge transfer states at the donor-

acceptor interface can also be strongly bound [41]. The multi-step interface introduced in this chapter destabilizes bound charge transfer states at the donor-acceptor interface, thereby reducing a potentially important cause of recombination losses [164]. However, devices with thin interfacial layers do not always exhibit higher performance. These results indicate that understanding energy levels alone is insufficient to fully understand exciton dissociation in organic solar cells. It remains unclear how widely the introduction of an interfacial layer can be deployed successfully.

Chapter 5

Conclusions and Future Work

In this thesis we have demonstrated two new device architectures for bilayer heterojunction organic semiconductor photovoltaics inspired by photosynthesis. These two device architectures are designed to overcome the two primary challenges facing organic photovoltaics.

First, the trade-off between light absorption and exciton diffusion was overcome by introducing an external light absorbing antenna layer. Light absorbed by the antenna layer was transferred to the charge generating semiconductor layers via coupling into waveguide modes and energy transfer mediated by surface plasmon polariton modes. Plasmon mediated coupling was found to be a viable method of transferring energy from the external antenna into the charge generating layers and fabricated devices exhibited energy coupling as high as 51%. In addition to single layer antennas we also demonstrated devices with resonant cavity antennas. Resonant cavity antennas were employed to achieve high absorption in the antenna within the distance from the silver cathode where surface plasmon polariton energy transfer is most efficient. We demonstrated an efficiency improvement for CuPc/C_{60} devices which exhibit weak absorption in the wavelength range 475 nm $< \lambda <$ 575 nm. On the basis of the results described in this thesis, we anticipate that the addition of external antennas

onto thin film organic photovoltaics provides a flexible route towards achieving higher efficiency devices. However, additional work is needed to achieve large increases in performance with this device architecture.

Additional efficiency gains are likely possible with more sophisticated antenna designs. Antenna materials should be selected for high optical absorption and photoluminescence efficiency. The materials do not need to efficiently transport excitons or charge. Therefore, materials can be used in external antenna layers that have not previously been used successfully in organic photovoltaics. Dyes like J-aggregates or quantum dots might be particularly attractive materials to integrate into antennas. Antennas could also be designed to include multiple materials or material orientations to maximize antenna absorption or to focus antenna emission near the metal film where it is most efficient.

In addition to designing more sophisticated antennas, the increase in performance achieved with this device architecture could be enhanced by designing PVs on the basis of high internal quantum efficiency, low series resistance, and high stability. With a well designed antenna, the PV could be designed to absorb strongly only at a single wavelength - the energy transfer energy. While the introduction of the antenna necessarily adds a step to the energy transduction process, the antenna decouples photon absorption and exciton dissociation; these two processes can be optimized independently, increasing PV design flexibility.

Antennas can be successfully employed with organic solar cells in spectral regions where the absorption fraction of the PV cell drops below the energy transfer efficiency. We expect external light antennas to be most effective for organic PVs that exhibit weak absorption in some spectral regions. However, this technique for improving the efficiency of organic solar cells is also applicable to other organic solar cell material pairs as the resonant antenna cavity can be tuned across the visible spectrum. Further improving the efficiency of energy transfer through judicious selection of cathode

structures or antenna materials could further expand the effectiveness of this device architecture.

Second, charge transfer state recombination at the donor-acceptor interface in organic photovoltaic devices was suppressed by adding a thin interfacial layer. Planar heterojunction organic solar cells with thin interfacial layers demonstrated simultaneous increases in both short-circuit current, J_{SC}, and open-circuit voltage, V_{OC}. The interfacial layer reduces recombination by destabilizing the charge transfer state populated immediately after exciton dissociation. Charges in the charge transfer state undergo a second electron transfer reaction to populate a more spatially separated charge transfer state. The electron transfer cascade in these devices is similar to the electron transfer cascade found in photosynthetic reaction centers. The interfacial layer also reduces the dark current by suppressing recombination of injected charges. Reduced dark current yields an increase in V_{OC}.

We found the optimal interfacial layer thickness to be approximately 1.5 nm in solar cells based on m-MTDATA and PTCBI and solar cells comprised of CuPc and C_{60}. In CuPc/C_{60} devices, the addition of a 1.5 nm interfacial layer increased the J_{SC} by 34% and V_{OC} by 33% under simulated solar illumination. The power conversion efficiency increased 49% in these devices.

However, while we demonstrated improved performance in several different devices using several different interfacial layers, the introduction of an interfacial layer does not always aid exciton dissociation. We described a number of hypotheses that could explain why performance enhancements were not observed in all devices. Further work is needed to identify which of the suggested mechanisms are most important. Unfortunately, conclusively confirming the specific physical mechanisms at work may be unattainable using current measurement techniques. In particular, methods to more accurately measure the lowest unoccupied molecular orbitals in organic semiconductors are needed. A more detailed understanding of the impact of morphology

on electron transfer and charge recombination rate constants is also needed. Ultimately, the introduction of thin interfacial layers can be used as a probe of the physics of exciton separation in organic PV cells. Further characterization of devices with interfacial layers could make important contributions to our understanding of how bilayer heterojunction organic solar cells work.

In conclusion, organic semiconductor photovoltaics are a promising route to low-cost, scalable, emissions-free electricity generation. Organic semiconductors are plentiful, inexpensive, and compatible with inexpensive large area manufacturing processes such as roll-to-roll or web-based deposition. However, achieving higher power conversion efficiencies is critical before OPVs can play a larger role in our future energy generation landscape. In this thesis we demonstrated two new device architectures exhibiting improved performance relative to conventional organic photovoltaic devices. These results indicate that device architecture engineering is one of the most promising routes to higher efficiency.

Appendix A

Luminescent Solar Concentrators

The external light absorbing antenna concept discussed in Chapter 2 can also be used with inorganic solar cells. However, the motivation for using an external light absorbing antenna with inorganic solar cells differs from that for using organic devices. Unlike organic devices, inorganic semiconductor photovoltaics typically exhibit efficient light absorption above the electronic bandgap of their semiconductor material. An external antenna is not needed to fill absorption gaps. Inorganic semiconductors also possess far lower binding energies for excitations and do not form bound excitons that must subsequently be dissociated. However, the crystalline nature of inorganic solar cells typically makes them expensive to manufacture over large areas. Reducing the cost of deploying inorganic solar cells remains one the primary barriers to broader adoption.

Photovoltaic concentrators have generated significant interest as a potential inexpensive alternative to conventional PV cells. In a PV concentrator, light is gathered by a large collector and focused on a small area of high-performance semiconductor PV such as crystalline Si or GaAs. Concentrator systems often employ large lenses or mirrors to concentrate sunlight. However, the focal point of a fixed lens- or mirror-based concentrator moves as the sun transits the sky [165, 166]. For a lens-based

concentrator, this imposes a limit on the achievable increase in power generated per unit area of PV cell [167]. To achieve larger flux gains, conventional solar concentrators must employ large mobile mirrors to track the sun during its transit across the sky each day. Unfortunately, these systems are typically expensive to deploy and maintain. Furthermore, solar cells at the focal point of conventional concentrators must be actively cooled as all of the energy above the bandgap of the PV's active semiconductor material is lost to heat during conversion. Furthermore, mechanical tracking also typically requires extra space around the perimeter to avoid shadowing neighboring concentrators.

External organic semiconductor light absorbing antennas can be used to concentrate light on an inorganic solar cell without the need for expensive optics or mechanical tracking. We demonstrate the use of this concept in a device architecture known as a luminescent solar concentrator (LSC). First proposed in the 1970's, LSCs consist of a planar waveguide with a thin-film dye coating on the face or embedded within the waveguide with solar cells attached to the edges [56, 57, 168, 169], as illustrated in Figure A-1a.

A.1 Mechanism of power conversion

Light incident on an LSC is first absorbed by the dye coating. Instead of emitting light into surface plasmon polariton modes, in these devices the dye layer re-emits light into waveguide modes in the glass substrate. After re-emission the light is collected by inorganic solar cells attached to the waveguide edges. Optical concentration is achieved because the dye behaves as an optical heat pump; light is absorbed at one energy and re-emitted at a lower energy [167]. The energy difference is lost to heat, but this allows the radiance at the lower energy to be increased far beyond the concentration limit conventionally achievable without mechanical tracking. Further-

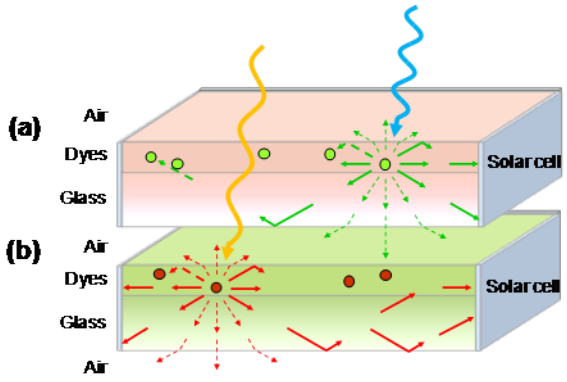

Figure A-1: Luminescent solar concentrator (LSC) device architecture. (a) LSCs consist of a thin film of organic chromophores deposited on high refractive index glass substrates. The chromophores absorb incident solar radiation and re-emit it at a lower energy. Approximately 80% of the re-emitted photons are trapped within the waveguide by total internal reflection for ultimate collection by a PV device mounted on the substrate edges. Photon loss (dashed lines) occurs via non-trapped emission or re-absorption by other chromophores. (b) Light transmitted through the first LSC can be captured and collected by a second LSC whose chromophores absorb and emit light at lower energies for electrical conversion at a second, lower bandgap PV device.

more, if the emission wavelength of the dye in an LSC is placed at the bandgap energy of the PV semiconductor, active cooling of the edge mounted solar cells may not be necessary; heat loss occurs in the waveguide instead of the solar cell.

To obtain higher efficiencies, LSCs can be utilized in a tandem configuration where multiple waveguides are used. In Figure A-1 we show a tandem LSC [168]. Incident solar radiation first encounters an LSC employing a short wavelength dye. Longer wavelengths of light are transmitted through the first LSC (Figure A-1a) and absorbed by a longer wavelength dye in a second LSC (Figure A-1b). If the PV cells in each LSC are matched to each emission wavelength, the power efficiency of the tandem system can surpass the single junction limit. Alternatively, solar radiation transmitted through the first waveguide could be gathered by a bottom PV cell or used to heat water in a hybrid PV thermal system.

A.2 Reducing self-absorption in LSCs

The performance of early LSCs was limited by self-absorption losses. Self-absorption refers to the ability of a dye to absorb its own emission. Self-absorption leads to the re-absorption and re-emission of waveguided photons many times in the LSC waveguide. Re-absorbed photons in the waveguide may be lost to free space photon emission outside the devices or be lost to non-radiative decay via phonons. Lower self-absorption allows waveguided photons to travel farther before reaching a solar cell at the edge of the glass. High self-absorption limits the ability of LSCs to economically achieve high concentration factors.

The ability to precisely control thin film composition and intermolecular energy transfer using low-cost manufacturing processes has advanced considerably since the early LSC studies. We exploit these abilities to reduce self absorption in LSCs. Specifically, we apply recent advances in organic optoelectronic devices to LSCs, exploiting Förster energy transfer [120], solid state solvation [170], and phosphorescence [171].

We first demonstrate an LSC consisting of the dye molecule DCJTB in host material Alq_3 [172]. We fabricate the LSC using thermal evaporation on a glass substrate. Thermal evaporation allows precise control of film composition. DCJTB belongs to the DCM class of laser dyes, characterized by large Stokes shifts and red emission with near unity quantum efficiency. DCJTB is characterized by low self-absorption due to its large Stokes shift. Similar to the initial antenna layers studied in Chapter 2, to reduce concentration quenching of photoluminescence, we dope the dye DCJTB into the host material Alq_3 at low concentration (2% v/v). In addition, self-absorption is reduced further when DCJTB is doped into Alq_3 as Alq_3 provides a polar environment that stabilizes the highly polar DCJTB excited states. This effect, know as solid-state solvation, red-shifts the DCJTB photoluminescence [170].

We fabricate a 5.7 μm thick film of Alq_3:DCJTB (2%), achieving an absorbance of 1.1 absorbance units (au) at the DCJTB absorption peak. We quantify self-absorption

losses in LSCs using the self-absorption ratio, S, defined as the ratio of the absorption coefficients at the absorption and emission maxima. The self absorption ratio for the Alq_3:DCJTB LSC is approximately $S = 80$, as illustrated in Figure A-2a.

Next, we utilize Förster energy transfer to reduce the required concentration of the emissive dye and achieve even lower self-absorption with DCJTB. We fabricate an LSC with a 1.6 μm film of Alq_3:rubrene (30%):DCJTB (1%) with an absorbance of 1.2 au at the rubrene absorption peak. Förster energy transfer from rubrene to DCJTB increases the self absorption ratio relative to the LSC with only Alq_3 and DCJTB. Unfortuneately, rubrene is nonpolar and, together with a slight reduction in the DCJTB concentration, the DCJTB PL blue-shifts 20nm negating some of the potential increase in self-absorption ratio. Nonetheless, as illustrated in Figure A-2a, we achieve a self-absorption ratio of $S = 220$ with rubrene.

Finally, we use phosphorescence to reduce self-absorption further. We fabricate an LSC using the phosphorescent material platinum tetraphenyltetrabenzoporphyrin (Pt(TPBP)). Pt(TPBP) is a phosphorescent material that emits in the infrared at $\lambda = 770$ nm with a PL efficiency of approximately 50% [171]. Compared to conventional fluorescent dyes, phosphorescent materials are particularly attractive as their emissive state is only weakly absorptive. We fabricate an LSC with a 5.8 μm film of Alq_3:DCJTB (2%):Pt(TPBP)(4%) with an absorbance of 2.1 au at the Pt(TPBP) absorption peak. The absorption of Pt(TPBP) is dominated by strong transitions from the Soret band at $\lambda = 430$ nm and the Q band at $\lambda = 611$ nm. To complete the absorption spectrum of Pt(TPBP)-based LSCs, we employ DCJTB to fill in the Pt(TPBP) absorption spectrum and transfer energy to Pt(TPBP). The self-absorption ratio for the Pt(TPBP)-based LSC is approximately $S = 500$, as illustrated in Figure A-2b. Energy transfer and phosphorescence are illustrated schematically in Figure A-2c and Figure A-2d, respectively.

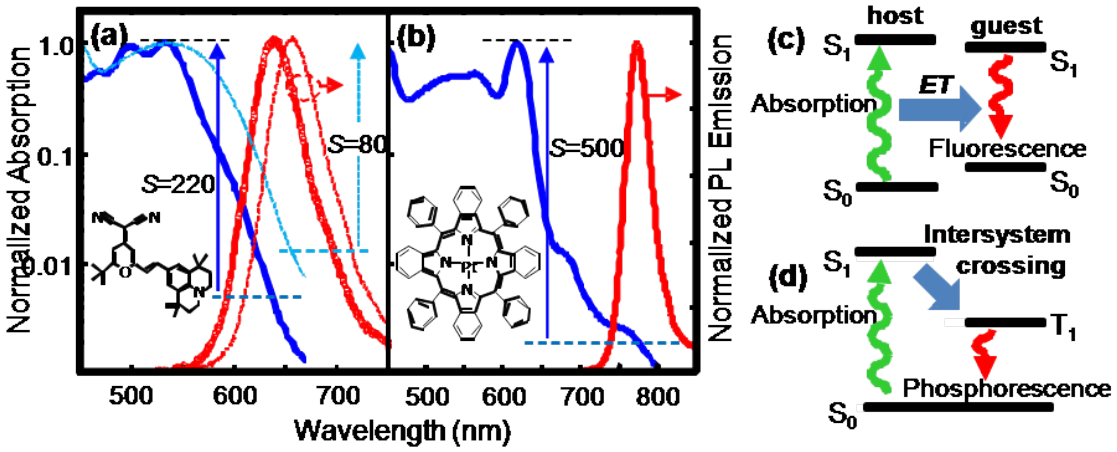

Figure A-2: Normalized absorption and emission spectra of LSC films. (a) The ratio between the peak absorption coefficient and the absorption coefficient at the emission wavelength provides a measure of the self-absorption in an LSC film. The self-absorption ratio in a DCJTB-based LSC is $S = 80$ (dotted lines). A larger self-absorption ratio of $S = 220$ is obtained in a rubrene-based LSC (solid lines). The self absorption ratio increases because the amount of DCJTB is reduced by a factor of three. DCJTB's absorption is replaced by rubrene, which then transfers energy to DCJTB; see (c). Inset: DCJTB chemical structure. (b) Phosphorescence is another method to reduce self-absorption; see (d). The self absorption ratio in a Pt(TPBP)-based LSC is $S = 500$. Inset: Pt(TPBP) chemical structure. Near field dipole-dipole coupling known as Förster energy transfer can efficiently transfer energy between host and guest molecules. The concentration of guest molecules can be less than 1%, significantly reducing self absorption. (d) Spin orbit coupling in a phosphor increases the PL efficiency of the triplet state and the rate of intersystem crossing from singlet to triplet manifolds. The exchange splitting between singlet and triplet states is typically about 0.7 eV, significantly reducing self-absorption.

A.2.1 Low self-absorption LSC performance

To characterize the performance of the LSCs described above, we first measure optical quantum efficiency (OQE), the fraction of incident photons emitted from the edges of the LSC waveguide. This metric is used to quantify the ability for LSCs to effectively waveguide light to edge-mounted solar cells. For an organic film with refractive index of $n = 1.7$, assuming isotropic emission, approximately 80% of the absorbed photons should be re-emitted into waveguide modes in the organic film or glass substrate [167]. If self-absorption and scattering losses are negligble, these waveguided photons will all emerge from the edges of the LSC and be incident upon solar cells. The remaining photons are not subject to total internal reflection upon emission and are lost into the air through the top and bottom faces of the LSC. Of course, scattering and self-absorption losses cannot be eliminated completely and some waveguide losses will inevitably occur.

We measure OQEs within an integrating sphere. We distinguish between edge and facial emission by selectively blocking edge emission using black tape and permanent black marker. The OQEs of the single waveguide LSCs at low geometric concentration ($G = 3$) are compared in Figure A-3a. The geometric concentration factor, G, also known as the geometric gain is the ratio of the area of the concentrator, A_{conc}, to the area of the PV cell, A_{PV}. Therefore, in this example, the area of the face of the collector is three times larger than the total area of the collectors edges. Our glass substrates measure 25 by 25 by 2mm. The OQE for the three LSCs described above all appear uniform throughout the regions where each LSC absorbs light. The Pt(TPBP) clearly has the advantage of absorbing light further into the infrared. At low geometric concentration, self-absorption is negligible for all three of these LSCs. Therefore, the ratio between OQEs are approximately equal to ratios between PL efficiencies for these devices.

Next, we combine LSCs to form tandem configurations. The rubrene-based LSC

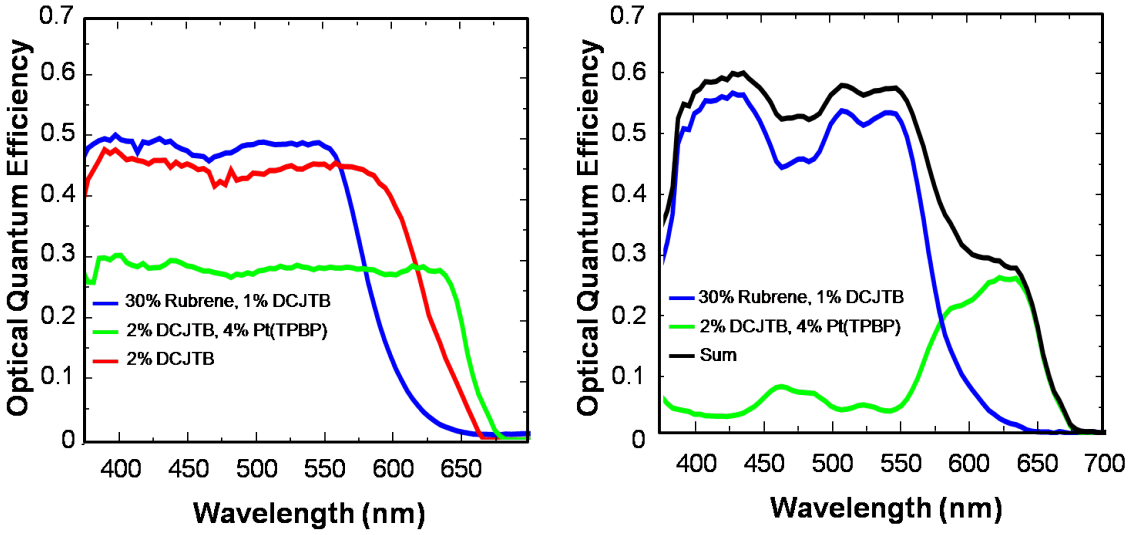

Figure A-3: Optical quantum efficiency (OQE) spectra of LSC films. The OQE is the fraction of incident photons that are emitted from the edges of the substrate. (a) The OQE spectra of the DCJTB- (red), rubrene- (blue) and Pt(TPBP)-based (green) single waveguide LSCs at a geometric gain of $G = 3$. (b) In the tandem configuration light is incident first on the rubrene-based LSC (blue). This filters the incident light incident on the second, mirror-backed, Pt(TPBP)-based LSC (green). The composite OQE is shown in black.

is used on top to collect blue and green light and the Pt(TPBP)-based LSC on the bottom to collect red light. Together, this tandem LSC combines higher efficiency collection in the blue and green with lower efficiency performance further into the red, as shown in Figure A-3B.

Next, we measure the external quantum efficiency (EQE) of the LSCs. EQE is the number of harvested electrons per incident photon. In addition to waveguide losses, EQE also includes the coupling losses at the PV interface and the quantum efficiency of the PV. To obtain the EQE in the range $G < 50$, thin films were evaporated onto a 100 mm $\times$ 100 mm $\times$ 1 mm glass substrate with $n = 1.72$. A 125 mm $\times$ 8 mm strip of solar cell, manufactured by Sunpower Corporation, was attached to one entire edge of the substrate using EpoTek 301 epoxy. The remaining edges were blackened with black permanent marker to prevent reflections from the other edges. EQE(G)

is measured by sweeping a monochromatic excitation perpendicular to the attached solar cell while monitoring the photocurrent. Figure A-4a shows the dependence of the EQE dependence with G for each of the films, taken at $\lambda = 534$nm and $\lambda = 620$ nm for the fluorescent and phosphorescent systems, respectively. The DCJTB-based LSC shows the strongest self-absorption. The self-absorption is lower in the rubrene-based LSC, consistent with the spectroscopic data in Figure A-2a. Finally, the Pt(TPBP)-based LSC shows no observable self absorption loss for $G < 50$.

The increase in PV power that is gained per unit area of the PV cell is known as the flux gain, F [56, 57]. The flux gain includes the possible changes in the power efficiency of the PV in the concentrator system, η_{conc}, compared to the efficiency of the detached PV cell. Flux gain determines the magnitude of power that is obtained per unit area of PV cell. A large flux gain allows the area of PV to be reduced further without reducing power harvesting capability. In Figure A-4b, the flux gain, F, for the three films coupled to bandgap-matched solar cells are compared. LSCs with emission from DCJTB are paired with GaInP solar cells [173]; those with emission from Pt(TPBP) are paired with GaAs [174]. For $G < 50$, all three films demonstrate increasing flux gain with G. We extend the theoretical fit of OQE versus G to project performance at high geometric gain. The DCJTB-based LSC is predicted to peak at $F = 12\pm2$ at $G = 80$. The rubrene-based LSC is predicted to peak at $F = 17\pm2$ at $G = 125$. Finally, the Pt(TPBP)-based is estimated to peak at $F = 46\pm15$ at $G = 630$.

Finally, the LSC power conversion efficiencies were estimated by integrating the product of the OQE, the AM1.5G standard solar spectrum, and the external quantum efficiency of the solar cell, weighted by the emission spectrum of each film. Again, the DCJTB LSCs are paired with GaInP solar cells [173] while those with emission from Pt(TPBP) are paired with GaAs [174]. The resulting power conversion efficiencies are listed in Table A.1. At $G = 3$, the DCJTB-, rubrene-, and Pt(TPBP)-based LSCs

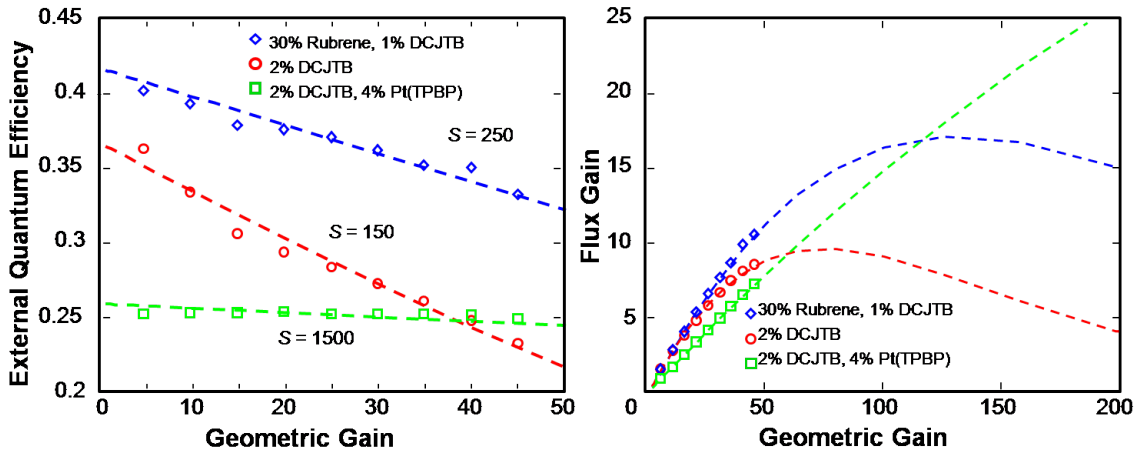

Figure A-4: LSC efficiency and flux gain as a function of geometric gain. (a) With increasing G, photons must take a longer path to the edge-attached PV, increasing the probability of re-absorption. The fit lines apply theory described in the text. (b) Flux gain compares the electrical power output from the solar cell when attached to the concentrator relative to direct solar illumination. The flux gain increases with G, but reaches a maximum when the benefit of additional G is canceled by self-absorption losses. Near field energy transfer and phosphorescence substantially improve the flux gain relative to the DCJTB-based LSC.

exhibit power conversion efficiencies of 5.9%, 5.5%, and 4.1%, respectively. The tandem structure achieves a power conversion efficiency of 6.8% at $G = 3$. Unfortunately, the power conversion efficiency decreases as the gain increases due to self-absorption. Achieving higher efficiency LSC performance at higher geometric gains remains a critical challenge.

A.3 Outlook for this device architecture

The results described in this appendix indicate that the external light absorbing antenna concept discussed in Chapter 2 can also be successfully employed with inorganic solar cells in the luminescent solar concentrator device architecture. The flux gains demonstrated in this appendix may enable the economical use of high performance PV cells in low cost systems. A large flux gain is likely most advantageous in > 1 MW scale PV installations where the cost of the solar cells is paramount. Usually

Table A.1: Calculated LSC power efficiency and flux gains. We calculate the power conversion efficiency of the LSCs by integrating the product of the OQE, the AM1.5G solar spectrum, and solar cell EQE curves. EQE values can be found in the literature: the DCJTB LSCs are paired with GaInP solar cells [173] while those with emission from Pt(TPBP) are paired with GaAs [174]. The Pt(TPBP) LSCs, with the lowest self-absorption, maintain high power conversion efficiency and flux gain at high geometric gain G. However, the performance at low G is reduced compared to the DCJTB- and rubrene-based LSCs due to the lower PL efficiency of Pt(TPBP).

Terminal absorber	Emitter	Power conversion efficiency at $G = 3$, 45	Flux gain at $G = 45$	Projected maximum flux gain
DCJTB	DCJTB	5.9%, 4.0%	9	12±2 at $G = 80$
Rubrene	DCJTB	5.5%, 4.7%	11	17±2 at $G = 125$
Pt(TPBP)	Pt(TPBP)	4.1%, 4.1%	7	46±15 at G=630
Tandem: Rubrene/ Pt(TPBP)	DCJTB/ Pt(TPBP)	6.8%, 6.1%	N/A	N/A

higher power efficiencies are desired in smaller scale domestic solar applications due to high installation costs and size constraints. Further, there remains significant opportunity to improve the efficiency of LSCs. The PL efficiency of the terminal dye can be increased, an antireflection coating could be applied to the waveguides, and the solar cells could be optimized for monochromatic excitation. Finally, the absorption spectrum should be expanded into the near infrared.

Bibliography

[1] A. Grubler, *Technology and Global Change*. Cambridge University Press, 1998.

[2] British Petroleum, "BP Statistical Review of World Energy," June 2009.

[3] United Nations Population Division, "World Population Prospects: The 2008 Revisions." http://esa.un.org/unpp/, 2009.

[4] Energy Information Administration, U.S. Department of Energy, "Annual energy review," 2008.

[5] Energy Information Administration, U.S. Department of Energy, "World crude oil prices." http://tonto.eia.doe.gov/dnav/pet/pet_pri_wco_k_w.htm, Dec. 2009.

[6] D. Yergin, "Ensuring energy security," *Foreign Affairs*, p. 69, March/April 2006.

[7] S. Gorman, "Electricity Grid in US Penetrated by Spies." Wall Street Journal, April 2009.

[8] IPCC Core Writing Team, Pachauri, R.K and Reisinger, A. (eds.), "IPCC, 2007: Climate Change 2007: Synthesis Report. Contribution of Working Groups I, II and III to the Fourth Assessment Report of the Intergovernmental Panel on Climate Change," 2007.

[9] A. P. Sokolov, P. H. Stone, C. E. Forest, R. Prinn, M. C. Sarofim, M. Webster, S. Paltsev, C. A. Schlosser, D. Kicklighter, S. Dutkiewicz, J. Reilly, C. Wang, B. Felzer, J. M. Melillo, and H. D. Jacoby, "Probabilistic forecast for twenty-first-century climate based on uncertainties in emissions (without policy) and climate parameters," *Journal of Climate*, vol. 22, no. 19, pp. 5175–5204, 2009.

[10] J. Schmidhuber and F. N. Tubiello, "Global food security under climate change," *Proceedings of the National Academy of Sciences*, vol. 104, no. 50, pp. 19703–19708, 2007.

[11] A. J. McMichael, R. E. Woodruff, and S. Hales, "Climate change and human health: present and future risks," *The Lancet*, vol. 367, no. 9513, pp. 859–869, 2006.

[12] S. Pacala and R. Socolow, "Stabilization Wedges: Solving the Climate Problem for the Next 50 Years with Current Technologies," *Science*, vol. 305, no. 5686, pp. 968–972, 2004.

[13] U.S. Department of Energy, "Basic Research Needs for Solar Energy Utilization," 2005.

[14] J. A. Turner, "A realizable renewable energy future," *Science*, vol. 285, no. 5428, pp. 687–689, 1999.

[15] National Renewable Energy Lab, "United states photovoltaic solar resource: Flat plate tilted at latitude." http://www.nrel.gov/gis/solar.html, Jan 2008.

[16] Y. B. Gershon Grossman, Ofira Ayalon and D. Kaufman, "Solar energy for the production of heat Summary and recommendations of the 4th assembly of the energy forum at SNI," 2007. Samuel Neaman Institute for Advanced Research in Science and Technology.

[17] S. A. Kalogirou, "Solar thermal collectors and applications," *Progress in Energy and Combustion Science*, vol. 30, no. 3, pp. 231–295, 2004.

[18] Sargent & Lundy LLC Consulting Group, "Assessment of Parabolic Trough and Power Tower Solar Technology Cost and Performance Forecasts," tech. rep., National Renewable Energy Laboratory, 2003.

[19] A. Becquerel, "Mmoire sur les effets lectriques produits sous l'influence des rayons solaires," *Comptes Rendus*, p. 561, 1839.

[20] D. M. Chapin, C. S. Fuller, and G. L. Pearson, "A new silicon p-n junction photocell for converting solar radiation into electrical power," *Journal of Applied Physics*, vol. 25, no. 5, pp. 676–677, 1954.

[21] M. Green, K. Emery, Y. Hishikawa, and W. Warta, "Solar cell efficiency tables (version 34)," *Progress in Photovoltaics: Research and Applications*, vol. 17, pp. 320–326, 2009.

[22] W. Shockley and H. J. Queisser, "Detailed balance limit of efficiency of p-n junction solar cells," *Journal of Applied Physics*, vol. 32, no. 3, pp. 510–519, 1961.

[23] S. R. Bull, "Renewable energy today and tomorrow," *Proceedings of the IEEE*, vol. 89, no. 8, pp. 1216–1226, 2001.

[24] S. G. Bailey and D. J. Flood, "Space photovoltaics," *Progress in Photovoltaics: Research and Applications*, vol. 6, pp. 1–14, 1998.

[25] E. Lorenzo, "Photovoltaic rural electrification," *Progress in Photovoltaics: Research and Applications*, vol. 5, pp. 3–27, 1997.

[26] A. Goetzberger and C. Hebling, "Photovoltaic materials, past, present, future," *Solar Energy Materials & Solar Cells*, vol. 62, pp. 1–19, 2000.

[27] SolarBuzz, "Solar electricity price index." http://solarbuzz.com/solarprices.htm, December 2009.

[28] R. M. Swanson, "Photovoltaics power up," *Science*, vol. 324, no. 5929, pp. 891–892, 2009.

[29] T. Bradford, *SOLAR REVOLUTION: The Economic Transformation of the Global Energy Industry*. Cambridge: MIT Press, 1 ed., 2006.

[30] M. Campbell, P. Aschenbrenner, J. Blunden, E. Smeloff, and S. Wright, "The drivers of the levelized cost of electricity for utility-scale photovoltaics," tech. rep., Sunpower Corporation, 2008.

[31] M. Green, *Third generation photovoltaics: advanced solar energy conversion*. Berlin: Springer Verlag, 2003.

[32] H. Ullal, "Overview and challenges of thin film solar electric technologies," in *Conference Presentation at the World Renewable Energy Congress X and Exhibition 2008*, (Glasgow, Scotland, United Kingdom), July 2008.

[33] First Solar Inc., "First solar passes $1 per watt industry milestone." Press Release, Feb 2009.

[34] J. Y. Kim, K. Lee, N. E. Coates, D. Moses, T.-Q. Nguyen, M. Dante, and A. J. Heeger, "Efficient tandem polymer solar cells fabricated by all-solution processing," *Science*, vol. 317, no. 5835, pp. 222–225, 2007.

[35] F. C. Krebs, "Fabrication and processing of polymer solar cells: A review of printing and coating techniques," *Solar Energy Materials and Solar Cells*, vol. 93, no. 4, pp. 394–412, 2009.

[36] T. Stubinger and W. Brutting, "Exciton diffusion and optical interference in organic donor–acceptor photovoltaic cells," *Journal of Applied Physics*, vol. 90, no. 7, pp. 3632–3641, 2001.

[37] V. I. Arkhipov, P. Heremans, and H. Bässler, "Why is exciton dissociation so efficient at the interface between a conjugated polymer and an electron acceptor?," *Applied Physics Letters*, vol. 82, no. 25, pp. 4605–4607, 2003.

[38] P. Peumans and S. R. Forrest, "Separation of geminate charge-pairs at donor-acceptor interfaces in disordered solids," *Chemical Physics Letters*, vol. 398, no. 1-3, pp. 27–31, 2004.

[39] A. Liu, S. Zhao, S. B. Rim, J. Wu, M. Knemann, P. Erk, and P. Peumans, "Control of electric field strength and orientation at the donor-acceptor interface in organic solar cells," *Advanced Materials*, vol. 20, no. 5, pp. 1065–1070, 2008.

[40] T. Offermans, S. C. J. Meskers, and R. A. J. Janssen, "Charge recombination in a poly(para-phenylene vinylene)-fullerene derivative composite film studied by transient, nonresonant, hole-burning spectroscopy," *The Journal of Chemical Physics*, vol. 119, no. 20, pp. 10924–10929, 2003.

[41] M. Muntwiler, Q. Yang, W. A. Tisdale, and X. Y. Zhu, "Coulomb barrier for charge separation at an organic semiconductor interface," *Physical Review Letters*, vol. 101, no. 19, p. 196403, 2008.

[42] K. Vandewal, A. Gadisa, W. D. Oosterbaan, S. Bertho, F. Banishoeib, I. Van Severen, L. Lutsen, T. J. Cleij, D. Vanderzande, and J. V. Manca, "The relation between open-circuit voltage and the onset of photocurrent generation by charge-transfer absorption in polymer:fullerene bulk heterojunction solar cells," *Advanced Functional Materials*, vol. 18, no. 14, pp. 2064–2070, 2008.

[43] T. Drori, C. X. Sheng, A. Ndobe, S. Singh, J. Holt, and Z. V. Vardeny, "Below-gap excitation of pi-conjugated polymer-fullerene blends: Implications for bulk organic heterojunction solar cells," *Physical Review Letters*, vol. 101, no. 3, pp. 037401–4, 2008.

[44] M. Hallermann, S. Haneder, and E. Da Como, "Charge-transfer states in conjugated polymer/fullerene blends: Below-gap weakly bound excitons for polymer photovoltaics," *Applied Physics Letters*, vol. 93, no. 5, pp. 053307–3, 2008.

[45] K. Tvingstedt, K. Vandewal, A. Gadisa, F. Zhang, J. Manca, and O. Inganas, "Electroluminescence from charge transfer states in polymer solar cells," *Journal of the American Chemical Society*, vol. 131, no. 33, pp. 11819–11824, 2009.

[46] K. H. Nealson and P. G. Conrad, "Life: past, present and future," *Philosophical Transactions of the Royal Society of London. Series B: Biological Sciences*, vol. 354, no. 1392, pp. 1923–1939, 1999.

[47] W. Purves, D. Sadava, G. Orians, and H. C. Heller, *Life, the science of biology*. Sunderland, MA; Gordonsville, VA: Sunauer Associates, Inc.; W.H. Freeman and Co., seventh ed., 2004.

[48] B. Green and W. Parson, *Light-Harvesting Antennas in Photosynthesis*. Dordrecht: Kluwer Academic, 2003.

[49] R. Blankenship, *Molecular Mechanisms of Photosynthesis*. Oxford: Blackwell Science, 1 ed., 2002.

[50] M. K. Sener, D. Lu, T. Ritz, S. Park, P. Fromme, and K. Schulten, "Robustness and optimality of light harvesting in cyanobacterial photosystem i," *The Journal of Physical Chemistry B*, vol. 106, no. 32, pp. 7948–7960, 2002.

[51] C. C. Moser, J. M. Keske, K. Warncke, R. S. Farid, and P. L. Dutton, "Nature of biological electron transfer," *Nature*, vol. 355, no. 6363, pp. 796–802, 1992.

[52] U. Ermler, G. Fritzsch, S. K. Buchanan, and H. Michel, "Structure of the photosynthetic reaction centre from rhodobacter sphaeroides at 2.65 åresolution: cofactors and protein-cofactor interactions," *Structure*, vol. 2, no. 10, pp. 925–936, 1994.

[53] N. Nelson and A. Ben-Shem, "The complex architecture of oxygenic photosynthesis," *Nat Rev Mol Cell Biol*, vol. 5, no. 12, pp. 971–982, 2004.

[54] A. J. Hoff and J. Deisenhofer, "Photophysics of photosynthesis. structure and spectroscopy of reaction centers of purple bacteria," *Physics Reports*, pp. 1–247, 1997.

[55] W. Humphrey, A. Dalke, and K. Schulten, "Vmd: Visual molecular dynamics," *Journal of Molecular Graphics*, vol. 14, no. 1, pp. 33–38, 1996.

[56] J. Batchelder, A. Zewail, and T. Cole, "Luminescent solar concentrators. 1: Theory of operation and techniques for performance evaluation," *Applied Optics*, vol. 18, pp. 3090–3110, 1979.

[57] J. Batchelder, A. Zewail, and T. Cole, "Luminescent solar concentrators. 2: Experimental and theoretical analysis of their possible efficiencies," *Applied Optics*, vol. 20, pp. 3733–3754, 1981.

[58] T. Heidel, D. Hochbaum, M. Bahlke, I. Hiromi, J. Lee, and M. Baldo, "Reducing recombination losses in planar organic photovoltaic cells using multiple step charge separation," *Applied Physics Letters*, 2010. Under Review.

[59] S. E. Gledhill, B. Scott, and B. A. Gregg, "Organic and nano-structured composite photovoltaics: An overview," *Journal of Materials Research*, vol. 20, Dec 2005.

[60] S. R. Forrest, "The limits to organic photovoltaic cell efficiency," *MRS Bulletin*, vol. 30, no. 1, pp. 28–32, 2005.

[61] G. A. Chamberlain, "Organic solar cells: A review," *Solar Cells*, vol. 8, no. 1, pp. 47–83, 1983.

[62] A. K. Ghosh, D. L. Morel, T. Feng, R. F. Shaw, and J. C. A. Rowe, "Photovoltaic and rectification properties of al/mg phthalocyanine/ag schottky-barrier cells," *Journal of Applied Physics*, vol. 45, no. 1, pp. 230–236, 1974.

[63] C. W. Tang, "Two-layer organic photovoltaic cell," *Applied Physics Letters*, vol. 48, no. 2, pp. 183–185, 1986.

[64] J. Xue, S. Uchida, B. Rand, and S. Forrest, "Asymmetric tandem organic photovoltaic cells with hybrid planar-mixed molecular heterojunctions," *Applied Physics Letters*, vol. 85, no. 23, pp. 5757–5759, 2004.

[65] J. Xue, B. Rand, S. Uchida, and S. Forrest, "Mixed donor-acceptor molecular heterojunctions for photovoltaic applications. ii. device performance," *Journal of Applied Physics*, vol. 98, no. 12, p. 124903, 2005.

[66] S. H. Park, A. Roy, S. Beaupre, S. Cho, N. Coates, J. S. Moon, D. Moses, M. Leclerc, K. Lee, and A. J. Heeger, "Bulk heterojunction solar cells with internal quantum efficiency approaching 100no. 5, pp. 297–302, 2009.

[67] P. Würfel, *Physics of Solar Cells*, vol. 2. Weinheim: Wiley-VCH, 2005.

[68] M. Pope and C. Swenberg, *Electronic Processes in Organic Crystals*. Oxford: Oxford University Press, 1st ed., 1982.

[69] A. Jonscher, "Electronic Properties of Amorphous Dielectric Films," *Thin Solid Films*, vol. 1, pp. 213–234, 1967.

[70] P. Peumans, A. Yakimov, and S. R. Forrest, "Small molecular weight organic thin-film photodetectors and solar cells," *Journal of Applied Physics*, vol. 93, no. 7, pp. 3693–3723, 2003.

[71] G. Yu and A. Heeger, "Charge separation and photovoltaic conversion in polymer composites with internal donor-acceptor heterojunctions," *Journal of Applied Physics*, vol. 78, no. 7, pp. 4510–4515, 1995.

[72] J. Halls, C. Walsh, N. Greenham, E. Marseglia, R. Friend, S. Moratti, and A. Holmes, "Efficient photodiodes from interpenetrating polymer networks," *Nature*, vol. 376, pp. 498–500, 1995.

[73] P. Peumans, S. Uchida, and S. Forrest, "Efficient bulk heterojunction photovoltaic cells using small-molecular-weight organic thin films," *Nature*, vol. 425, pp. 158–162, 2003.

[74] B. Rand, J. Xue, S. Uchida, and S. Forrest, "Mixed donor-acceptor molecular heterojunctions for photovoltaic applications. i. material properties," *Journal of Applied Physics*, vol. 98, no. 12, 2005.

[75] B. Maennig, J. Drechsel, D. Gebeyehu, P. Simon, F. Kozlowski, A. Werner, F. Li, S. Grundmann, S. Sonntag, M. Koch, K. Leo, M. Pfeiffer, H. Hoppe, D. Meissner, N. S. Sariciftci, I. Riedel, V. Dyakonov, and J. Parisi, "Organic p-i- n solar cells," *Applied Physics A: Materials Science & Processing*, vol. 79, no. 1, pp. 1–14, 2004.

[76] A. Yakimov and S. Forrest, "High photovoltage multiple-heterojunction organic solar cells incorporating interfacial metallic nanoclusters," *Applied Physics Letters*, vol. 80, no. 9, pp. 1667–1669, 2002.

[77] L. Pettersson, L. Roman, and O. Inganäs, "Enhanced photo conversion efficiency utilizing interference inside organic heterojunction photovoltaic devices," *Journal of Applied Physics*, vol. 86, no. 1, pp. 487–496, 1999.

[78] T. Stũbinger and W. Brütting, "Exciton diffusion and optical interference in organic donor-acceptor photovoltaic cells," *Journal of Applied Physics*, vol. 90, no. 7, pp. 3632–3641, 2001.

[79] L. Roman, O. Inganäs, T. Granlund, T. Nyberg, M. Svensson, M. Andersson, and J. Hummelen, "Trapping light in polymer photodiodes with soft embossed gratings," *Advanced Materials*, vol. 12, no. 3, pp. 189–195, 2000.

[80] M. Niggemann, M. Glatthaar, A. Gombert, A. Hinsch, and V. Wittwer, "Diffraction gratings and buried nano-electrodes-architectures for organic solar cells," *Thin Solid Films*, vol. 451-452, pp. 619–623, 2004.

[81] M. Niggemann, M. Glatthaar, P. Lewer, C. M*ü*ller, J. Wagner, and A. Gombert, "Functional microprism substrate for organic solar cells," *Thin Solid Films*, vol. 511-512, pp. 628–633, 2006.

[82] M. Ihara, K. Tanaka, K. Sakaki, I. Homma, and K. Yamada, "Enhancement of the absorption coefficient of *cis*-$(ncs)_2$ bis*2,2'-bipyridyl-4,4'-dicarboxylate) ruthenium(ii) dye in dye-sensitized solar cells by a silver island film," *Journal of Physical Chemistry B*, vol. 101, pp. 5153–5157, 1997.

[83] B. Rand, P. Peumans, and S. Forrest, "Long-range absorption enhancement in organic tandem thin-film solar cells containing silver nanoclusters," *Journal of Applied Physics*, vol. 96, no. 12, pp. 7519–7526, 2004.

[84] L. Pettersson, L. Roman, and O. Inganäs, "Modeling photocurrent action spectra of photovoltaic devices based on organic thin films," *Journal of Applied Physics*, vol. 86, no. 1, pp. 487–496, 1999.

[85] O. Stenzel, A. Stendal, K. Voigtsberger, and C. von Borczyskowski, "Enhancement of the photovoltaic conversion efficiency of copper phthalocyanine thin film devices by incorporation of metal clusters," *Solar Energy Materials and Solar Cells*, vol. 37, pp. 337–348, 1995.

[86] M. Westphalen, U. Kreibig, J. Rostalski, H. L*ddotu*th, and D. Meissner, "Metal cluster enhanced organic solar cells," *Solar Energy Materials and Solar Cells*, vol. 61, no. 1, pp. 97–105, 2000.

[87] C. J. Brabec, A. Cravino, D. Meissner, N. S. Sariciftci, M. T. Rispens, L. Sanchez, J. C. Hummelen, and T. Fromherz, "The influence of materials work function on the open circuit voltage of plastic solar cells," *Thin Solid Films*, vol. 403-404, pp. 368–372, 2002.

[88] C. J. Brabec, A. Cravino, D. Meissner, N. S. Sariciftci, T. Fromherz, M. T. Rispens, L. Sanchez, and J. C. Hummelen, "Origin of the open circuit voltage of plastic solar cells," *Advanced Functional Materials*, vol. 11, no. 5, pp. 374–380, 2001.

[89] A. Gadisa, M. Svensson, M. R. Andersson, and O. Inganas, "Correlation between oxidation potential and open-circuit voltage of composite solar cells based on blends of polythiophenes/ fullerene derivative," *Applied Physics Letters*, vol. 84, no. 9, pp. 1609–1611, 2004.

[90] M. C. Scharber, D. Mhlbacher, M. Koppe, P. Denk, C. Waldauf, A. J. Heeger, and C. J. Brabec, "Design rules for donors in bulk-heterojunction solar cells-towards 10% energy-conversion efficiency," *Advanced Materials*, vol. 18, no. 6, pp. 789–794, 2006.

[91] D. C. Olson, S. E. Shaheen, M. S. White, W. J. Mitchell, M. F. A. M. van-Hest, R. T. Collins, and D. S. Ginley, "Band-offset engineering for enhanced open-circuit voltage in polymer-oxide hybrid solar cells," *Advanced Functional Materials*, vol. 17, no. 2, pp. 264–269, 2007.

[92] H. Frohne, S. E. Shaheen, C. J. Brabec, D. C. Mller, N. S. Sariciftci, and K. Meerholz, "Influence of the anodic work function on the performance of organic solar cells," *ChemPhysChem*, vol. 3, no. 9, pp. 795–799, 2002.

[93] K. Sarangerel, C. Ganzorig, M. Fujihira, M. Sakomura, and K. Ueda, "Influence of the work function of chemically modified indium-tin-oxide electrodes on the open-circuit voltage of heterojunction photovoltaic cells," *Chemistry Letters*, vol. 37, no. 7, pp. 778–779, 2008.

[94] C. M. Heller, I. H. Campbell, D. L. Smith, N. N. Barashkov, and J. P. Ferraris, "Chemical potential pinning due to equilibrium electron transfer at metal/c[sub 60]-doped polymer interfaces," *Journal of Applied Physics*, vol. 81, no. 7, pp. 3227–3231, 1997.

[95] J. A. Barker, C. M. Ramsdale, and N. C. Greenham, "Modeling the current-voltage characteristics of bilayer polymer photovoltaic devices," *Physical Review B*, vol. 67, no. 7, p. 075205, 2003.

[96] J. Nelson, J. Kirkpatrick, and P. Ravirajan, "Factors limiting the efficiency of molecular photovoltaic devices," *Physical Review B*, vol. 69, no. 3, p. 035337, 2004.

[97] J. Nelson, "Diffusion-limited recombination in polymer-fullerene blends and its influence on photocurrent collection," *Physical Review B*, vol. 67, no. 15, p. 155209, 2003.

[98] J. Nelson and J. Kirkpatrick, "Analysis of the photovoltaic efficiency of a molecular solar cell based on a two-level system," *Applied Physics A: Materials Science & Processing*, vol. 79, no. 1, pp. 15–20, 2004.

[99] R. A. Marcus, "Electron transfer reactions in chemistry. theory and experiment," *Reviews of Modern Physics*, vol. 65, July 1993.

[100] R. A. Marsh, C. R. McNeill, A. Abrusci, A. R. Campbell, and R. H. Friend, "A unified description of current-voltage characteristics in organic and hybrid photovoltaics under low light intensity," *Nano Letters*, vol. 8, no. 5, pp. 1393–1398, 2008.

[101] D. Cheyns, J. Poortmans, P. Heremans, C. Deibel, S. Verlaak, B. P. Rand, and J. Genoe, "Analytical model for the open-circuit voltage and its associated resistance in organic planar heterojunction solar cells," *Physical Review B (Condensed Matter and Materials Physics)*, vol. 77, no. 16, pp. 165332–10, 2008.

[102] B. Rand, D. Burk, and S. Forrest, "Offset energies at organic semiconductor heterojunctions and their influence on the open-circuit voltage of thin-film solar cells," *Physical Review B*, vol. 75, p. 11, 2007.

[103] M. D. Perez, C. Borek, S. R. Forrest, and M. E. Thompson, "Molecular and morphological influences on the open circuit voltages of organic photovoltaic devices," *Journal of the American Chemical Society*, vol. 131, no. 26, pp. 9281–9286, 2009.

[104] T. D. Heidel, J. K. Mapel, M. Singh, K. Celebi, and M. A. Baldo, "Surface plasmon polariton mediated energy transfer in organic photovoltaic devices," *Applied Physics Letters*, vol. 91, no. 9, pp. 093506–3, 2007.

[105] E. H. Sargent, "Infrared quantum dots," *Advanced Materials*, vol. 17, no. 5, pp. 515–522, 2005.

[106] P. Peumans, V. Bulovic, and S. Forrest, "Efficient, high-bandwidth organic multilayer photodetectors," *Applied Physics Letters*, vol. 76, no. 20, pp. 3855–3857, 2000.

[107] P. Andrew and W. Barnes, "Energy transfer across a metal film mediated by surface plasmon polaritons," *Science*, vol. 306, pp. 1002–1005, 2004.

[108] S. A. Maier and H. A. Atwater, "Plasmonics: Localization and guiding of electromagnetic energy in metal/dielectric structures," *Journal of Applied Physics*, vol. 98, no. 1, pp. 011101–10, 2005.

[109] W. L. Barnes, A. Dereux, and T. W. Ebbesen, "Surface plasmon subwavelength optics," *Nature*, vol. 424, no. 6950, pp. 824–830, 2003.

[110] H. Raether, *Surface plasmons on smooth and rough surfaces and on gratings*, vol. 111. Berlin: Springer-Verlag, 1987.

[111] E. Kretschmann and H. Raether, "Radiative decay of non-radiative surface plasmons excited by light," *Zeitschrift für Naturforschung*, vol. 23A, pp. 2135–2136, 1968.

[112] R. Chance, A. Prock, and R. Silbey, "Molecular fluorescence and energy transfer near metal interfaces," in *Advances in Chemical Physics Vol. 37* (I. Prigogine and S. Rice, eds.), vol. 37, pp. 1–65, New York: Wiley, 1978.

[113] D. Drexhage, "Interaction of light with monomolecular dye layers," in *Progress in Optics XII* (E. Wolf, ed.), New York: North-Holland, 1974.

[114] W. Barnes, "Fluorescence near interfaces: the role of photonic mode density," *Journal of Modern Optics*, vol. 45, pp. 661–699, 1998.

[115] W. Weber and C. Eagen, "Energy transfer from an excited dye molecule to the surface plasmons of an adjacent metal," *Optics Letters*, vol. 4, no. 8, pp. 236–238, 1979.

[116] V. Bulovic, V. Khalfin, G. Gu, P. Burrows, D. Garbuzov, and S. Forrest, "Weak microcavity effects in organic light emitting devices," *Physical Review B*, vol. 58, pp. 3730–3740, 1998.

[117] M. H. Lu and J. C. Sturm, "Optimization of external coupling and light emission in organic light-emitting devices: modeling and experiment," *Journal of Applied Physics*, vol. 91, no. 2, pp. 595–604, 2002.

[118] M. H. Lu and J. C. Sturm, "External coupling efficiency in planar organic light-emitting devices," *Applied Physics Letters*, vol. 78, no. 13, pp. 1927–1929, 2001.

[119] K. Celebi, T. Heidel, and M. Baldo, "Simplified calculation of dipole energy transport in a multilayer stack using dyadic green's functions," *Optics Express*, vol. 15, no. 4, pp. 1762–1772, 2007.

[120] T. Förster, "Transfer mechanisms of electronic excitation," *Discussions of the Faraday Society*, vol. 27, pp. 7–17, 1959.

[121] D. M. Basko, G. C. La Rocca, F. Bassani, and V. M. Agranovich, "Electronic energy transfer in a planar microcavity," *Physica Status Solidi a-Applied Research*, vol. 190, no. 2, pp. 379–382, 2002.

[122] D. Garbuzov, V. Bulovic, P. Burrows, and S. Forrest, "Photoluminescence efficiency and absorption of aluminum-tris-quinolate (Alq3) thin films," *Chemical Physics Letters*, vol. 249, pp. 433–437, 1996.

[123] H. Mattoussi, H. Murata, C. Merritt, Y. Iizumi, J. Kido, and Z. Kafafi, "Photoluminescence quantum yield of pure and molecularly doped organic solid films," *Journal of Applied Physics*, vol. 86, no. 5, pp. 2642–2650, 1999.

[124] D. Magde, R. Wong, and P. G. Seybold, "Fluorescence quantum yields and their relation to lifetimes of rhodamine 6G and fluorescein in nine solvents: Improved absolute standards for quantum yields," *Photochemistry and Photobiology*, vol. 75, no. 4, pp. 327–334, 2002.

[125] J. Mapel, K. Celebi, M. Singh, and M. Baldo, "Plasmonic excitation of organic double heterostructure solar cells," *Applied Physics Letters*, vol. 90, no. 121102, 2007.

[126] Y. Kinoshita, R. Takenaka, and H. Murata, "Independent control of open-circuit voltage of organic solar cells by changing film thickness of MoO[sub 3] buffer layer," *Applied Physics Letters*, vol. 92, no. 24, pp. 243309–3, 2008.

[127] N. Li, B. E. Lassiter, R. R. Lunt, G. Wei, and S. R. Forrest, "Open circuit voltage enhancement due to reduced dark current in small molecule photovoltaic cells," *Applied Physics Letters*, vol. 94, no. 2, p. 023307, 2009.

[128] M. Hiramoto, H. Fukusumi, and M. Yokoyama, "Organic solar cell based on multistep charge separation system," *Applied Physics Letters*, vol. 61, pp. 2580–2582, Nov. 1992.

[129] K. Triyana, T. Yasuda, K. Fujita, and T. Tsutsui, "Improvement of Heterojunction Donor/Acceptor Organic Photovoltaic Devices by Employing Additional Active Layer," *Japanese Journal of Applied Physics*, vol. 44, p. 1974, Apr. 2005.

[130] G. Zhang, W. Li, B. Chu, L. Chen, F. Yan, J. Zhu, Y. Chen, and C. S. Lee, "Cascade-energy-level alignment based organic photovoltaic cells by utilizing copper phthalocyanine as bipolar carrier transporting layer," *Applied Physics Letters*, vol. 94, no. 14, p. 143302, 2009.

[131] J. Dai, X. Jiang, H. Wang, and D. Yan, "Organic photovoltaic cells with near infrared absorption spectrum," *Applied Physics Letters*, vol. 91, no. 25, pp. 253503–3, 2007.

[132] F. Yang, R. R. Lunt, and S. R. Forrest, "Simultaneous heterojunction organic solar cells with broad spectral sensitivity," *Applied Physics Letters*, vol. 92, no. 5, pp. 053310–3, 2008.

[133] S. Sista, Y. Yao, Y. Yang, M. L. Tang, and Z. A. Bao, "Enhancement in open circuit voltage through a cascade-type energy band structure," *Applied Physics Letters*, vol. 91, no. 22, p. 3, 2007.

[134] Y. Kinoshita, T. Hasobe, and H. Murata, "Control of open-circuit voltage in organic photovoltaic cells by inserting an ultrathin metal-phthalocyanine layer," *Applied Physics Letters*, vol. 91, no. 8, p. 3, 2007.

[135] L. Onsager, "Initial recombination of ions," *Physical Review*, vol. 54, pp. 554–557, 1938.

[136] J.-L. Bredas, D. Beljonne, V. Coropceanu, and J. Cornil, "Charge-transfer and energy-transfer processes in [pi]-conjugated oligomers and polymers: A molecular picture," *Chemical Reviews*, vol. 104, no. 11, pp. 4971–5004, 2004.

[137] R. Marcus, "On the theory of oxidation-reduction reactions involving electron transfer," *Journal of Chemical Physics*, vol. 24, no. 5, pp. 966–978, 1955.

[138] V. Lemaur, M. Steel, D. Beljonne, J.-L. Bredas, and J. Cornil, "Photoinduced charge generation and recombination dynamics in model donor/acceptor pairs for organic solar cell applications: A full quantum-chemical treatment," *Journal of the American Chemical Society*, vol. 127, no. 16, pp. 6077–6086, 2005.

[139] S. Larsson and A. Volosov, "Distance dependence in photo-induced intramolecular electron transfer," *The Journal of Chemical Physics*, vol. 85, no. 5, pp. 2548–2554, 1986.

[140] R. A. Street, "Carrier mobility, structural order, and solar cell efficiency of organic heterojunction devices," *Applied Physics Letters*, vol. 93, no. 13, p. 133308, 2008.

[141] Y. Yi, V. Coropceanu, and J.-L. Bredas, "Exciton-Dissociation and Charge-Recombination Processes in Pentacene/C60 Solar Cells: Theoretical Insight into the Impact of Interface Geometry," *Journal of the American Chemical Society*, vol. 131, no. 43, pp. 15777–15783, 2009.

[142] N. S. Sariciftci, L. Smilowitz, A. J. Heeger, and F. Wudl, "Photoinduced Electron Transfer from a Conducting Polymer to Buckminsterfullerene," *Science*, vol. 258, no. 5087, pp. 1474–1476, 1992.

[143] P. A. van Hal, R. A. J. Janssen, G. Lanzani, G. Cerullo, M. Zavelani-Rossi, and S. De Silvestri, "Full temporal resolution of the two-step photoinduced energy-electron transfer in a fullerene-oligothiophene-fullerene triad using sub-10 fs pump-probe spectroscopy," *Chemical Physics Letters*, vol. 345, no. 1-2, pp. 33–38, 2001.

[144] C. J. Brabec, G. Zerza, G. Cerullo, S. De Silvestri, S. Luzzati, J. C. Hummelen, and S. Sariciftci, "Tracing photoinduced electron transfer process in conjugated polymer/fullerene bulk heterojunctions in real time," *Chemical Physics Letters*, vol. 340, no. 3-4, pp. 232–236, 2001.

[145] S. Yoo, B. Domercq, and B. Kippelen, "Highly efficient pentacene/c[sub 60] organic solar cells," in *Organic Photovoltaics VI*, vol. 5938, (San Diego, CA, USA), pp. 59380M–8, SPIE, 2005.

[146] D. M. Russell, A. C. Arias, R. H. Friend, C. Silva, C. Ego, A. C. Grimsdale, and K. Mullen, "Efficient light harvesting in a photovoltaic diode composed of a semiconductor conjugated copolymer blend," *Applied Physics Letters*, vol. 80, no. 12, pp. 2204–2206, 2002.

[147] V. D. Mihailetchi, L. J. A. Koster, J. C. Hummelen, and P. W. M. Blom, "Photocurrent generation in polymer-fullerene bulk heterojunctions," *Physical Review Letters*, vol. 93, no. 21, p. 216601, 2004.

[148] L. J. A. Koster, E. C. P. Smits, V. D. Mihailetchi, and P. W. M. Blom, "Device model for the operation of polymer/fullerene bulk heterojunction solar cells," *Physical Review B*, vol. 72, no. 8, p. 085205, 2005.

[149] P. Schilinsky, C. Waldauf, and C. J. Brabec, "Recombination and loss analysis in polythiophene based bulk heterojunction photodetectors," *Applied Physics Letters*, vol. 81, no. 20, pp. 3885–3887, 2002.

[150] L. Goris, A. Poruba, L. Hod'akova, M. Vanecek, K. Haenen, M. Nesladek, P. Wagner, D. Vanderzande, L. De Schepper, and J. V. Manca, "Observation of the subgap optical absorption in polymer-fullerene blend solar cells," *Applied Physics Letters*, vol. 88, no. 5, pp. 052113–3, 2006.

[151] D. Abramavicius, V. Gulbinas, and L. Valkunas, "Acceleration of charge separation by oscillations of the environment polarization," *Chemical Physics Letters*, vol. 368, pp. 480–485, 2003.

[152] D. M. Basko and E. M. Conwell, "Hot exciton dissociation in conjugated polymers," *Physical Review B*, vol. 66, no. 15, p. 155210, 2002.

[153] V. I. Arkhipov, E. V. Emelianova, and H. Bässler, "Hot exciton dissociation in a conjugated polymer," *Physical Review Letters*, vol. 82, no. 6, p. 1321, 1999.

[154] H. Ohkita, S. Cook, Y. Astuti, W. Duffy, S. Tierney, W. Zhang, M. Heeney, I. McCulloch, J. Nelson, D. D. C. Bradley, and J. R. Durrant, "Charge carrier formation in polythiophene/fullerene blend films studied by transient absorption spectroscopy," *Journal of the American Chemical Society*, vol. 130, no. 10, pp. 3030–3042, 2008.

[155] I. G. Hill, A. Kahn, Z. G. Soos, and J. R. A. Pascal, "Charge-separation energy in films of [pi]-conjugated organic molecules," *Chemical Physics Letters*, vol. 327, no. 3-4, pp. 181–188, 2000.

[156] C. Adachi, R. Kwong, and S. R. Forrest, "Efficient electrophosphorescence using a doped ambipolar conductive molecular organic thin film," *Organic Electronics*, vol. 2, no. 1, pp. 37–43, 2001.

[157] A. Kahn, N. Koch, and W. Gao, "Electronic structure and electrical properties of interfaces between metals and pi-conjugated molecular films," *Journal of Polymer Science Part B: Polymer Physics*, vol. 41, no. 21, pp. 2529–2548, 2003.

[158] Y. Hamada, H. Kanno, T. Tsujioka, H. Takahashi, and T. Usuki, "Red organic light-emitting diodes using an emitting assist dopant," *Applied Physics Letters*, vol. 75, no. 12, pp. 1682–1684, 1999.

[159] C. Goldmann, S. Haas, C. Krellner, K. P. Pernstich, D. J. Gundlach, and B. Batlogg, "Hole mobility in organic single crystals measured by a "flip-crystal" field-effect technique," *Journal of Applied Physics*, vol. 96, no. 4, pp. 2080–2086, 2004.

[160] D. Alloway and N. Armstrong, "Organic heterojunctions of layered perylene and phthalocyanine dyes: characterization with UV-photoelectron spectroscopy andluminescence quenching," *Applied Physics A: Materials Science & Processing*, vol. 95, no. 1, pp. 209–218, 2009.

[161] J. Ye, H.-Z. Chen, and M. Wang, "Enhanced photoconductivity in organic single-layered photoreceptors with bipolar charge transport materials," *Materials Chemistry and Physics*, vol. 82, no. 1, pp. 210–215, 2003.

[162] J. Hwang, A. Wan, and A. Kahn, "Energetics of metal-organic interfaces: New experiments and assessment of the field," *Materials Science and Engineering: R: Reports*, vol. 64, no. 1-2, pp. 1–31, 2009.

[163] R. F. Bailey-Salzman, B. P. Rand, and S. R. Forrest, "Near-infrared sensitive small molecule organic photovoltaic cells based on chloroaluminum phthalocyanine," *Applied Physics Letters*, vol. 91, no. 1, p. 013508, 2007.

[164] A. C. Morteani, P. Sreearunothai, L. M. Herz, R. H. Friend, and C. Silva, "Exciton regeneration at polymeric semiconductor heterojunctions," *Physical Review Letters*, vol. 92, no. 24, p. 247402, 2004.

[165] W. T. Welford and R. Winston, *Optics of nonimaging concentrators. Light and solar energy.* New York: Academic Press, 1978.

[166] H. Mousazadeh, A. Keyhani, A. Javadi, H. Mobli, K. Abrinia, and A. Sharifi, "A review of principle and sun-tracking methods for maximizing solar systems output," *Renewable and Sustainable Energy Reviews*, vol. 13, no. 8, pp. 1800–1818, 2009.

[167] G. Smestad, H. Ries, R. Winston, and E. Yablonovitch, "The thermodynamic limits of light concentrators," *Solar Energy Materials*, vol. 21, pp. 99–111, 1990.

[168] A. Goetzberger and W. Greube, "Solar energy conversion with fluorescent collectors," *Applied Physics A: Materials Science & Processing*, vol. 14, no. 2, pp. 123–139, 1977.

[169] E. Yablonovitch, "Thermodynamics of the fluorescent planar concentrator," *Journal of the Optical Society of America*, vol. 70, no. 11, pp. 1362–1363, 1980.

[170] V. Bulovic, A. Shoustikov, M. Baldo, E. Bose, V. Kozlov, M. Thompson, and S. Forrest, "Bright, saturated, red-to-yellow organic light -emitting devices based on polarization-induced spectral shifts," *Chemical Physics Letters*, vol. 287, pp. 455–460, 1998.

[171] M. Baldo, D. O'Brien, Y. You, A. Shoustikov, S. Sibley, M. Thompson, and S. Forrest, "High efficiency phosphorescent emission from organic electroluminescent devices," *Nature*, vol. 395, pp. 151–154, 1998.

[172] M. J. Currie, J. K. Mapel, T. D. Heidel, S. Goffri, and M. A. Baldo, "High-efficiency organic solar concentrators for photovoltaics," *Science*, vol. 321, no. 5886, pp. 226–228, 2008.

[173] C. Baur, A. W. Bett, F. Dimroth, G. Siefer, M. Meusel, W. Bensch, W. Kostler, and G. Strobl, "Triple-junction iii–v based concentrator solar cells: Perspectives and challenges," *Journal of Solar Energy Engineering*, vol. 129, no. 3, pp. 258–265, 2007.

[174] R. P. Gale, R. W. McClelland, D. B. Dingle, J. V. Gormley, R. M. Burgess, N. P. Kim, R. A. Mickelsen, and B. J. Stanbery, "High-efficiency GaAs/$CuInSe_2$ and AlGaAs/$CuInSe_2$ thin-film tandem solar cells," in *21st Institute of Electrical and Electronics Engineers (IEEE) Photovoltaic Specialists Conference*, (Kissimimee, FL), May 1990.